Journal of Chemical Reviews, 2019, Volume 1, Issue 3, Pages 183-232

Review Article

Reviewing of Synthesis and Computational Studies of Pyrazolo Pyrimidine Derivatives

Hussein Shaban Hussein Mohamed [a,*], **Sayed Abdelkader Ahmed** [b]

[a] *Research Institute of Medicinal and Aromatic Plants (RIMAP), Beni-Suef University, Beni-Suef, Egypt*
[b] *Chemistry Department, Faculty of Science, Beni-Suef University, Beni-Suef, Egypt*

Receive Date: 11 Jun 2019, **Revise Date:** 24 June 2019, **Accept Date:** 24 June 2019

Abstract: In this review we synthesized and conducted a computational studies on Pyrazolo pyrimidine's derivatives that were carried out through density functional theory level utilizing HF/6−311+G**and B3LYP/6−311+G**. Charge transfer occured through molecule was shown by the calculation of HOMO and LUMO energies. The electric dipole moment values (l) of the molecule were counted calculations of DFT. Some geometrical and structural parameters such as total energies (E), relative energies (DE), (bond length in Å, angles in degree), energy gap, relative Gibbs free energy, dipole moment, and molecular electrostatic potentials (MEP) were studied.

DOI: 10.33945/SAMI/JCR.2019.3.3

Keywords: GAUSSIAN09, DFT, HOMO-LUMO, pyrazolo pyrimidine derivatives, quantum chemical calculation.

Graphical Abstract:

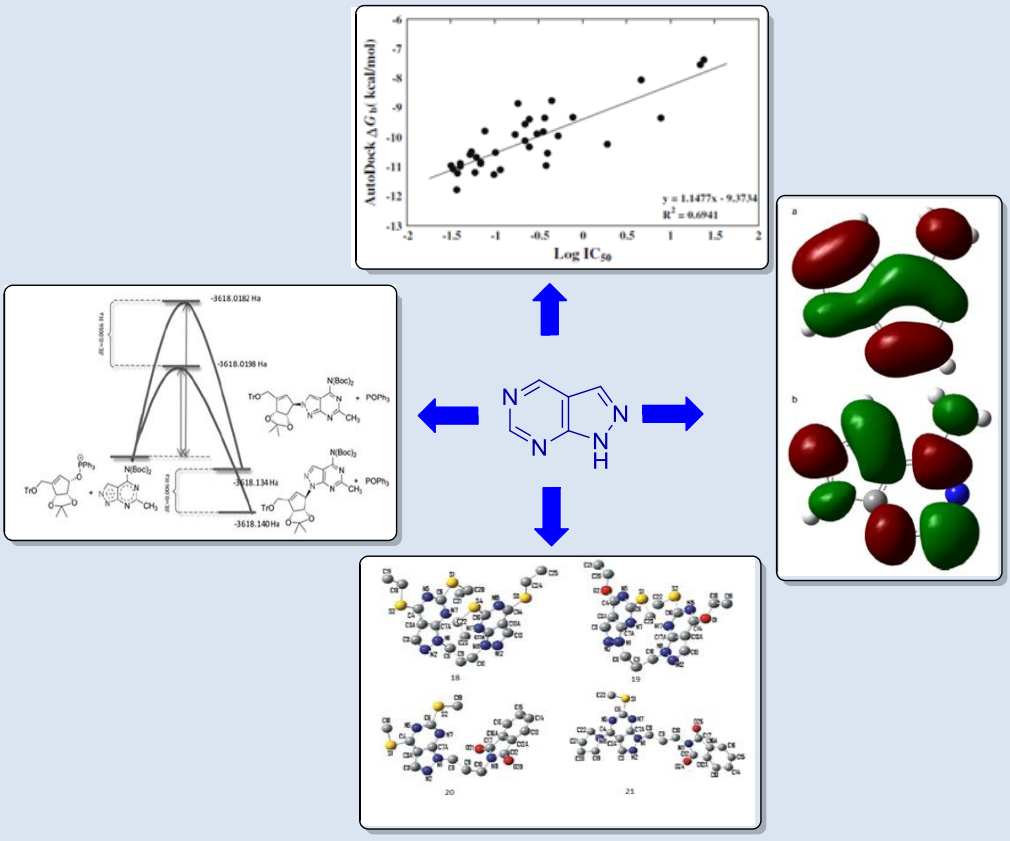

*Corresponding author: H. S. Mohamed, Email: h_gendy_2010@yahoo.com

Biography:

Hussein S. H. Mohamed Was born Beni-Suef (Egypt) in 1980, obtained his Ph.D. degree in Organic chemistry in 2015 under the supervisor of Prof. Dr. Ahmed Elghandour and Prof. Dr. Sayed A. Ahmed. Later on, he is currently working as Senior Researcher in Natural Products of Research Institute of Medicinal and Aromatic Plants (RIMAP), Beni-Suef University. He has been actively involved Synthesis of Heterocyclic compounds and its applications in biological activities, recently he interested in Removal of dyes and heavy metals from wastewater by different synthesized compounds.

Sayed A. Ahmed Has completed his Ph.D under the supervision of Professor Galal Elgemie and Prof. Dr. Ahmed Elghandour in the Department of Chemistry at Beni-Suef University, Egypt. He currently works as a full professor in Organic Chemistry at Beni-Suef University Egypt. His studies focused on organic synthesis of Organic compounds and he has published more than 100 papers. He is a Dean of Faculty of Earth Sciences, Beni-Suef University Egypt. He has received several national and international awards.

1. Introduction

Heterocyclic pyrimidine nucleus includes four carbon and two nitrogen atoms and is pharmacologically in active; however, its synthetic derivatives have important roles in pharmaceutical applications [1-3]. The properties are demonstrated by their hydrogen and bonding systems. They belong to the family of nucleic acids. Nucleic acids are of great interest, since, they have role in the manufacture of proteins and the functions of the cells in living organisms [4-6]. For example Pyrazolo[3,4-*d*]pyrimidine derivatives are shown to exhibit anti-amoebic activity [7-13] and are potential anti-inflammatory agents [14, 15], anti-coagulation inhibitors [16], xanthine oxidase inhibitors [17], antiproliferative and proapoptotic agents in various tumor types [18,19]. They are called SRC kinase inhibitors [20] and are beneficial in human cancers treating sustaining oncogenic activation of RET [21]. After the knowing of scaled quantum mechanical (SQM) calculations, the philosophy of computational methods of vibrational spectroscopy [22-25] were changed significantly. The most applied spectroscopic methods by organic chemists for the characterization of compounds are ultra-violet, IR, NMR, and mass spectroscopy. IR measurement through liquid mixtures supplies an excellent tool to investigate inter and intramolecular interactions between like and unlike molecules. The density functional theory has become a great method for the description of vibrational spectra and molecular structure. Completed by a visualization program, the assignments can accurately be made [26-28]. The advance in the graphic and computational devices has increased the significance of MEP surfaces, highest occupied molecular orbital (HOMO) and lowest unoccupied molecular orbital (LUMO) as tools for studying molecular reactivities, interactions, charge transfers and other molecular properties [29-34]. These characteristics are the highest occupied molecular orbital energy E_{HOMO}, the lowest unoccupied molecular orbital energy E_{lumo}, energy gap ΔE, dipole moment μ, total energy E_T, activation energy E_a, absorption maximum λ_{max} and factor of oscillation f(SO). The geometry of the systems has been improved at the B3LYP /6-31G (d) [35-38] computational level. As per the computations, the molecules concerned to energy minima on the Potential Energy Surface (PES). The Gaussian-09 program was used for all this calculations [39-42].The density functional used this form:

$$Exc= (1-\alpha_0)E_X^{LSDA} +\alpha_0 E_X^{HF} +\alpha_X \Delta E_X^{B88}+\alpha_C E_c^{LYP} + (1-\alpha_C)E_C^{VWN}$$

2. Synthesis and Computational Studies of Pyrazolo[3,4-*d*]Pyrimidine

2.1. 4- Aminopyrazolo[3,4-d]pyrimidine

The theoretical UV–Vis spectrum is used to detect this compound using CIS method and the electronic properties, such as HOMO and LUMO energies, were perfected by time-dependent DFT (TD-DFT) approach. Charge transfer occurs within the molecule was shown by HOMO and LUMO energies calculations. The first order hyperpolarizability (β_0) of this molecular system and related properties (β, α_0 and $\Delta\alpha$) of 4-APP are computed using DFT/6-31G (d) method on the finite-field approach. The Mulliken

charges, the values of electric dipole moment (μ) of the molecule were calculated utilizing DFT calculations. They used natural bond (NBO) analysis to compute The diversity in electron density (ED) in the antibonding orbitals and stabilization energies giving clear evidence of stabilization originating in the hyper conjugation of hydrogen-bonded interactions [43].

2.1.1. Structure of 4-aminopyrazolo[3,4-d]pyrimidine

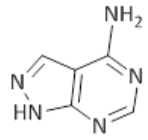

1

Scheme 1. Structure of *4*-aminopyrazolo*[3,4-d]pyrimidine*

2.1.2. Computational

Gaussian 09W software package used to calculate the energy and dipole moment of tautomer [44], using the B3LYP functional [45,46] combined with standard 6-31G* basis set.

In the Table 1 Prabavathi, *et al*. reported that the total energies, dipole moment and their relative energies of various tautomer of 4-APP were computed at B3LYP/6-31G* level.

We can realize from Table 1 that for 4-APP the energies of the tautomers are in the following order

(1a) < (1b) < (1c) < (1d) < (1e) < (1f) < (1g) < (1h) < (1i) < (1j) < (1k) < (1L) < (1m) < (1n) < (1o) < (1p).

It was found that the amino-N(1)*H* tautomer has the lowest energy and is the most stable form.

Xue *et al*. utilizing the computed geometrical parameters for 4-APP (as it contains both a pyrimidine ring and an imidazole ring) which are parallel with some of the purine derivatives [47,48] (6-aminopurine and adenine) for the possible bond lengths and bond angles. So it was predicted that the bond length and bond angle agree with adenine parameters obtained in Table 3.

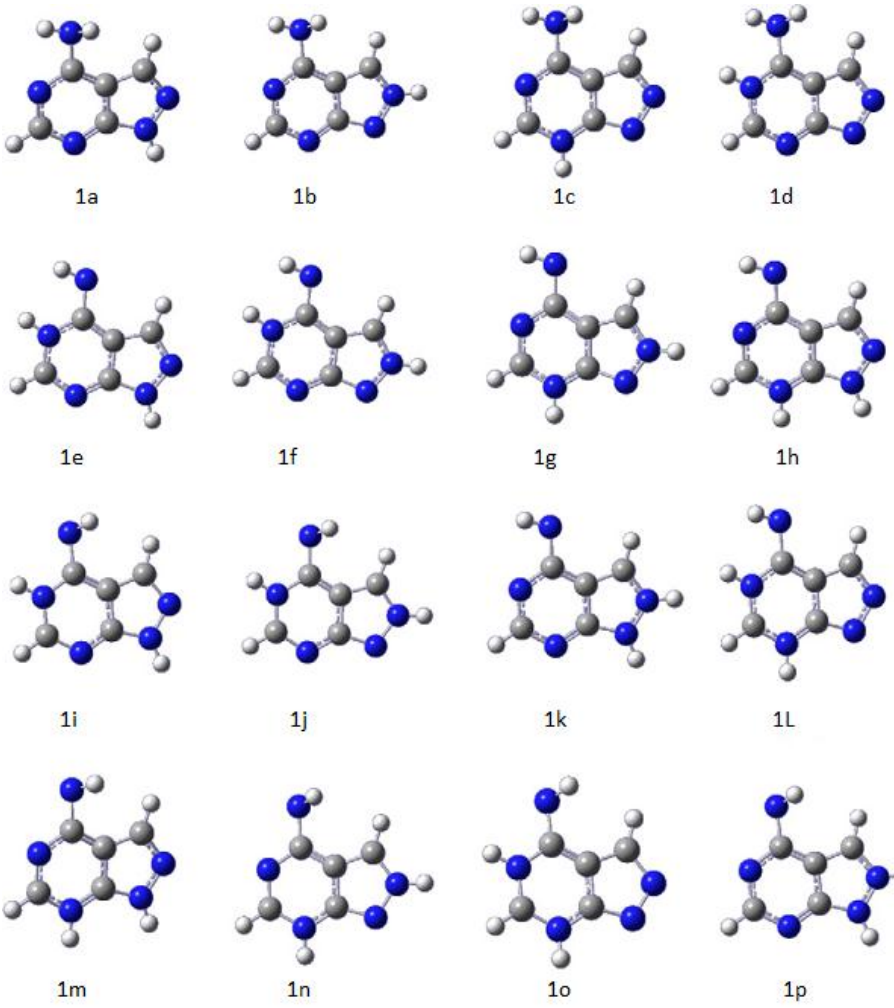

Figure 1. Tautomers of 4-aminopyrazolo[3,4-*d*]pyrimidine.

Through Table 4 the values of the polarizabilities (α) and hyperpolarizability (β) of the Gaussian 09 output, Data *et al*. found that the extent of π electron delocalization control the ground-state dipole moment and the hyperpolarizability, which relies on the structural details of the molecules [49].

The six peaks of 4-APP appeared at 1587, 1580, 1478, 725 cm^{-1} in both IR and Raman spectra and the IR bands at 1606, and 1512 cm^{-1} are attributed to ring C–N stretching vibrations. Analogical bands are theoretically calculated at 1633, 1612, 1563, 1512, 1466, 705 cm^{-1} with a PED contribution in the range 58–35% at 6-31G** level.

Table 1. Energy and dipole moment of 4-aminoPyrazolo[3,4-*d*]pyrimidine.

Tautomer[a]	Total energy (Hartree) B3LYP/ 631-G*	Dipole moment (Debye) B3LYP/ 631-G*	Relative energies (kJ mol^{-1})
	4-Aminopyrazolo [3 4-*d*]pyrimidine		
1a	-467.238374	1.7170	0.0
1b	-467.218458	5.5250	52.3
1c	-467.215798	6.2607	59.3
1d	-467.198521	11.2556	104.6
1e	-467.197957	4.8652	106.1
1f	-467.185872	1.9407	137.8
1g	-467.185169	4.5492	139.7
1h	-467.184202	7.9895	142.2
1i	-467.180848	3.8361	151.0
1j	-467.166858	1.1979	187.8
1k	-467.157364	8.5522	212.4
1l	-467.154937	10.8967	219.1
1m	-467.154623	8.6543	219.9
1n	-467.154076	6.1545	221.3
1o	-467.138857	9.2026	261.3
1p	-467.126886	10.6410	292.7

[a] For the tautomeric figures.

Table 2. Theoretical computed energies (a.u.), energies (Kcal Mol^{-1}), Rotational constant (GHZ), entropy (Cal mol^{-1} k^{-1}) and Dipole moment (Debye).

Structural parameter	B3LYP/6-31G* 4-APP	B3LYP/6-31G** 4-APP
Total energy(thermal) E_{total}	75.22	75.17
Heat capacity at const. Volume ,*Cv*	27.84	27.86
Entropy ,*S*	83.15	83.11
Vibrational energy E_{vib}	73.45	73.40
Zero-point vibrational Energy , E_0	70.82	70.78
Rotational constant		
A	2.403	2.404
B	1.493	1.493
C	0.922	0.922
Dipole moment		
μ_x	-0.4060	0.3975
μ_y	-1.4263	-1.5064
μ_z	1.3911	1.3441
μ_{total}	2.0332	2.0578

Table 3. Optimized geometrical parameters of 4-aminoPyrazolo[3,4-*d*]pyrimidine obtained by B3LYP/6-31G* and B3LYP/6-31G** density functional calculations.

Bond length	Value (Å)		Bond angle	Value (º)	
	6-31G*	6-31G**		6-31G*	6-31G**
N1–N2	1.36	1.36	N1–N2–C3	105.81	105.85
C3–N2	1.32	1.32	N2–C3–C4	111.19	111.12
C4–C3	1.42	1.42	C3–C4–C5	140.36	140.33
C5–C4	1.41	1.41	C4–C5–N6	119.81	119.78
N6–C5	1.33	1.33	C5–N6–C7	118.25	118.29
C7–N6	1.34	1.34	N6–C7–N8	128.61	128.57
N8–C7	1.32	1.32	C7–N8–C9	111.80	111.82
C9–N8	1.34	1.34	C9–N1–H10	127.62	127.49
H10–N1	1.00	1.00	N2–C3–H11	119.38	119.46
H11–C3	1.08	1.08	C4–C5–N12	122.43	122.44
N12–C5	1.38	1.38	C5–N12–H13	111.79	111.76
H13–N12	1.01	1.01	C5–N12–H14	108.53	108.48
H14–N12	1.01	1.01	N6–C7–H15	115.20	115.22
H15–C7	1.08	1.08	C4–C3–N2–N1	0.0	0.0
			C5–C4–C3–N2	180.0	180.0
			N6–C5–C4–C3	-180.0	-180.0
			C7–N6–C5–C4	0.0	0.0
			N8–C7–N6–C5	0.0	0.0
			C9–N8–C7–N6	0.0	0.0
			H10–N1–C9–N8	0.0	0.0
			H11–C3–N2–N1	180.0	180.0
			N12–C5–C4–C3	6.0	6.0
			H13–N12–C5–C4	-46.0	-46.0
			H14–N12–C5–C4	-161.0	-161.0
			H15–C7–N6–C5	180.0	180.0

[a] For the tautomeric figures.

Table 4. Vibrational spectral data (cm^{-1})

No	Observed		Calculated frequency (cm^{-1}) with		B3LYP/6-31G** force field		TED (%) among type of internal coordinates[c]
	Infrared	Raman	Unscaled	Scaled	IR[a](Ai)	Raman[b](Ii)	
1	3318	_	3644	3318	14.89	1.07	N–H Stretching
2	3135	_	3553	3135	94.00	3.83	NH_2ass(95)
3	_	3102	3504	3102	22.60	72.71	NH_2ss(95)
4	3060	_	3337	3079	4.02	10.57	C–H(99)
5	3030	_	3261	3010	29.03	1.14	C–H(99)
6	1677	1675	1670	1668	220.69	17.93	NH_2sci(54)
7	1606	_	1630	1633	190.18	29.66	C–N(51), NH_2Sci(26)
8	1587	1585	1611	1612	64.95	4.24	C–N(43), bCCH(32)

9	1580	1580	1511	1563	4.36	25.17	C–N(54), bCCH(29)
10	1512	_	1488	1512	165.42	19.41	C–N(58), C–C(16)
11	1478	1478	1450	1466	84.69	26.12	C–N(49), bCCH(22)
12	1398	_	1389	1407	4.18	4.10	bCCH(52), C–N(16)
13	_	1394	1368	1387	9.63	23.17	C–N(57), C–C(19)
14	1340	1337	1336	1335	8.02	10.30	C–C(42), C–N(35)
15	1339	_	1332	1325	180.20	3.14	bNNH(47), C–N(16)
16	1265	_	1283	1265	45.52	3.62	bCCH (59), bNNH (15)
17	1199	_	1211	1200	40.66	9.27	C–C(41), C–N(22)
18	_	1154	1160	1147	11.30	12.00	bring2(35), C–N(27)
19	1067	1066	1075	1069	34.15	8.14	N–N(78), bNNH(9)
20	1029	1031	1053	1035	22.96	8.31	NH_2roc(54), C–N(37)
21	962	939	981	972	150.30	1.43	C–C(53), bring2(18)
22	903	898	947	914	100.47	2.83	bring1(54), C–C(17)
23	900	900	906	895	11.79	2.12	gCH(59), bring2 (17)
24	870	_	871	856	70.71	1.02	gHN(77), tring2(15)
25	796	796	853	805	15.64	1.94	gCH(31), tring1(27)
26	785	_	800	775	115.94	1.51	gCH(30), tring1(29)
27	725	725	713	705	2.87	18.67	C–N(30), C–C(24)
28	693	_	681	701	17.42	0.08	tring2(82), tButt(7)
29	636	_	659	633	30.89	1.29	gCN(39), tring1(30)
30	609	615	608	594	0.23	8.34	bring2(31), C–C (29)
31	549	_	573	554	57.46	2.13	tring1(46), gNH(23)
32	527	527	525	526	0.56	4.51	bring1(74), C–N(12)
33	_	_	511	508	3.66	2.77	bring1(32), bCN(31)
34	_	_	499	488	34.03	2.12	gNH(58), tring2(30)
35	_	_	353	337	69.94	1.98	tNH_2(68), gHN(19)
36	_	_	299	292	3.05	0.06	tring1(35), tring2(25)
37	_	_	285	280	2.64	0.58	bCN(45), bring1(15)
38	_	_	209	209	2.64	0.43	tbutt(48), tring1(31)
39	_	_	164	155	1.81	0.37	tring1(72), tring2(12)

Abbreviations used: b, bending; g, deformation; ass, asymmetric; ss, symmetric; t, torsion; sci, scissoring; gHN, twisting.
[a] Relative absorption intensities normalized with highest peak absorption.
[b] Relative Raman intensities calculated and normalized to 100.
[c] For the notations used.

Chemical shifts of the carbon atoms in 4-APP theoretically are calculated, lies between 105 and 165 ppm. The studies show the chemical shifts calculated for the hydrogen atoms of amino group are quite low. The N atom(s) have electronegative property polarizes

the electron distribution in its bond to close carbon atom and lowering the electron density of the molecule [50].

Table 5. Theoretical isotropic chemical shifts calculated using HF/6-31G* (with respect to TMS, all values in ppm) for 4-aminopyrazolo[3,4-*d*]pyrimidine [43].

Calculated chemical shift (ppm)

Atom	HF/6-31G*
N1	180.7
N2	308.5
C3	134.8
C4	109.2
C5	162.1
N6	248.3
C7	160.2
N8	235.3
C9	157.4
H10	9.1
H11	7.9
N12	78.3
H13	3.6
H14	3.9
H15	8.9

All the exocyclic atoms have atomic charges corresponds to their electro-negativity while the charges at all the C atoms of the ring are corresponds to the net flow of π electrons (delocalization of electron density) [51]. The Mulliken atomic charges of every atomic site of 4-APP are gathered in Table 6.
The visible absorption maximum was found to be a function of electron availability, oscillator strength, and theoretical electronic excitation energies (as shown in Table 7).
Depending on the calculated potential energy distribution results, assignments of the fundamental vibrational frequencies have been made unambiguously. The lesser value of HOMO–LUMO energy gap has essential effect on the intramolecular bioactivity of the molecule and charge transfer. The energies of essential MOs and the λ_{max} of the compounds were also evaluated from TD-DFT strategy [43].

2.2. 4-Aminopyrazolo[3,4-d]Pyrimidine & Computational details

One electron excitation from the highest occupied molecular orbital (HOMO) to the lowest unoccupied molecular orbital (LUMO) describe the electronic absorption related to the transition from the ground to the first excited state.

Table 6. Atomic charges for optimized geometry of 4-APP using DFT B3LYP/6-31G(d,p).

Atomic number	4-APP	
	Mulliken charges	**Natural atomic charges**
N1	-0.522	-0.37630
N2	-0.242	-0.25642
C3	-0.002	-0.02723
C4	0.044	-0.24706
C5	0.369	0.45339
N6	-0.480	-0.55445
C7	0.169	0.26115
N8	-0.478	-0.51883
C9	0.554	0.38261
H10	0.350	0.44117
H11	0.153	0.23834
N12	-0.723	-0.82628
H13	0.322	0.40198
H14	0.331	0.40839
H15	0.153	0.21953

Table 7. Theoretical electronic absorption spectra values of 4-APP using TD-DFT/B3LYP/6-31G.

Excited state	Wavelength λ (nm)	Excitation energies (eV)	Oscillator strengths (f)
	4-APP	**4-APP**	**4-APP**
S1	206.37	6.0079	0.1907
S2	204.00	6.0777	0.1014
S3	187.27	6.6204	0.0082
S4	173.42	7.1494	0.0095
S5	166.95	7.4263	0.0017

Table 8. The HOMO–LUMO energy gap of 4-aminopyrazolo(3,4-*d*)pyrimidine[4AP(3,4-D)P] was calculated at ab initio HF/6−31+G** (d, p) and B3LYP/6−31+G** (d, p)".

Parameters	B3LYP/6−311+ G** (d,p)	HF/6−311+ G**(d,p)
HOMO energy (a.u.)	−0.285697	−0.31699
LUMO energy (a.u.)	−0.162230	−0.19304
HOMO–LUMO energy gap (a.u.)	−0.123467	−0.12395

ab initio HF and density functional methods utilizing 6−31+G (d,p) demonstrate various thermodynamic properties as heat capacity, zero point energy, entropy along with the global minimum energy of [4AP(3,4-D) P]. As shown in Table 9, we present the total energy and the change in the total entropy of [4AP(3,4-D)P] at room temperature.

The C–H out-of-plane bending modes were given within the characteristic region and are shown in Table 10.

The vibrational properties of 4AP(3,4-d)P have been investigated by FTIR and Laser Raman spectroscopy and were performed accordingly to the SQM force field method based on the ab initio HF/6−311+G**(d,p) and B3LYP/6−311+G**(d,p) levels. It was discussed the importance of amino and other groups in the vibrational frequencies of 4AP(3,4-d)P. The various techniques of vibrations were unambiguously assigned depend on the results of the TED output [26].

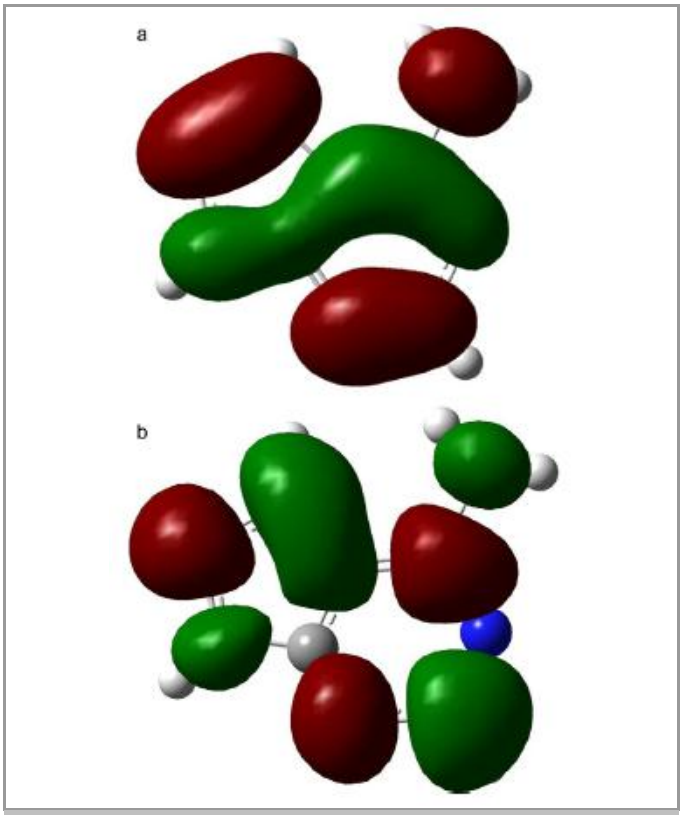

Figure 2. Atomic orbital **(a)** HOMO and **(b)** LUMO compositions of the frontier. Molecular Orbital for pyrazolo(3,4-*d*)pyrimidine.

Table 9. Thermodynamic parameters of 4-aminoPyrazolo (3,4-*d*)pyrimidine calculated at HF/6−311+G** (d, p) and B3LYP/6−31+G**(d,p) methods.

Structural parameter	Method/basis set	
	HF/6−311+G(d,p)**	**B3LYP/6−311+G**(d,p)**
Optimized global minimum Energy (Hartrees)	−467.6102.	−467.4267
Total energy (thermal), E_{total} (kcal mol^{-1})	79.822	74.560
Heat capacity, C_v (kcal mol^{-1} k^{-1})	0.0369	0.0399
Entropy, S (cal mol^{-1} k^{-1})	26.800	29.023
Total	82.824	84.609
Translational	40.614	40.614
Rotational	28.893	28.951
Vibrational	13.318	15.044
Vibrational energy, E_{vib} (mol^{-1} k^{-1})	91.859	85.698
Zero point vibrational energy, (Kcal mol^{-1})	75.492	69.927
Rotational constants (GHZ)		
A	2.4673	2.4186
B	1.5277	1.4989
C	0.9436	0.9255
Dipole moment (Debye)	2.6914	2.6270

Table 10. Vibrational assignments of fundamental frequencies in cm^{-1} and wave numbers (characterized by TED) obtained for 4-aminoPyrazolo(3,4-*d*)pyrimidine at HF/6−311+G**(d,p) and B3LYP/6 311+G**(d,p) level: [wave numbers (cm^{-1}); IR intensities (km mol^{-1}); reduced mass (amu), FORCE constant (m dyn A^{-1}); Raman activity (A^4/amu)] [26].

S. no.	Symm species C_s	Observed frequencies (cm^{-1})		B3LYP/6−311+G**(d,p)					HF/6−311+G**(d,p)					Assignment (% TED)
		FTIR	Laser Raman	Calculated frequencies (cm^{-1})	IR Intensity	Raman activity	Force constant	Reduced mass	Calculated frequencies (cm^{-1})	IR intensity	Raman Activity	Force constant	Reduced Mass	
1	A'	3472(w)	–	3730	3.03	46.06	9.051	5.791	3961	5.96	37.36	6.861	7.095	NH_2 ass(98)
2	A'	–	3406(w)	3661	18.23	130.86	8.539	7.271	3913	25.71	99.45	4.042	9.917	NH_2 ss(96)
3	A'	3306 (w)	–	3601	509.74	180.33	7.990	8.101	3829	539.33	123.80	9.728	7.454	V NH(94)
4	A'	3125 (w)	–	3229	46.73	34.29	10.868	2.002	3385	60.79	19.96	10.216	4.324	V CH(92)
5	A'	–	3110(w)	3167	113.29	44.74	4.356	2.001	3343	146.89	4.55	9.771	1.432	V CH(90)
6	A'	–	1680(vw)	1651	86.48	32.80	4.724	5.619	1800	162.43	59.30	9.039	6.589	V NN(89)
7	A'	1674(ms)	–	1630	19.09	2.86	1.945	1.377	1794	23.33	84.38	3.133	2.789	NH_2 sciss(86)
8	A'	–	1610(vw)	1611	0.55	31.11	1.739	4.830	1776	1.45	116.01	2.509	2.553	V CN(85)
9	A'	1593 (s)	–	1508	49.67	14.89	4.499	3.961	1699	58.06	26.41	5.571	6.009	V CN(84)
10	A'	–	1580(w)	1496	33.68	24.80	5.631	1.312	1635	1.62	24.31	7.418	3.617	V CN(82)
11	A'	1493(ms)	1491(w)	1449	34.37	3.82	2.771	6.446	1585	1.41	25.20	7.201	2.174	V CN(81)
12	A'	–	1478(w)	1399	35.99	14.02	3.255	3.858	1532	53.97	21.48	5.520	5.717	V CN(82)
13	A'	–	1462(w)	1373	1.20	98.01	4.6153	6.946	1481	221.07	0.28	6.144	1.266	V CN(84)
14	A'	–	1394(ms)	1347	12.61	138.17	3.747	2.851	1452	22.44	0.37	3.856	5.619	V CN(82)
15	A'	–	1351(w)	1311	32.98	9.87	3.072	3.527	1398	37.97	16.69	3.975	3.777	V CC(83)
16	A'	1333(ms)	–	1284	9.91	4.56	6.734	5.068	1381	67.5	5.89	2.684	1.365	V CC(80)
17	A'	–	1298(w)	1214	7.48	6.64	6.445	2.591	1291	10.04	6.74	0.819	5.721	V CC(79)
18	A'	1248(w)	–	1166	20.91	9.66	2.908	3.210	1254	34.37	13.09	3.756	3.532	b NH(78)
19	A'	1220(vw)	–	1092	113.02	0.47	2.198	3.502	1184	556.26	44.93	5.391	1.099	b CH(76)
20	A'	–	1202(vw)	1016	1.54	0.75	2.219	3.027	1129	57.89	3.84	2.202	1.093	b CN(75)
21	A'	1184(vw)	–	985	17.56	1.91	2.299	2.664	1107	23.21	8.96	2.628	2.891	b CH(72)
22	A'	1151(vw)	1154(w)	952	195.81	0.13	2.666	3.562	1026	86.95	7.94	3.355	3.901	R symd(70)
23	A'	1075(w)	–	905	101.76	8.04	1.147	6.072	986	37.19	0.25	3.545	2.603	Rt rigd(69)
24	A'	–	1067(w)	855	16.47	1.06	0.828	2.395	984	21.78	4.74	2.596	2.875	R bend 1(71)
25	A'	1049(w)	–	803	55.03	4.53	2.284	8.335	896	260.39	5.55	2.977	3.575	R bend 2(70)
26	A'	–	1043(w)	720	26.81	2.16	3.938	1.957	779	5.43	0.94	1.106	6.028	R asymd(78)
27	A'	–	1030(w)	694	15.18	0.75	0.605	1.859	769	9.75	1.38	1.385	2.356	NH_2 rocking(65)
28	A"	873(w)	–	668	222.51	5.59	0.937	1.096	722	28.33	0.28	1.097	4.172	tR symd(63)
29	A"	760(w)	–	613	0.26	1.95	1.342	1.091	658	0.93	0.19	1.539	1.773	tR asymd(64)
30	A"	–	724(w)	566	5.89	0.36	0.451	1.811	603	6.17	1.25	0.506	2.283	tR trigd(62)
31	A"	–	651(w)	531	25.37	0.11	1.382	3.793	570	12.95	0.32	1.596	3.605	tR bend 1(63)
32	A"	613(w)	615(w)	516	3.75	24.34	0.307	1.886	555	6.69	5.85	0.604	1.473	tR bend

													2(64)
33	A"	600(w)	–	505	5.12	0.33	0.279	1.449	537	3.62	0.75	0.234	1.917	ω CH(61)
34	A"	561(w)	–	494	8.16	2.38	0.197	4.278	525	47.76	2.95	0.206	8.327	ω CH(60)
35	A"	544(w)	–	293	8.13	0.13	0.244	8.153	315	4.82	0.32	0.329	3.331	ω NH(62)
36	A"	–	538(w)	291	5.08	0.17	0.198	1.404	314	3.37	0.36	0.219	1.375	NH_2 wagging(59)
37	A"	432(w)	–	235	13.63	9.41	0.043	1.104	246	34.82	2.37	0.049	1.105	ω CN(60)
38	A"	354(w)	–	202	5.47	5.25	0.155	1.082	217	3.71	2.57	0.159	1.083	NH_2 twisting(59)
39	A"	129(w)	–	154	3.51	0.11	0.054	1.046	174	3.07	0.99	0.063	1.047	Butterfly(58)

2.3. Synthesis of 1- and 2-aryl-pyrazolo[4,3-d]pyrimidine 2, 1- and 2-aryl-pyrazolo[3,4-d]pyrimidine

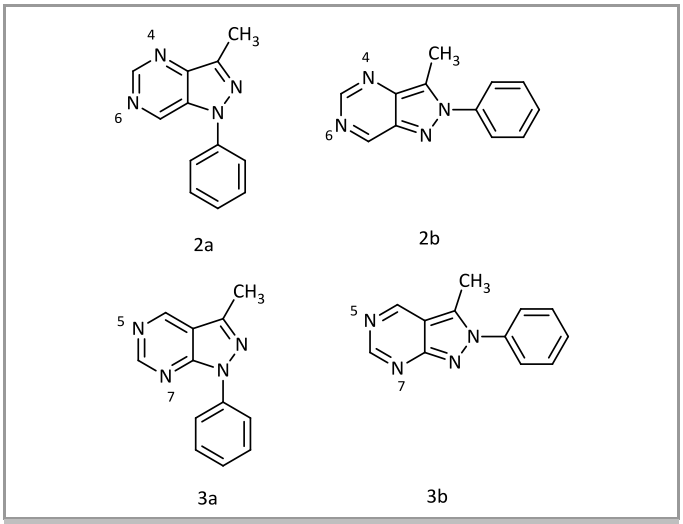

Scheme 2. pyrazolo[3,4-*d*]pyrimidine derivatives

2.3.1. Computational details

The system uses the B3LYP /6-31G (d) [35] computational level. Relatively the calculations, the molecules with minimum energy where λ is the number of negative eigenvalues of the Hessian matrix for a given stationary point) on the Potential Energy Surface.

It was found, that the Relative energies (kJ/mol) of isomers, classified by families (without aza, monoaza, diaza and triaza). Relative energy minima in bold (the compounds of only an isomer calculated have no reltive energy value). The negative values of the last column mean that **a** are more stable than **b**.

Table 11. Relative energy of isomers (Kj/mol)

Compound	Isomer a	Isomer b	a vs. B
2 (diaza-4,6)	21.5	1.9	-22.3
3 (diaza-5,7)	0.0	0.0	-41.8

The geometries of compounds in the solid state it is useful to use theoretical calculations in the gas phase. This allows to have a complete set of related structures and to differentiate the intrinsic effects from crystal field ones [52-55].

None the less , from the present survey, several conclusions can be drawn: **i)** N internal angles are more reliable than NC distances for structural characterization; **ii)** 1- and 2-aryl series form two separated sets; **iii)** a rationale has been found for the N-aryl torsion angles [56].

2.4. Synthesis of 4-Alkylidenehydrazino-1H-pyrazolo[3,4-d]pyrimidines and arylmethylidene hydrazino-1H-pyrazolo[3,4-d]pyrimidines

4-Alkylidenehydrazino-1*H*-pyrazolo[3,4-*d*]pyrimidines, 4-arylmethylidenehydrazino-1*H*-pyrazolo[3,4-*d*]-pyrimidines, and 2-substituted 7H-pyrazolo[4,3-e]-1,2,4-triazolo-[1,5-*c*]-pyrimidines as potential xanthine oxidase inhibitors were docked into the active site of the bovine milk xanthine dehydrogenase using two scoring functions involved in the CACHe 6.1.10 and Auto Dock 3.05.

Through the docking investigation into the active site of XDH (PDB codes it was obtained Structures of different bicyclic pyrazolo pyrimidines **4–6** and tricyclic Pyrazolo triazolo pyrimidines **7a–s.**

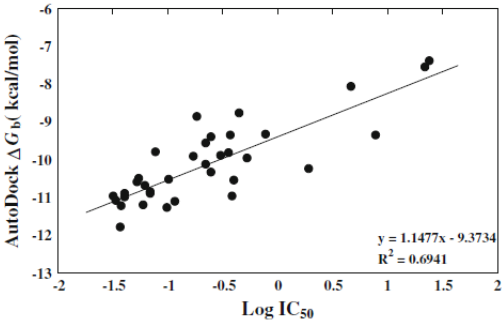

Figure 3. Correlation feature between the AutoDock binding free energy (ΔGb) and log IC50 of **allopurinol**, **oxipurinol**, **6b**, **e–k**, **m–r**, and **7a–s** docked against XDH (1n5x)".

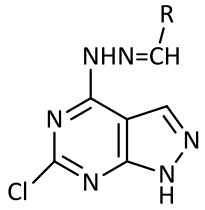

4a-g

4-aldhydehydrazones of 6-chloropyrazolo[4,3-d]pyrimidines

4,5 a: R = n-C_7H_{15}
b: R = Ph
c: R = 4-F-C_6H_4
d: R = 4-Cl-C_6H_4
e: R = 4-Me-C_6H_4
f: R = 4-MeO-C_6H_4
g: R = 4-O_2N-C_6H_4

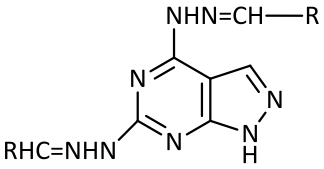

5a-g

4,6-Bis-aldehydehdrazones of pyrazolo[4,3-d]pyrimidines

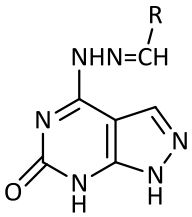

6a-s

4-Alkylidenehydrazino- and 4-arylmethylidenehydrazino-1H-pyrazolo[4,3-d]pyrimidin-6(7H)-ones

6,7 a: R = H
b: R = Me
c: R = Et
d: R = n-Bu
e: R = n-C_7H_{15}
f: R = CH_2=CH-$(CH_2)_8$
g: R = Ph
h: R = 4-F-C_6H_4
i: R = 2-Cl-C_6H_4
j: R = 3-Cl-C_6H_4
k: R = 4-Cl-C_6H_4
l: R = 4-Br-C_6H_4
m: R = 4-Me-C_6H_4
n: R = 4-MeO-C_6H_4
o: R = 3,4-OCH_2O-C_6H_3
p: R = 4-HOOC-C_6H_4
q: R = 4-HO-C_6H_4
r: R = 4-O_2N-C_6H_4
s: R = 3-O_2N-4-HO-C_6H_4

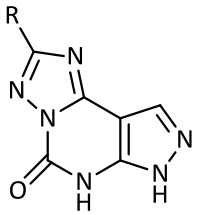

7a-s

7H-pyrazolo[4,3-e]1,2,4-triazolo [1,5-c]pyrimidin-5(6H)-one

Scheme 3. Structure of pyrazolo[3,4-*d*]pyrimidine derivatives

Table 12. The best docking results based on the binding free energies (ΔG_b) of the compounds docked against XDH (PDB code: 1n5x), the distance and angle of hydrogen bonds between compounds and amino acid residues involved in XDH, and RMSD from the crystallized TEI- 6720 ligand [57].

Compound	IC_{50} (μM)[a]	ΔG_b (kcal/mol)[b]	Hydrogen bonds between atoms of compounds and amino acids				RMSD (A°)[d]
			Atom of compound	Amino acid	Distance (A°)	Angle (°)	
Allopurinol	24.3	-7.39	N_8–N	HN of Thr 1010	2.05	167.0	5.55
			C_6–OH	OE2 of Glu 802	2.17	155.5	
Oxipurinol	22.1	-7.54	C_2–Oxo	HO of Ser 876	2.31	146.7	3.93
			C_6–Oxo	HN of Thr 1010	2.06	135.4	
			C_6–Oxo	Hn(HH22) of Arg 880	1.76	162.8	
6a	–[d]	-7.72	C_6–Oxo	HN of Thr 1010	2.08	136.6	5.05

			C_6–Oxo	HN(HH22) of Arg 880	1.87	151.3	
6b	4.670	-8.07	N_7–H	OH of Thr 1010	2.19	138.9	3.90
			C_6–Oxo	HN(HH22) of Arg 880	1.71	146.1	
6c	–	-8.53	C_6–Oxo	HN(HH22) of Arg 880	1.72	141.5	4.38
6d	–	-9.23	N_2–N	HE of Arg 880	1.99	138.0	4.86
			N_2–N	HH22 of Arg 880	1.72	145.8	
6f	7.894	-9.34	C_6–Oxo	HN of Ala 1079	2.21	164.6	2.14
6g	0.305	-9.88	N_2–N	HN(HE) of Arg 880	2.27	135.9	4.83
			N_2–N	HN(HH22) of Arg 880	1.67	159.1	
			N_1–H	OH of Thr 1010	1.84	147.2	
6h	0.373	-9.35	N_2–N	HN Ala 1079	2.07	145.9	2.86
			C_4–NH	OE1 of Glu 802	1.86	136.1	
			C_6–Oxo	HN(HH22) of Arg 880	2.03	157.7	
			C_6–Oxo	HN of Thr 1010	1.90	141.1	
6i	0.077	-9.79	C_6–Oxo	HN of Thr 1010	2.05	137.3	3.08
			C_6–Oxo	HN(HH22) of Arg 880	1.87	153.8	
			N_2–N	HN of Ala 1079	2.19	148.8	
6j	0.223	-9.35	N_2–N	HN Ala 1079	2.27	147.5	3.10
			C_6–Oxo	HN(HH22) of Arg 880	1.83	150.8	
6k	0.224	-9.55	N_2–N	HN Ala 1079	2.22	143.4	2.93
			C_6–Oxo	HN(HH22) of Arg 880	2.06	155.3	
			C_6–Oxo	HN of Thr 1010	1.92	141.5	
6l[e]	>10	-10.39	C_6–Oxo	HN of Thr 1010	1.94	138.4	3.09
			C_6–Oxo	HN(HH22) of Arg 880	1.91	162.1	
			C_1–N	HN of Ala 1079	2.26	147.0	
6m	0.247	-10.34	C_6–Oxo	HN of Thr 1010	1.96	140.0	2.95
			C_6–Oxo	HN(HH22) of Arg 880	1.96	158.9	
			C_4–NH	OE1 of Glu 802	1.74	137.7	
			N_2–N	HN of Ala 1079	2.24	146.4	
6n	0.172	-9.91	C_6–Oxo	HN of Thr 1010	2.03	162.6	2.94

			C_6–Oxo	HN(HH22) of Arg 880	2.05	154.7	
6o	0.385	-10.96	C_6–Oxo	HN of Thr 1010	2.08	143.0	3.04
			C_6–Oxo	HN(HH22) of Arg 880	2.07	152.8	
			N_2–N	HN of Ala 1079	1.97	144.6	
6p	0.399	-10.55	p–COO	HN(HZ1) of Lys 771	1.99	145.2	2.14
			C_6–Oxo	HN(HH22) of Arg 880	1.92	171.0	
			N_2–N	HN of Ala 1079	2.23	152.6	
6q	0.359	-9.81	C_6–Oxo	HN of Thr 1010	2.07	143.4	2.82
			C_6–Oxo	HN(HH22) of Arg 880	2.13	150.8	
6r	1.925	−10.23	*p*–N=O	HN(HE) of Arg 880	2.14	137.5	1.21
			p–N=O	HN(HH22) of Arg 880	2.49	139.1	
			p–N=O	HN of Thr 1010	1.71	155.1	
			p–N^+–O^-	HN(HH22) of Arg 880			
6s	–	−11.85	C_6–Oxo	HN of Thr 1010	1.88	143.2	2.16
			C_6–Oxo	HN(HH22) of Arg 880	2.12	156.3	
			N_2–N	HN of Ala 1079	2.07	143.1	
7a	0.184	−8.86	C_5–Oxo	HH22 of Arg 880	1.85	158.2	5.59
7b	0.250	−9.40	C_5–Oxo C_5–Oxo	HN of Thr 1010	1.96	138.2	5.35
				HN(HH22) of Arg 880	1.90	158.6	
7c	0.782	−9.33	C_5–Oxo	HN(HH22) of Arg 880	1.77	153.5	4.82
			N_8–N	HN of Ala 1079	2.24	147.0	
7d	0.529	−10.15	C_5–Oxo	HN(HH22) of Arg	1.83	138.2	4.32
			N_6–H	OH of Thr 1010	1.85	149.9	
7e	0.069	−10.84	C_5–Oxo	HN(HH22) of Arg 880	1.67	152.3	3.49
			N_8–N	HN of Ala 1079	2.33	146.7	
7f	0.117	−11.11	C_5–Oxo	HN(HH22) of Arg 880	1.87	136.2	2.27
			N_8–N	HN of Ala 1079	1.93	145.8	
7g	0.103	−10.53	C_5–Oxo	HN of Thr 1010	1.95	139.8	3.92
			C_5–Oxo	HN(HH22) of Arg 880	1.95	159.9	
			N_8–N	HN of Ala 1079	2.44	146.4	

7h	0.062	−10.68	C_5–Oxo	HN of Thr 1010	1.96	142.9	3.58
			C_5–Oxo	HN(HH22) of Arg 880	2.06	158.4	
7i	0.070	−10.90	C_5–Oxo	HN of Thr 1010	1.95	140.7	3.75
			C_5–Oxo	HN(HH22) of Arg 880	1.98	160.8	
7j	0.038	−11.21	C_5–Oxo	HN of Thr 1010	1.94	142.5	3.62
			C_5–Oxo	HN(HH22) of Arg 880	2.05	158.6	
7k	0.032	−10.97	C_5–Oxo	HN of Thr 1010	1.99	142.1	3.54
			C_5–Oxo	HN(HH22) of Arg 880	2.04	155.7	
7l	0.034	−11.08	C_5–Oxo	HN of Thr 1010	1.99	140.8	3.55
			C_5–Oxo	HN(HH22) of Arg 880	1.98	156.7	
			N_8–N	HN of Ala 1079	2.28	146.5	
7m	0.041	−10.98	C_5–Oxo	HN of Thr 1010	2.00	141.6	3.55
			C_5–Oxo	HN(HH22) of Arg 880	2.02	155.7	
			N_8–N	HN of Ala 1079	2.23	146.3	
7n	0.053	−10.60	C_5–Oxo	HN of Thr 1010	1.98	141.9	3.23
			C_5–Oxo	HN(HH22) of Arg 880	2.03	156.4	
			N_8–N	HN of Ala 1079	2.27	146.0	
7o	0.041	−10.89	C_5–Oxo	HN of Arg Thr 1010	1.97	144.1	2.88
			C_5–Oxo	HN(HH22) of Arg	2.03	157.3	
7q	0.055	−10.49	C_5–Oxo	HN of Arg Thr 1010	1.98	141.4	3.26
			C_5–Oxo	HN(HH22) of Arg 880	2.01	156.5	
			N_8–N	HN of Ala 1079	2.29	146.1	
7r	0.060	−11.19	C_5–Oxo	HN of Thr 1010	1.89	142.8	2.52
			C_5–Oxo	HN(HH22) of Arg 880	2.06	161.4	
			N_8–N	HN of Ala 1079	2.34	145.4	
7s	0.037	-11.78	N_5–H	OH of Thr 1010	1.75	140.7	1.30

[a] Through reference .
[b] Binding free energy.
[c] Root mean square deviation.
[d] Not determined.
[e] This value is inaccurate because of the insolubility in DMSO.

2.5. Pyrazolo[3,4-d]pyrimidines

Pyrazolo[3,4-*d*]pyrimidines have a class of naturally occurring fused uracils that appear diverse biological activities. Through each method, Docking results make obvious that Pyrazolo[3,4-*d*]pyrimidine molecules with trimethylene linker can bond to both anti-coagulation and enzymatic regions of Phospholipase A_2 (PLA_2) [16]. The pyrazolo[3,4-

d]pyrimidine molecules considered for docking studies are 1,3-bis(4,6-diethylthio-1*H*-pyrazolo[3,4-*d*]pyrimidin-1-yl)propane [58] **8**; 1,3-bis(4-ethoxy-6-methyl-sulfanyl-1*H*-pyrazolo[3,4-*d*] pyrimidin-1-yl)propane **9** [59]; 1,10-(1,3-propanediyl)bis(5-methyl-6-methylthio-4,5-Pyrazolo[3,4-*d*]pyrimidines as inhib-itor of viper Phospholipase A_2 421 dihydro-1*H*-pyrazolo[3,4-*d*]pyrimidin-4-one) **10** [60]; 1,10-(1,3-propanediyl)bis(5-ethyl-6-methylthio-4,5-dihydro-1*H*-pyrazolo[3,4-*d*]pyrimidin-4-one) **11** [61]; 1,10-(1,3- propanediyl)bis(5-benzyl-6-methylsulfanyl-4,5-dihy-dro-1*H*-pyrazolo[3,4-*d*]pyrimidin-4-one) **12** [62]; 1-(4,6-dimethylsulfanyl-1*H*-pyrazolo[3,4-*d*]pyrimidin-1-yl)-3-(5-methyl-6-methylsulfanyl-4-oxo-1,5-dihydropyra-zolo[3,4-*d*]pyrimidin-1-yl)prop-ane **13** [63]; 4,6-bis(methylsulfanyl)-1-phthalimidopropyl-1*H*-pyrazo-lo[3,4-*d*]-pyrimidine **14** [64]; 6-methylsulfanyl-1-phthalimidopropyl-4(pyrrolidin-1-yl)-1H-pyrazolo-[3,4-*d*]pyrimidine **15** [64]; and 6-methylsulfanyl-1-(3-phenylpropyl)-4,5-dihydro-1*H*-pyrazolo[3,4-*d*]pyrimidine-4-one **16** [65].

2.5.1. Computational details

The Conformational search and docking studies using AUTODOCK4.2 show that electronic interaction has an important role in ligand–channel interaction. Table 13 show the result. For the best degree of the docked poses, with comparable to the indomethacin binding to PLA_2, molecules **8**, **9**, **11** and **13** have poor binding energies., molecule **15** has the comparable energy while molecules **10**, **12**, **14** and **16** have better bound energy values.

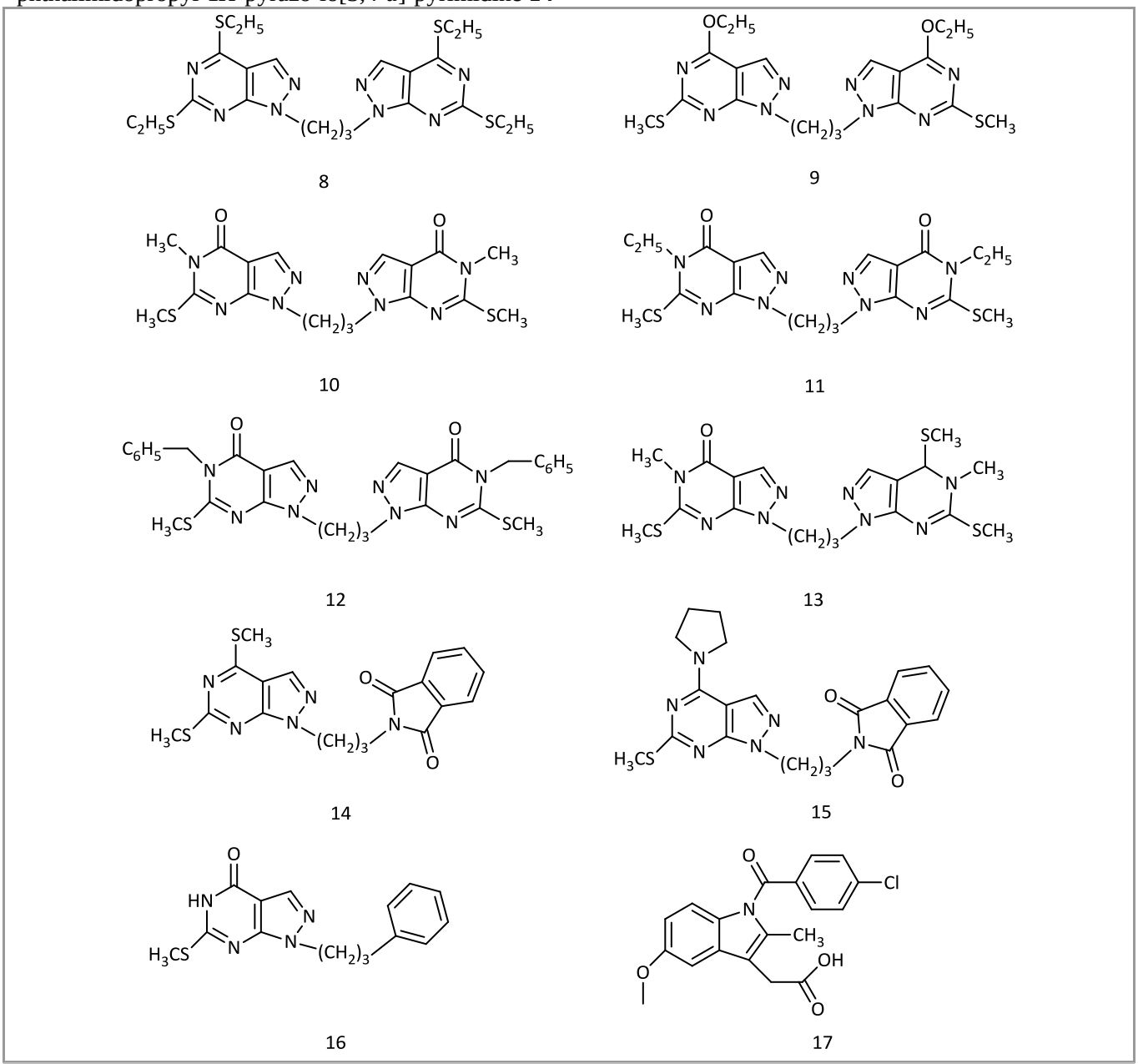

Scheme 4. Chemical diagram of ligands (molecules 8–16 and IMN)".

Table 13. Inhibition coefficient (KI) and different energy values of the ligands as obtained through the docking with 3H1X using AUTODOCK4.2.

Molecules	Rank	Kl (μM)	Intramolecular energy (kcal/mol)	Internal energy (kcal/mol)	Torsional energy (kcal/mol)	Binding Energy (kcal/mol)
8	1-1	74.69	−9.21	0.19	3.58	−5.63
	2-1	131.66	−8.87	−0.83	3.58	−5.29
	3-1	160.42	−8.76	−0.55	3.58	−5.18
	3-2	388.60	−8.23	−0.60	3.58	−4.65
	4-1	249.63	−8.49	−0.80	3.58	−4.91
9	1-1	290.50	−7.80	−0.59	2.98	−4.83
	2-1	295.25	−7.80	−0.23	2.98	−4.82
	3-1	368.95	−7.67	−0.35	2.98	−4.68
	3-2	375.14	−7.66	−0.66	2.98	−4.67
	4-1	504.85	−7.48	−0.70	2.98	−4.50
10	1-1	9.21	−8.66	−0.12	1.79	−6.87
	1-2	10.95	−8.56	−0.14	1.79	−6.77
	1-3	20.45	−8.19	−0.20	1.79	−6.40
	2-1	10.76	−8.57	0.30	1.79	−6.78
	2-2	32.88	−7.91	−0.25	1.79	−6.12
11	1-1	91.64	−7.90	−0.50	2.39	−5.51
	2-1	115.41	−7.76	−0.54	2.39	−5.37
	2-2	178.43	−7.50	−0.25	2.39	−5.11
	3-1	233.02	−7.34	−0.49	2.39	−4.96
	4-1	282.48	−7.23	−0.73	2.39	−4.84
12	1-1	18.62	−9.44	−0.74	2.98	−6.45
	2-1	34.87	−9.06	−1.44	2.98	−6.08
	3-1	79.36	−8.58	−1.11	2.98	−5.59
	4-1	84.09	−8.54	−1.29	2.98	−5.56
	5-1	142.00	−8.23	−1.11	2.98	−5.25
13	1-1	81.41	−7.67	−0.18	2.09	−5.58
	2-1	333.24	−6.83	−0.88	2.09	−4.74
	3-1	349.47	−6.80	−0.61	2.09	−4.72
	4-1	456.35	−6.65	−0.16	2.09	−4.56
	5-1	480.47	−6.62	−0.60	2.09	−4.53
14	1-1	8.56	−8.70	−0.29	1.79	−6.91
	1-2	11.47	−8.53	−0.31	1.79	−6.74
	1-3	13.87	−8.42	−0.15	1.79	−6.63
	2-1	69.00	−7.47	−0.38	1.79	−5.68
	3-1	74.44	−7.42	−1.23	1.79	−5.63
15	1-1	27.26	−8.02	−0.63	1.79	−6.23
	1-2	38.61	−7.81	−0.82	1.79	−6.02
	2-1	118.32	−7.15	−1.50	1.79	−5.36
	3-1	128.14	−7.10	−1.36	1.79	−5.31
	4-1	171.61	−6.93	−1.29	1.79	−5.14

16	1-1	13.88	−8.12	−0.6	1.49	−6.63
	2-1	45.30	−7.42	−0.32	1.49	−5.93
	2-2	58.17	−7.27	−0.32	1.49	−5.78
	3-1	51.53	−7.34	−0.51	1.49	−5.85
	3-2	58.36	−7.27	−0.48	1.49	−5.78
IMN	1-1	22.90	−7.52	−0.66	1.19	−6.33
	2-1	24.65	−7.48	−0.70	1.19	−6.29
	2-2	27.00	−7.43	−0.68	1.19	−6.23
	3-1	27.26	−7.42	−0.66	1.19	−6.23
	3-2	32.31	−7.32	−0.69	1.19	−6.13

Table 14. Glide scores and average electrostatic (coul), van der Waals (vdw), site energy (site) and Glide energy obtained through Glide SP docking.

Molecules (SP)	**Entry ID**	**Glide score**	**E_{coul} (kcal/mol)**	**E_{vdw} (kcal/mol)**	**E_{site} (kcal/mol)**	**Glide energy (kcal/mol)**
8	32	−5.565	−3.270	−48.226	−0.157	−51.496
	40	−5.367	−0.968	−49.591	−0.167	−50.559
	44	−5.307	−2.830	−48.543	−0.185	−51.372
	47	−5.247	−2.134	−49.201	−0.180	−51.335
	56	−5.187	−1.967	−48.731	−0.183	−50.698
9	69	−4.856	−2.183	−43.014	−0.163	−45.197
	76	−4.791	−3.310	−42.334	−0.193	−45.644
	86	−4.694	−2.842	−42.245	−0.204	−45.087
	93	−4.565	−3.323	−44.350	−0.142	−47.673
	110	−4.073	−4.202	−43.388	−0.170	−47.589
10	8	−6.417	−4.752	−48.490	−0.017	−53.243
	13	−5.887	−5.426	−47.934	−0.111	−53.360
	14	−5.884	−5.442	−47.828	−0.017	−53.270
	24	−5.787	−5.894	−43.697	−0.091	−49.592
	25	−5.757	−5.637	−44.583	−0.090	−50.221
11	2	−6.705	−4.248	−50.535	−0.010	−54.783
	3	−6.688	−4.189	−50.629	−0.010	−54.819
	4	−6.668	−4.200	−50.783	−0.012	−54.983
	5	−6.493	−4.304	−50.249	−0.010	−54.554
	6	−6.435	−0.814	−52.373	0.0000	−53.187
12	89	−4.636	−2.338	−46.642	0.000	−48.980
	100	−4.318	−7.057	−42.092	−0.042	−49.149
	102	−4.283	−2.417	−43.022	−0.046	−45.439
	103	−4.273	−3.476	−42.849	−0.002	−46.325
	105	−4.216	−6.989	−39.835	−0.045	−46.823
13	7	−6.433	−1.882	−52.926	0.0000	−54.809
	36	−5.429	−3.008	−43.402	−0.162	−46.410
	37	−5.420	−2.630	−43.489	−0.173	−46.119
	38	−5.392	−2.871	−43.764	−0.177	−46.635

	42	−5.380	−3.307	−41.347	−0.168	−44.655
14	17	−5.822	−3.086	−44.766	−0.018	−47.852
	19	−5.818	−2.983	−45.060	−0.018	−48.043
	20	−5.817	−2.871	−45.000	−0.017	−47.872
	21	−5.815	−2.970	−45.107	−0.018	−48.077
	22	−5.812	−2.854	−45.048	−0.017	−47.902
15	15	−5.866	−2.921	−46.758	−0.017	−49.679
	34	−5.489	−1.316	−44.899	−0.043	−46.215
	92	−4.591	−0.780	−41.055	−0.029	−41.836
	94	−4.543	−1.039	−41.186	−0.045	−42.225
	97	−4.396	−0.641	−40.911	−0.032	−41.553
16	71	−4.828	−3.552	−31.002	0.000	−34.554
	74	−4.819	−3.611	−30.910	0.000	−34.521
	75	−4.809	−3.538	−30.922	0.000	−34.460
	77	−4.786	−3.340	−31.093	0.000	−34.432
	78	−4.776	−3.606	−30.638	0.000	−34.244
IMN	84	−4.709	−8.409	−24.405	−0.087	−32.814
	87	−4.672	−8.357	−24.488	−0.088	−32.846
	111	−4.064	−6.586	−21.505	−0.100	−28.091
	121	−3.243	−5.559	−23.459	−0.100	−29.018

In Table 14, the results of Glide docking in Standard Precision mode are summarized. Docking of Pyrazolo[3, 4-*d*]pyrimidine ligands and IMN appeared a great variation in their binding energy.

From Autodock calculations, it was noted that molecules **10, 12, 14** and **16** have better binding capabilities and minimum inhibitory concentrations than indomethacin. almost all the Pyrazolo[3,4-*d*]pyrimidine molecules have better binding energies than indomethacin by obtaining Docking simulations through Standard Precision and Extra Precision protocols of Glide [16].

2.6. Synthesis of pyrazolo[3,4-d]pyrimidine derivatives

By using the density functional B3LYP/6-31G** and dispersion corrected density functional DFT-D/B97D methods, the conformational stabilities and computations of optimized geometrical parameters of 1,3-bis(4,6-diethylthio-1*H*-pyrazolo[3,4-*d*]pyrimidin-1-yl)propane **18**; 1,3-bis(4-ethoxy-6-methylsulfanyl-1*H*-pyrazolo[3,4-*d*]pyrimidin-1-yl)propane **19**; 4,6-bis(methylsulfanyl)-1-phthalimidopropyl-1*H*-pyrazolo[3,4-*d*]pyrimidine **20** and 6-methylsulfanyl-1-phthalimidopropyl-4(pyrollidin-1-yl)-1*H*-pyrazolo[3,4-*d*]pyrimidine **21** molecules have been detected.

Geometries at the minimum energies were fully optimized without any constraints. Since B3LYP method does not include the dispersion term, M06-2X/6-311++G** method is used to define the energies of the B3LYP optimized geometries, which is known to better convenient for non-covalent interactions.

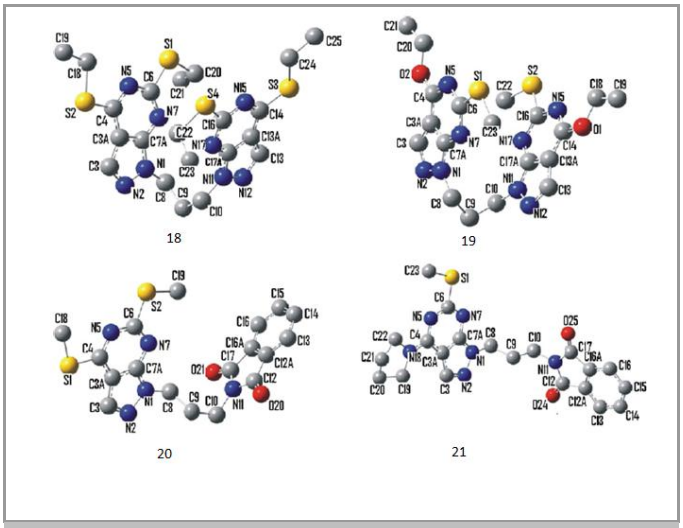

Figure 4. Chemical Structures with atomic numbering scheme of molecules **18**, **19**, **20** and **21**. (Hydrogen atoms have been omitted for clarity. Torsion angles chosen for conformational variations are N1-C8-C9-C10 (τ_1) and C8-C9-C10-N11 (τ_2).

2.6.1. Computational details

Figures (5,6) show molecular structures function of lowest energy conformation of all the four studied compounds and this conformation is a folded one donating ample scope for arene–arene (aromatic Π–Π) interactions.

Table 15a. Total energies (E), relative energies (ΔE) and torsion angles (τ_1, τ_2) corresponding to different conformations of molecule **18**. The crystallographic value of torsion angles are (-52.26, -52.26°).

Conf. (mol.18)	E (Hartree)			ΔE (kcal/mol)			τ_1		τ_2	
	B3LYP	M06-2X	B97D	B3LYP	M06-2X	B97D	B3LYP/M06-2X	B97D	B3LYP/M06-2X	B97D
I	-2847.8947	-2847.67026	-2847.0021	0.02	4.78	7.26	66.6	62.0	176.9	186.2
II	-2847.8946	-2847.67008	-2847.0020	0.04	4.89	7.29	177.3	-173.1	67.7	61.7
III	-2847.8935	-2847.66981	-2846.9958	0.73	5.06	11.18	-179.5	-172.7	-65.7	-60.1
IV	-2847.8935	-2847.66968	-2846.9958	0.75	5.14	11.15	-66.6	-61.4	179.4	186.4
V	-2847.8947	-2847.67787	-2847.0136	0.00	0.00	0.00	-56.7	-49.4	-56.5	-49.5

Table 15b. Total energies (E), relative energies (ΔE) and torsion angles (τ_1, τ_2) corresponding to different conformations of molecule **19**. The crystallographic value of torsion angles is (47.9°, 54.2°).

Conf. (mol.19)	E (Hartree)			ΔE (kcal/mol)			τ_1		τ_2	
	B3LYP	M06-2X	B97D	B3LYP	M06-2X	B97D	B3LYP/M06-2X	B97D	B3LYP/M06-2X	B97D
I	-2123.3325	-2123.13605	-2122.4071	21.13	5.49	11.63	66.0	56.3	179.8	166.5
II	-2123.3325	-2123.13610	-2122.4071	21.13	5.45	11.63	179.7	167.2	66.0	57.0
III	-2123.3662	-2123.13637	-2122.4116	0.00	6.97	8.75	183.3	171.9	-66.9	-63.2
IV	-2123.3662	-2123.13635	-2122.4117	0.00	5.29	8.73	-66.9	-62.6	-176.5	172.1
V	-2123.3335	-2123.14479	-2122.4256	20.51	0.00	0.00	54.0	49.1	54.4	48.6

Table 15c. Total energies (E), relative energies (ΔE) and torsion angles (τ_1, τ_2) corresponding to different conformations of molecule **20**.The crystallographic value of torsion angles are (167.3°, 69.8°).

Conf. (mol. 20)	E (Hartree)			ΔE (kcal/mol)			τ_1		τ_2	
	B3LYP	M06-2X	B97D	B3LYP	M06-2X	B97D	B3LYP/M06-2X	B97D	B3LYP/M06-2X	B97D
I	-1916.7796	-1916.62037	-1915.9895	0.08	0.58	8.82	67.1	62.4	177.2	-174.7
II	-1916.7801	-1916.62129	-1915.9936	0.00	0.00	6.27	177.0	-162.8	66.6	68.4
III	-1916.7795	-1916.62078	-1916.0036	0.17	0.27	0.00	179.4	55.3	-66.9	-80.3
IV	-1916.7793	-1916.62104	-1915.9901	0.28	0.16	8.45	-64.8	-61.9	-176.9	-175.7
V	-1916.7797	-1916.62118	-1916.0007	0.01	0.07	1.84	-57.9	-49.1	-58.4	-49.5

Table 15d. Total energies (E), relative energies (ΔE) and torsion angles (τ_1, τ_2) corresponding to different conformations of molecule **21**. The crystallographic value of torsion angles are (67.3°, 169.3°).

Conf. (mol.21)	E (Hartree)			ΔE (kcal/mol)			τ_1		τ_2	
	B3LYP	M06-2X	B97D	B3LYP	M06-2X	B97D	B3LYP/M06-2X	B97D	B3LYP/M06-2X	B97D
I	-1690.6875	-1690.50018	-1689.7786	15.50	1.08	6.92	67.2	63.3	178.9	184.9
II	-1690.6873	-1690.50047	-1689.7808	15.63	0.90	5.56	177.3	-147.3	65.9	68.6
III	-1690.6868	-1690.50004	-1689.7779	15.90	1.17	7.38	177.7	179.3	-68.5	-64.5
IV	-1690.6873	-1690.50081	-1689.7790	15.65	0.68	6.66	-65.8	-62.8	178.3	179.8
V	-1690.7122	-1690.50190	-1689.7897	0.00	0.00	0.00	-64.8	-70.1	75.6	65.5

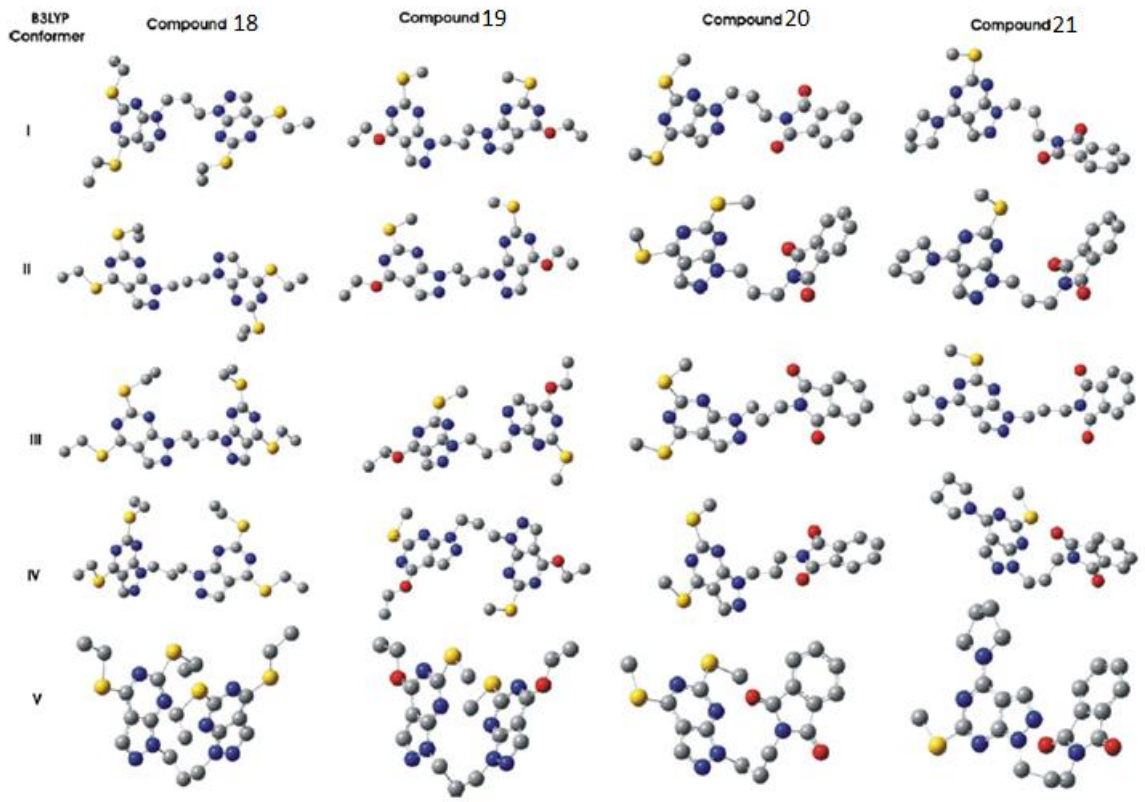

Figure 5. Different conformers of the molecules obtained from B3LYP/6-31G** method.

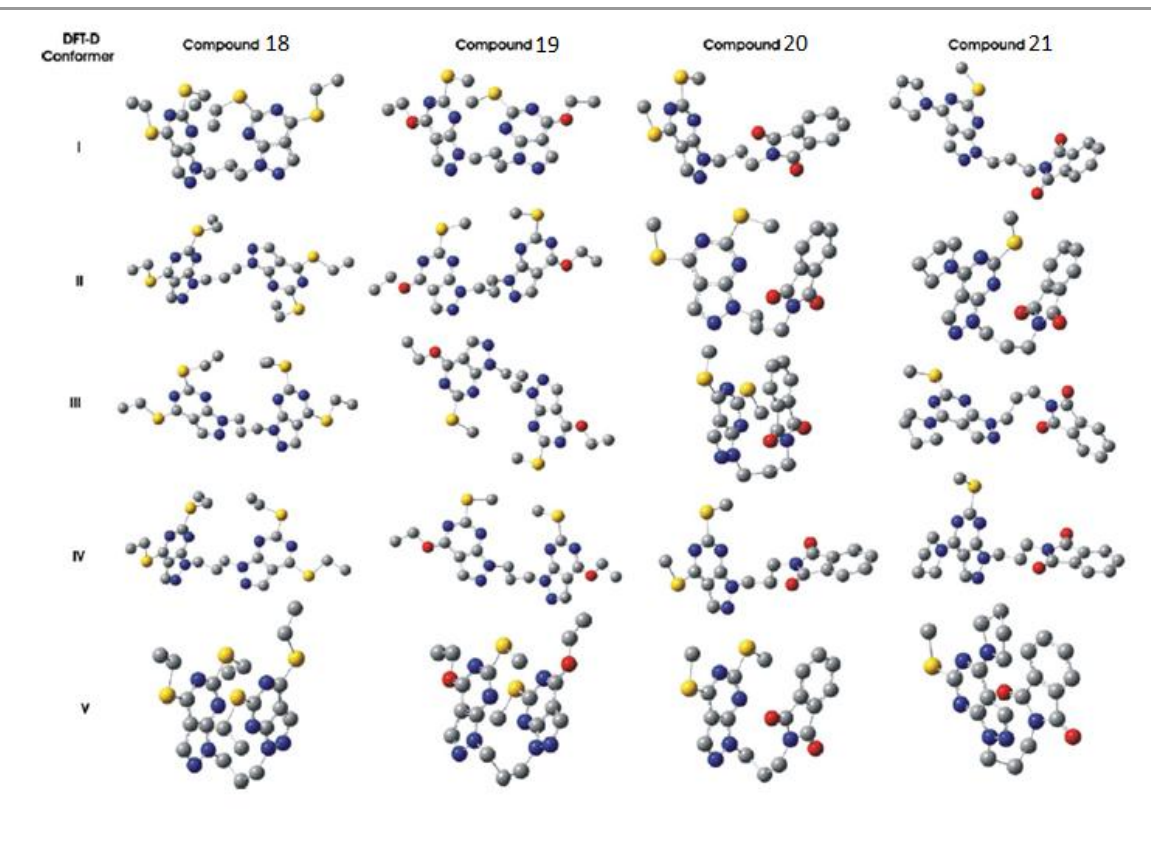

Figure 6. Different conformers of the molecules obtained from DFT-D/B97D method.

Table 16. Comparison of crystallographic and theoretical values (obtained from B3LYP and B97D methods) of some selected torsion angles of molecule **21** in different conformers

Torsions	Conformers										
	Cyst. Values	B3LYP					B97D				
		I	II	III	IV	V	I	II	III	IV	V
N1-C8-C9-C10 (τ_1)	67.3(4)	67.2	177.3	177.7	-65.8	-64.8	63.3	-147.3	179.2	-62.8	-70.1
C8-C9-C10-N11 (τ_2)	169.3(3)	178.9	65.9	-68.5	178.3	75.6	184.9	68.6	-64.5	179.8	65.5
N5-C4-N18-C19	176.1(3)	177.2	175.8	176.3	176.9	177.6	177.6	176.6	176.9	177.3	176.2
C4-N18-C19-C20	-165.7(4)	-170.2	-168.2	-168.7	-169.5	-170.3	-170.1	-169.0	-169.4	-169.4	-170.3
N18-C19-C20-C21	-13.5(6)	-29.1	-29.1	-29.2	-29.3	-29.0	-30.1	-29.9	-30.0	-30.3	-29.6
N5-C4-N18-C22	4.5(4)	-3.0	-2.4	-2.6	-3.0	-2.8	-3.2	-2.6	-2.9	-2.9	-4.1
C19-C20-C21-C22	15.5(7)	37.4	37.4	37.4	37.4	37.3	38.5	38.6	38.6	38.7	38.4
C20-C21-C22-N18	-10.7(6)	-30.9	-30.9	-30.8	-30.8	-30.8	-31.7	-31.9	-31.9	-31.7	-31.9
C21-C22-N18-C19	1.8(4)	13.2	13.1	13.0	12.9	13.1	13.4	13.8	13.7	13.3	13.9
C21-C22-N18-C4	174.3(3)	-166.7	-168.5	-167.9	-167.2	-166.5	-165.9	-166.9	-166.6	-166.5	-165.8
C22-N18-C19-C20	6.7(4)	10.1	10.1	10.3	10.4	10.1	10.6	10.2	10.4	10.8	9.9

Table 17. Substituions of pyrazolo[3,4-*d*]pyrimidine

Mol.N°	R1	R2	R3	Mol.N°	R1	R2	R3
22 a	Et			22 n	Et	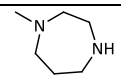	
22 b	Me			22 O	Et	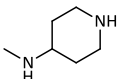	
22 c	Et			22 p	Et	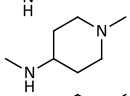	
22 d	Me		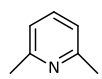	22 q	Et	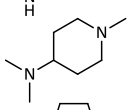	
22 e	Et		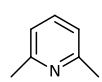	22 r	Et	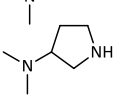	
22 f	Me		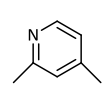	22 s	Me	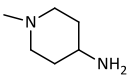	
22 g	Et		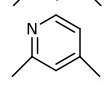	22 t	Et	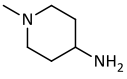	
22 h	Et		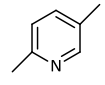	22 u	Me	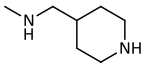	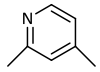
22 i	Et		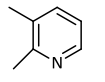	22 v	Me	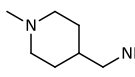	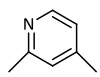
22 j	Me	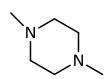		22 w	Me	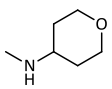	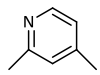
22 k	Et			22 x	Et		
22 l	Et			22 y	Et		
22 m	Et			22 z	Et		

Different theoretical strategies have exhibited that all the four pyrazolo[3,4-*d*]pyrimidine derivatives have five theoretically possible stable conformers of about equivalent energies.
For molecule, both theoretical methods B3LYP and B97D, utilized to examine the conformational preferences, do not agree consistently while distinguishing the global minimum.
The π-π interaction energy in the state of molecules **18** and **19** has values 4.78 kcal/mol and 5.49 kcal/mol respectively. In instances of molecules **20** and **21** all the conformers are practically broadened and have approximately same energy which indicates that intermolecular π-π interaction is missing in these particles [66].

2.7. Synthesis of 1-(2-ethoxyethyl)-1H-pyrazolo[4,3-d]pyrimidines

Phosphodiesterase V works as an appealing target for cardiovascular, Quantitative Structure–Activity Relationship (QSAR) consider as useful procedure for the optimization of structure necessities of twenty-six 1-(2-ethoxyethyl)-1*H*-pyrazolo[4,3-*d*]pyrimidines as phosphodiesterase V inhibitors.

2.7.1. The structural template of 1-(2-ethoxyethyl)-1H-pyrazolo[4,3-d]pyrimidine

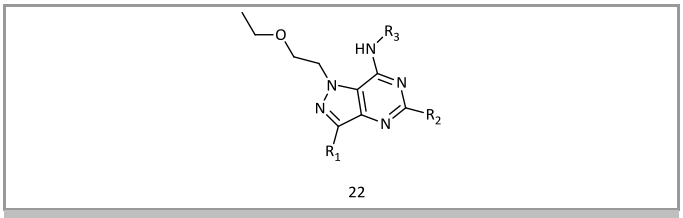

22

Scheme 5. 1-(2-ethoxyethyl)-1H-pyrazolo[4,3-*d*]pyrimidines structure

Various quantum chemical methods and quantum-chemistry calculations have been performed for studying the molecular structure and electronic 1-(2-ethoxyethyl)-1*H*-pyrazolo[4,3-*d*]pyrimidine derivate-ives properties [67,68]. The properties of biological Activity of organic compounds related to the geometry and additionally the nature of their molecular orbital, HOMO (highest occupied molecular orbital) and LUMO (lowest unoccupied molecular orbital).
In the next Table (Table 19), we summarized The Pearson correlation coefficients. The obtained matrix provides Information on the negative or positive correlation between variables.

Table 18. Values of the calculated parameters obtained by DFT/B3LYP 6-31G* optimization and ACD/ChemSketch program of the studied compounds.

N⁰	pIC$_{50}$	MW	MR (cm^3)	MV (cm^3)	Pc (cm^3)	n	α_e (dyne /cm)	D (g/ cm^3)	E$_T$ (ua)	E$_{Homo}$ (ev)	E$_{Lumo}$ (ev)	ΔE (ev)	μ (D)	E$_a$ (ev)	λ_{max} (nm)	f(so)
22 a	1,155	395,5	113,33	306,3	817,1	1,661	50,6	1,29	-34750	-5,096	-1,09	4,006	2,48	2,214	560,1	0,0139
22 b	0,398	382,46	107,17	278,8	759,7	1,694	55	1,37	-33052,9	-5,511	-1,58	3,935	2,53	3,499	354,4	0,0024
22 c	1,155	396,49	111,77	294,9	798,3	1,682	53,6	1,34	-35186,6	-5,007	-1,07	3,934	3,53	2,149	576,8	0,0134
22 d	0,187	396,49	111,59	294	790,8	1,683	52,3	1,34	-35194,8	-5,141	-1,24	3,903	3,86	3,072	403,6	0,0244
22 e	0,18	410,52	116,2	310,1	829,4	1,672	51,1	1,32	-36257,6	-5,195	-1,22	3,975	1,30	3,472	357,1	0,0006
22 f	-0,146	396,49	111,59	294	790,8	1,683	52,3	1,34	-35194,6	-5,189	-1,31	3,881	5,29	3,561	348,2	0,002
22 g	0,420	410,52	116,2	310,1	829,4	1,672	51,1	1,32	-36265,3	-5,202	-1,32	3,881	5,38	3,065	404,6	0,0216
22 h	-0,519	410,52	116,2	310,1	829,4	1,672	51,1	1,32	-36257,5	-5,182	-1,22	3,964	2,8	2,112	587,1	0,0156
22 i	-0,74	410,52	116,2	310,1	829,4	1,672	51,1	1,32	-36257,5	-5,005	-0,98	4,028	2,34	3,253	381,2	0,0694
22 j	-0,415	410,51	116,92	315,3	836,2	1,663	49,4	1,3	-36257,7	-5,004	-1,08	3,926	4,43	3,554	348,8	0,0021
22 k	0,051	424,54	121,52	331,3	874,8	1,654	48,5	1,28	-37328,2	-5,21	-1,25	3,957	1,89	2,761	449,1	0,0083
22 l	-0,398	424,54	120,62	325,2	860,5	1,663	48,9	1,30	-37328,4	-5,153	-1,21	3,942	1,40	3,494	354,8	0,0024
22 m	-0,079	424,54	120,62	325,2	860,5	1,663	48,9	1,30	-37328	-4,904	-0,96	3,939	4,73	3,549	349,3	0,006
22 n	0,119	424,54	120,81	326,1	868	1,662	50,1	1,30	-37328,1	-4,915	-1,09	3,825	4,01	3,406	364,0	0,0577
22 o	0,699	424,54	119,91	320	853,6	1,672	50,6	1,32	-37328,1	-5,213	-1,25	3,964	2,41	3,384	366,4	0,0611
22 p	0,143	438,57	125,23	341,3	899,1	1,654	48,1	1,28	-38398,6	-5,059	-1,05	4,013	4,44	3,221	384,9	0,0236
22 q	1,060	452,6	130,56	362,5	944,5	1,639	46	1,24	-39468,7	-4,900	-0,99	3,91	4,79	2,633	470,8	0,0055
22 r	0,377	424,54	120,62	325,2	860,5	1,663	48,9	1,30	-36257,9	-5,028	-1,09	3,94	5,6	3,737	331,8	0,0463
22 s	-0,362	410,52	115,06	302,1	816,8	1,686	53,3	1,35	-36257,9	-5,028	-1,09	3,94	5,6	3,452	359,2	0,0032

22 t	0,108	424,54	119,67	318,2	855,4	1,675	52,2	1,33	-37328,4	-5,008	-1,09	3,916	3,48	3,742	331,4	0,0754
22 u	0,456	424,54	119,91	320	853,6	1,672	50,6	1,32	-37328,1	-5,038	-1,07	3,97	4,77	3,326	372,8	0,0545
22 v	1,155	424,54	119,67	318,2	855,4	1,675	52,2	1,33	-37310,3	-4,846	-1,00	3,843	4,08	3,754	330,3	0,062
22 w	-0,079	411,5	113,63	305,8	814,4	1,665	50,3	1,34	-36798,6	-5,112	-1,12	3,996	3,55	4,051	306,1	0,0659
22 x	1,155	439,55	123,21	334,7	892,5	1,657	50,5	1,31	-38948	-5,092	-1,28	3,812	5,27	3,448	359,6	0,0635
22 y	1,097	452,55	125,13	331,5	899,7	1,679	54,2	1,36	-40414,7	-4,859	-0,92	3,939	5,85	1,932	641,7	0,0078
22 z	1,398	453,54	124,07	332	898,2	1,67	53,5	1,36	-40956,1	-5,079	-1,12	3,956	5,43	3,319	373,6	0,0197

Table 19. Correlation matrix (Pearson (n)) between different obtained descriptors:

	pIC_{50}	**MW**	**MR**	**MV**	**Pc**	**N**	**α_e**	**D**	**E_T**	**E_{HOMO}**	**E_{LUMO}**	**□E**	**μ**	**Ea**	**λmax**	**f(so)**
pIC_{50}	**1**															
MW	0,367	**1**														
MR	0,301	**0,962**	**1**													
MV	0,270	0,917	**0,984**	**1**												
Pc	0,344	**0,962**	**0,995**	**0,987**	**1**											
N	-0,096	-0,577	-0,720	-0,831	-0,746	**1**										
□	0,197	-0,360	-0,555	-0,674	-0,547	0,905	**1**									
D	0,059	-0,317	-0,547	-0,668	-0,551	0,898	**0,942**	**1**								
E_T	-0,374	**-0,974**	-0,897	-0,843	-0,904	0,496	0,246	0,194	**1**							
E_{HOMO}	0,192	0,546	0,563	0,532	0,556	-0,342	-0,235	-0,271	-0,540	**1**						
E_{LUMO}	0,088	0,504	0,523	0,503	0,515	-0,355	-0,273	-0,284	-0,501	0,928	**1**					
E	-0,273	-0,110	-0,104	-0,077	-0,107	-0,036	-0,098	-0,035	0,101	-0,189	0,191	**1**				
μ	0,292	0,392	0,306	0,245	0,298	0,007	0,097	0,134	-0,397	0,452	0,300	-0,400	**1**			
Ea	-0,311	-0,047	-0,085	-0,084	-0,115	0,047	-0,103	0,104	0,082	-0,092	-0,161	-0,180	0,053	**1**		
Λmax	0,317	0,046	0,061	0,051	0,091	0,001	0,161	-0,029	-0,087	0,134	0,204	0,184	-0,031	**-0,984**	**1**	
f(so)	0,070	0,169	0,126	0,110	0,125	-0,068	-0,026	0,045	-0,151	0,241	0,190	-0,132	0,021	0,400	-0,365	**1**

The Energy of activation **E_a** is negatively correlated with the maximum of absorption **λ_{max}** (r = -0.984 and p <0.05) at a significant level.

The Density **D** is correlated positively with the surface tension **α_e** (r =0.942 and p< 0.001) at a significant level. The analysis of projections is according to the planes F1–F2 and F1-F3 (59.53% and 58.28% of the total variance respectively) of the studied molecules [69].

2.8. Synthesis of 3-phenyl-1-tosyl-1H-pyrazolo[3,4-d]pyrimidin-4-amine

Using Hartree Fock (HF/6-31G**) and density functional theory (B3LYP/6-31G**) techniques to obtain the electronic structure calculations and vibrational assignments of a biologically important molecule namely, 3- phenyl-1-tosyl-1*H*-pyrazolo[3,4-*d*]pyrimidin-4-amine. The optimized geometrical parameters, molecular electrostatic potentials (MEP), and HOMO–LUMO gaps as acquired through the two techniques are analysed.

The optimized structure of 3-phenyl-1-tosyl-1*H*-pyrazolo[3,4-*d*]pyrimidin-4-amine, by an ab-initio (HF) and B3LYP (DFT) methods, in conjugation with

6-31G** basis set using Gaussian03, shown in the following Figure 9.

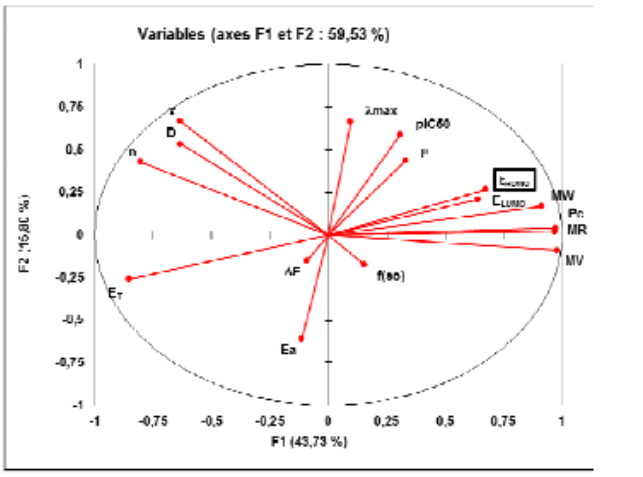

Figure 7. Correlation circle

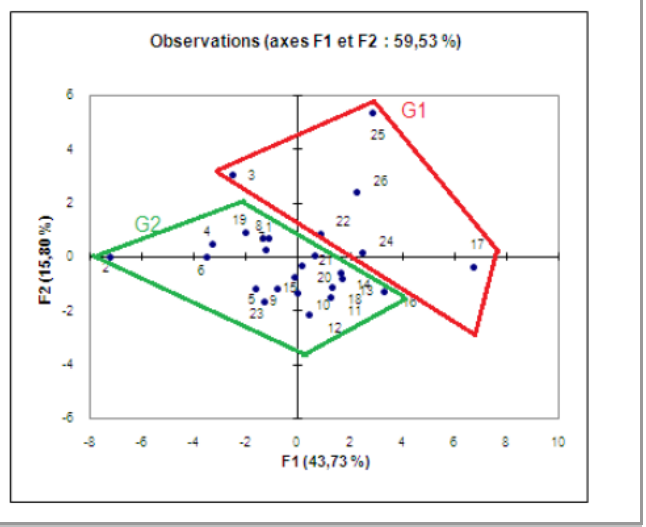

Figure 8. Cartesian diagram according to F1-F2.

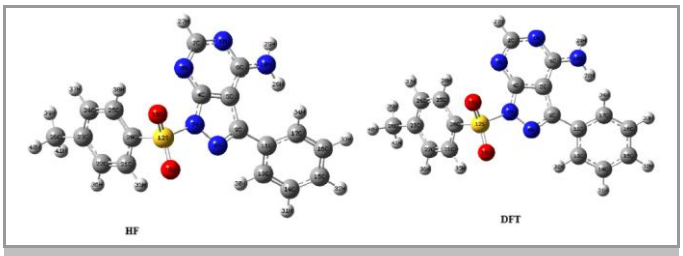

Figure 9. Optimized geometry of the 3-phenyl-1-tosyl-1*H*-pyrazolo[3,4-d]pyrimidine-4-amine at HF/6-31G** and B3LYP/6 – 31G** level".

2.8.1. Computational details

From two methods have been compared and are described in Table 20, Bond lengths and bond angles of the optimized structures as obtained.

Utilizing HF and DFT methods to detect Total and HOMO–LUMO energies of the 3-phenyl-1-tosyl-1*H*-pyrazolo [3,4-*d*]pyrimidin-4-amine. The HOMO and LUMO energies gap are 0.18837 a.u. by HF and0.17687 a.u. by DFT method, which is very small, and it indicates that 3-phenyl-1-tosyl-1*H*-pyrazolo [3,4-*d*]pyrimidin-4-amine is chemically highly reactive and biologically active for charge transfer intermolecular (Table 21).

On the premise of vibrational analysis at B3LYP/6-3G** and HF/6-31G** levels, various thermodynamic parameters are computed and are introduced in Table 22. We calculate the zero point vibrational energies (ZPVE), rotational constants, thermal energy, heat capacity and the entropy S_{vib} (T) to the degree of accuracy it is also clear from Table 22 that the rotational constant is directly proportional to rotational temperature. The rotational constant is inversely proportional to the moment of inertia of the molecule [70].

Theoretically computed vibrational (IR) frequencies of 3-phenyl-1-tosyl-1*H*-pyrazolo[3,4-*d*]pyrimidin-4-amine have been contrasted with the experimental observations [71] which is delineated in Table **23** [72].

Table 20. Comparison of calculated bond lengths (Å) and bond angles (°) using Gaussian03

Bond length (Å)			**Bond angle (°)**			**Dihedral angle (°)**		
Parameter	**HF**	**DFT**	**Parameter**	**HF**	**DFT**	**Parameter**	**HF**	**DFT**
C3–C2	1.386	1.408	C2–C3–C4	115.3	114.7	C2–N3–S–O2	−171.9	−172.5
C4–N1	1.326	1.324	C2–N3–N4	111.2	111.9	C3–C2–N3–N4	−1.1	−0.3
C5–N4	1.284	1.476	C3–C5–C6	129.2	130.0	C3–C2–N3–S	−180.0	176.9
C6–C5	1.483	1.405	C5–C6–C11	120.6	121.1	C4–C3–C5–C6	5.8	6.5
C6–C11	1.391	1.404	C13–C12–C17	121.2	121.7	C4–C3–C5–N4	−174.1	−173.3
C9–C10	1.385	1.395	N1–C4–C3	119.0	119.6	C4–C3–C2–N2	−1.3	−2.2
C10–C11	1.386	1.784	N1–C4–N5	117.1	116.7	C4–C3–C2–N3	176.5	175.5
C12–S	1.760	1.784	N3–N4–C5	107.4	106.7	C5–N4–N3–C2	1.4	0.7
C13–C12	1.388	1.396	N3–S–C12	103.7	102.7	C5–N4–N3–S	−179.6	−176.7

C14–C13	1.307	1.393	N3–S–O1	106.1	105.4	C7–C6–C11–C10	0.7	1.2
C15–C14	1.393	1.402	N4–C5–C6	120.3	119.6	C7–C6–C5–C3	−132.6	−141.0
C15–C16	1.390	1.403	N4–N3–S	120.1	119.6	C7–C6–C5–N4	47.2	38.8
N3–S	1.695	1.762	O1–S–O2	121.9	122.9	C11–C6–C5–C3	48.9	40.7
S–O2	1.419	1.455	S–C12–C13	119.2	118.8	C13–C12–S–N3	90.1	97.9
S–O1	.420	1.456				C13–C12–S–O2	−21.9	−13.2
N5–C4	1.341	1.356				C13–C12–S–O1	−157.2	−150.5
						C14–C13–C12–S	179.6	178.8
						C17–C12–S–O2	157.4	165.5
						C17–C12–S–O1	22.1	28.2
						C18–C15–C14–C13	−178.5	180.0
						C18–C15–C16–C17	178.5	180.0
						N2–C2–N3–N4	176.6	177.4
						N2–C2–N3–S	−2.3	−5.4
						N4–N3–S–C12	−105.3	−109.8
						N4–N3–S–O2	9.3	4.5
						N4–N3–S–O1	139.8	135.6

Table 21. Total and HOMO–LUMO energies of the 3-phenyl-1-tosyl-1*H*-pyrazolo [3,4-*d*]pyrimidin-4-amine obtained from HF and DFT methods

	HF	**DFT**
Total energy (a.u.)	−1509.8034	−1517.3056
Dipole moment (debye)	7.8696	6.7696
HOMO (a.u.)	−0.2339	−0.2279
LUMO (a.u.)	−0.0455	−0.0511
HOMO–LUMO energy gap(a.u)	0.1884	0.1768

Table 22. Theoretically computed thermodynamical parameters of 3-phenyl-1-tosyl-1*H*-pyrazolo[3,4-*d*] pyrimidine-4-amine.

Thermodynamical parameters	**HF**	**DFT**
Zero-point vibrational energy (kcal/mol)	209.6500	194.91907
Rotational temperature (K)	0.01493	0.01490
	0.00592	0.00574
	0.00531	0.00512
Rotational constants(GHz)	0.31114	0.31050
	0.12334	0.11959
	0.11060	0.10665
Energy(kcal/mol)		
Total	222.472	208.698
Translational	0.889	0.889

Rotational	0.889	0.889
Vibrational	220.694	206.921
Molecular capacity at constant volume(cal/mol-K)		
Total	78.176	84.769
Translational	2.981	2.981
Rotational	2.981	2.981
Vibrational	72.215	78.807
Entropy (cal/mol-Kelvin)		
Total	156.154	161.142
Translational	43.578	43.578
Rotational	35.581	35.650
Vibrational	76.995	81.915

Table 23. Vibrational assignments of fundamental frequencies (cm^{-1}) for 3-phenyl-1-tosyl-1*H*-pyrazolo[3,4-*d*] pyrimidin-4-amine at B3LYP/6–311 + G level.

Experimental frequencies	**Theoretical frequency**	**Intensity (km/mol)**	**Vibrational Assignments**
411	416.10	0.102	Ring out of plane
	422.39	6.447	Deformation
	430.01	2.932	
474	511.51	1.080	C–H out of plane bending
527	530.80	81.554	
551	547.35	28.531	
637	566.81	263.589	
	628.03	3.476	
693	694.60	21.253	CCC out-of-plane bending
	710.96	6.531	
776	772.58	22.985	C–H out of plane
807	784.40	33.450	Deformation
824	816.55	16.038	
	818.62	9.968	
	828.25	24.525	
1003	1010.94	23.630	Inter ring C–C stretching
1019	1016.50	0.445	C–C stretching
1061	1064.67	11.928	
1121	1125.82	104.333	In-plane ring HCC bending
1179	1146.28	4.568	
	1157.45	166.133	
1215	1208.88	3.510	C–H in-plane bending
1265	1215.25	6.612	
	1235.35	1.639	
1306	1319.98	32.032	N–N stretching
1339	1334.05	28.455	C–N stretching
	1350.16	20.809	
	1370.97	44.534	

	1396.57	6.135	
	1443.37	10.438	
1466	1443.37	10.438	C–C stretching
1478	1483.85	3.714	
	1627.16	9.199	
	1633.95	1.896	
1674	1663.74	418.137	NH_2 scissoring
3032	3042.48	22.488	Aromatic C–H stretching
3070	3104.35	14.758	
3125	3132.14	11.917	
	3180.85	28.780	
	3182.30	1.393	
	3187.92	14.356	
	3190.31	4.856	
	3208.22	21.772	
	3218.57	5.300	
	3226.66	1.594	
	3233.78	5.604	
3472	3600	85.002	NH_2 asymmetric stretching
	3736.84	91.085	NH_2 symmetric stretching

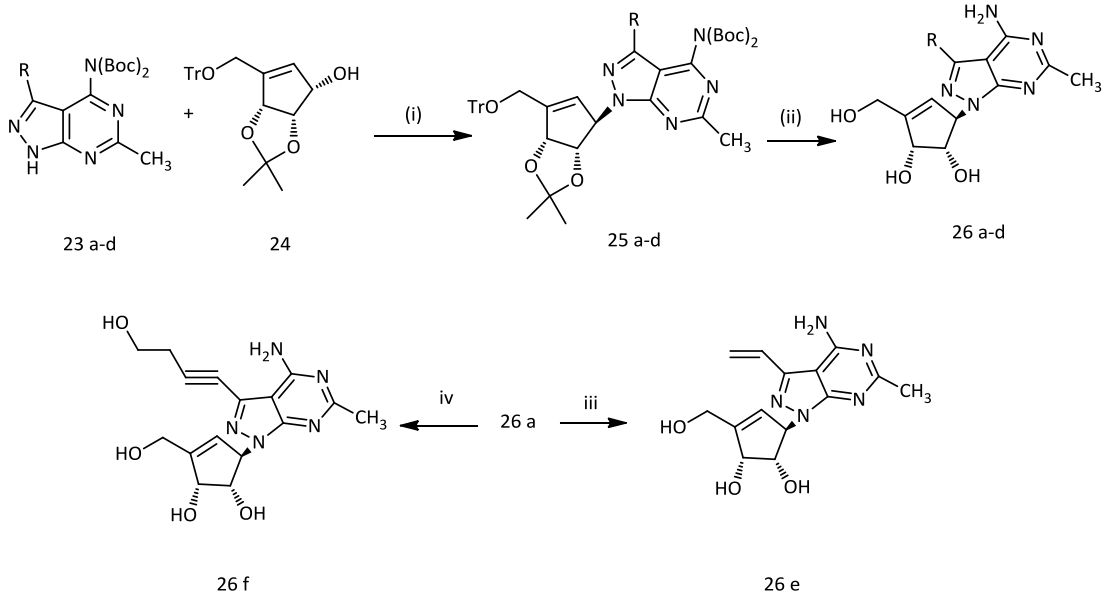

Scheme 6. Synthesis of 6-methyl-4-APP based carbocyclic nucleoside analogs 26a-e.

2.9. Synthesis of 4-amino-pyrazolo[3,4-d]pyrimidine; 6-methyl-4-APP; 6- methyl-4-amino-pyrazolo[3,4-d]pyrimidine

Compound **25 a-d** obtained by coupling of compound **23 a-d** with compound **24** (Mitsunobu coupling).

2.9.1. Computational details

The structures were limited utilizing Macro model with Optimized Potentials for Liquid Simulation. Spin restricted DFT with B3LYP (Becke-3-Lee-Yang-Parr) density functional and the 6–31-G** basis set were used to obtain the calculations.

The molecularmechanics (MM) energy optimization showed that the potential energy of the N2 is higher than the corresponding N1 isomer as shown in Figure 10.

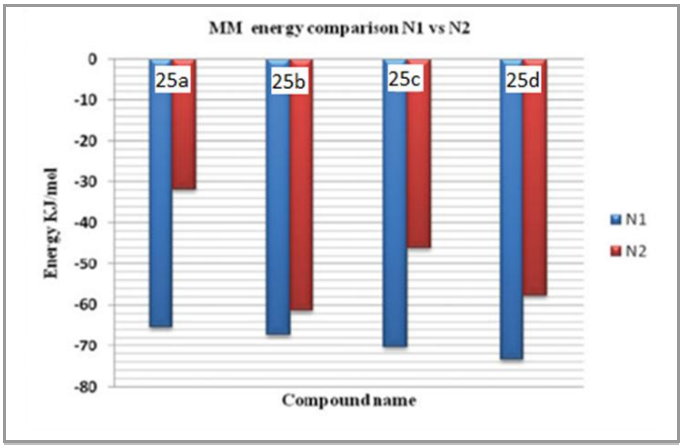

Figure 10. MM energy analyses showing the N1-regioisomer to have lower energy than N2-isomer.

The quantum mechanics (QM) computation for the activation energy for the formation of **25a** (N1) and **25a** (N2) were done. The result demonstrates that the transition state for N2 higher in energy than that of N1 is 0.0016 Ha (4.27 kJ/mol) (schematic representation in Figure 11).
The relative energy of is N2 isomer higher than that of N1 isomer. Thus, QM calculation likewise supports the formation of N1 product [73].

2.10. Synthesis of fluorine-substituted pyrazolo[3,4-d]pyrimidine derivative

New fluorine-substituted pyrazolo[3,4-*d*]pyrimidine derivatives **29–31** obtained by the reaction of (4-fluorophenyl)malanonitrile **27** with guanidine, then forming cyclization reaction with hydrazine producing 2,4-diamino-6-aryl-pyrimidine-5-carbonitrile **28.**
Scheme 7 describe fluorinated pyrazolo[3,4-*d*]pyrimidine derivatives **30** and **31** that produced from fluorinated acylation and/or benzeylation of compound **29** by warming with trifluoroacetamide and/or 4-fluorobeneyl chloride in acetic acid or dry C_6H_6-TEA.
HOMO, LUMO, energy gap, and the optimized geometric structure of the studied compounds **27-31,** by B3LYP/6-311 + G** theory level, introduced in Table 24 and Figure 12.
At Figure 12, The LUMO is delocalized among all the atoms for all molecules, except compounds **30** and **31**. But, the HOMOs are localized on the nitrogen atoms, except in compounds **27** and **31**.

2.10.1. Synthesis of fluorine-substituted pyrazolo[3,4-d]pyrimidine derivative

The computational calculation of compounds **27-31** was performed by using SPARTAN'08 Windows graphical software with density functional theory, DFT/6-31G* basis set [74].
We find theoretically that the compound with lower LUMO value and higher density value has shown the highest activity. The theoretical results were found in good corroboration with the experimental results. Structure activity relationship studies show that fluorinesubstituted derivatives play an important role in antimicrobial activity [75].

3. Synthesis and computational studies of pyrazolo[1,5-*a*]pyrimidine

3.1. Synthesis and computational studies of pyrazolo[1,5-a]pyrimidine

Through a dimroth rearrangement, in quantitative yields, Derivatives of the new ring system Pyrazolo[3,4-*d*] [1,2,3]triazolo[1,5-*a*]pyrimidine were synthesized from the comparing angular isomers. This class of compounds could be the best candidate as DNA intercalating agents as explained by Preliminary computational studies.

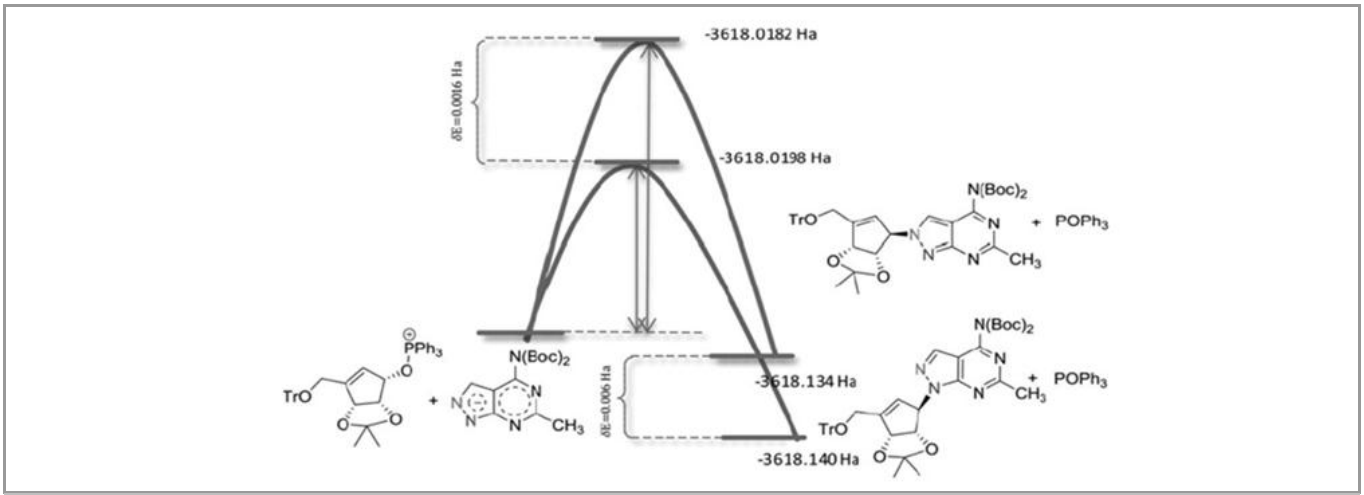

Figure 11. Schematic representation of the energy barrier for the formation of N1 and N2 isomer.

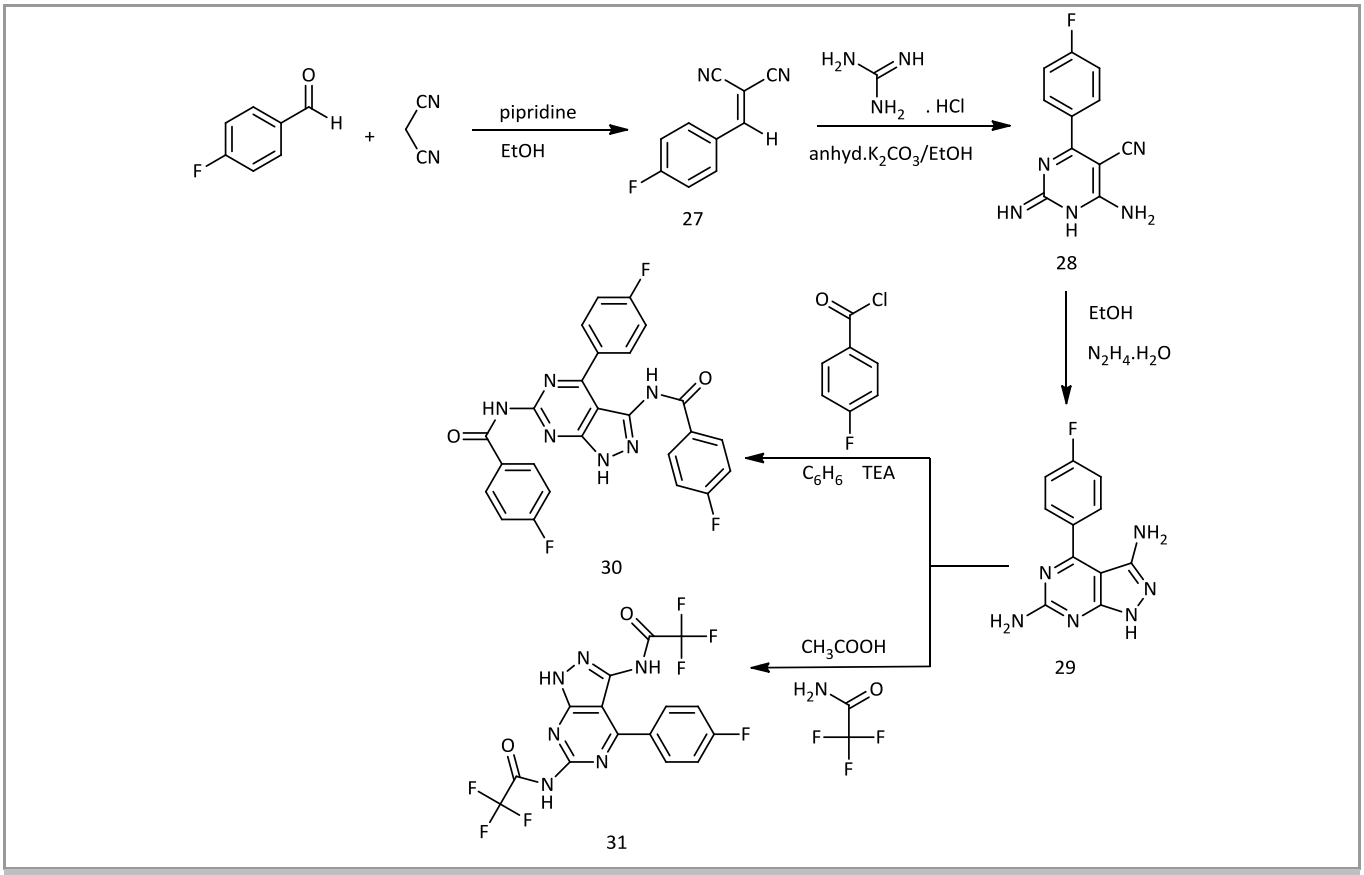

Scheme 7. Synthesis of fluorin-substituted pyrazolo[3,4-*d*]pyrimidine derivatives.

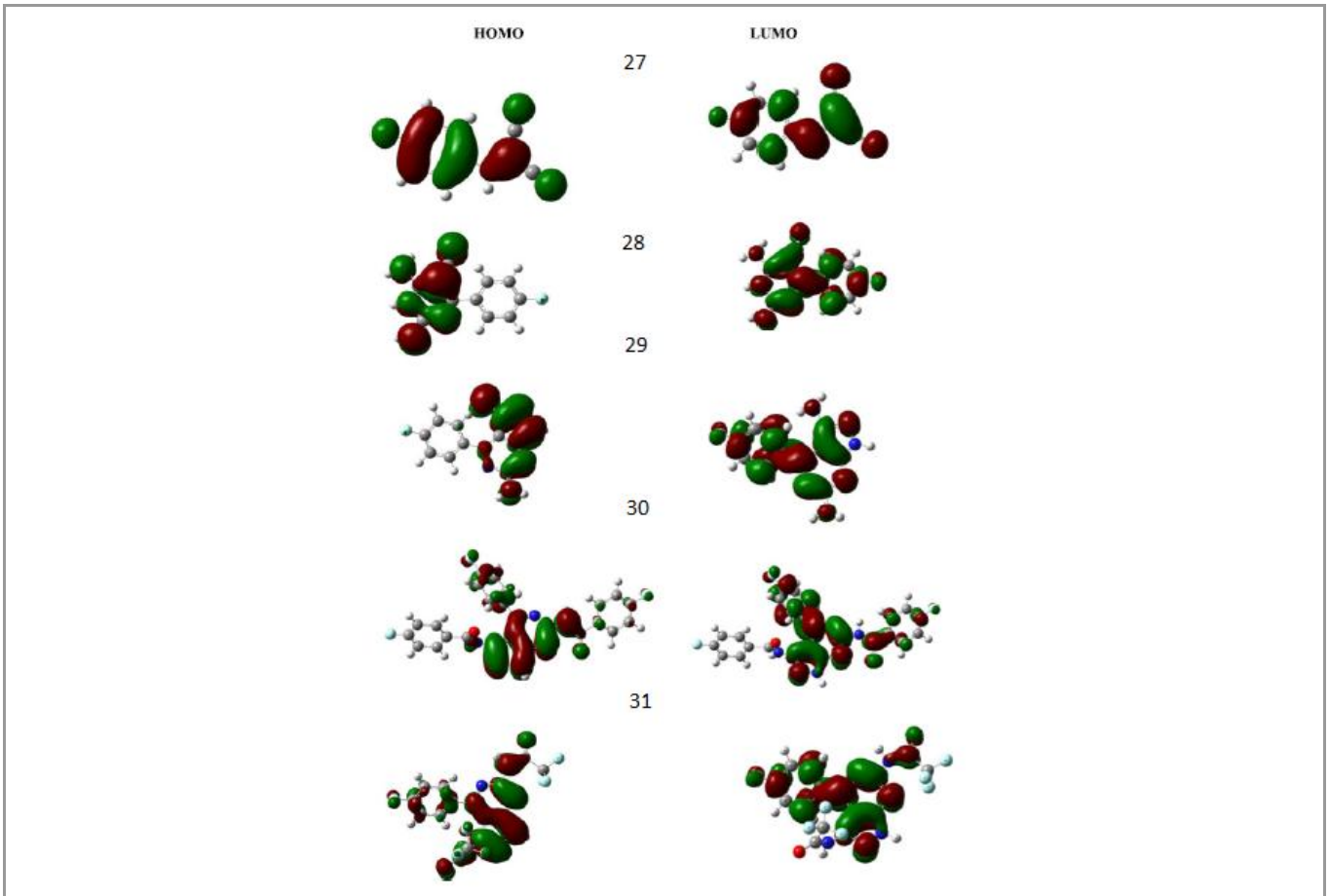

Figure 12. The electronic densities of HOMO and LUMO for compounds **27–31** using B3LYP/6-311 + G** level of theory.

Table 24. Optimized geometric structures and FMO energies of compounds **27** to **31** calculated by using DFT/RB3LYP/6-311 + G** level of theory.

Structures	HOMO	LUMO	Energy gap
	eV		
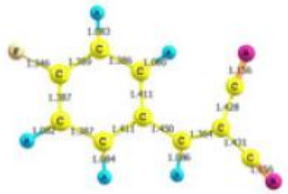	-7.452	-3.345	4.107
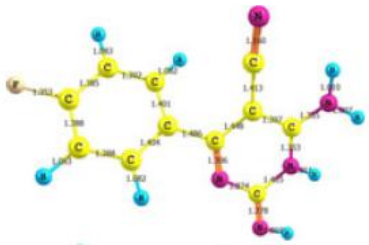	-6.429	-2.130	4.298
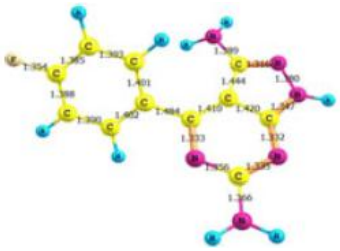	-5.965	-1.857	4.108
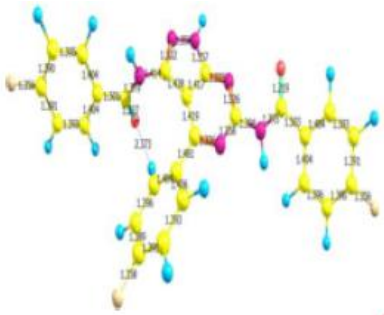	-6.813	-2.319	4.494
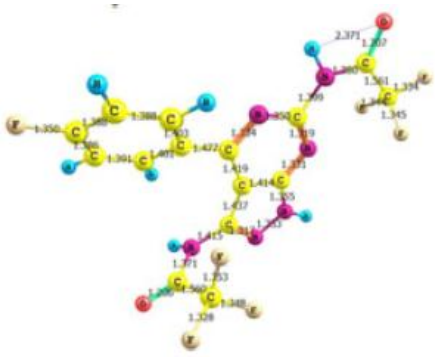	-7.385	-2.964	4.421

The Dimroth rearrangement (DR), in basic conditions, could be applied to the angular isomer **33** for preparing polyheterocyclic ring **34**.

The new compounds **38**, derivatives of the ring system Pyrazolo[4,3-*d*][1,2,3]triazolo[1,5-*a*]pyrimidine, were generally isolated in high yields (70–90%). It appears that in this situation the bond-forming efficiency relies upon the first reaction step, comprising in the 1,3-dipolar cycloaddition to form the triazole moiety [76].

According to the docking scores reported in Table 25 the pyrazolotriazolopyrimidine derivatives **38** and **40** can form stable complexes with DNA.

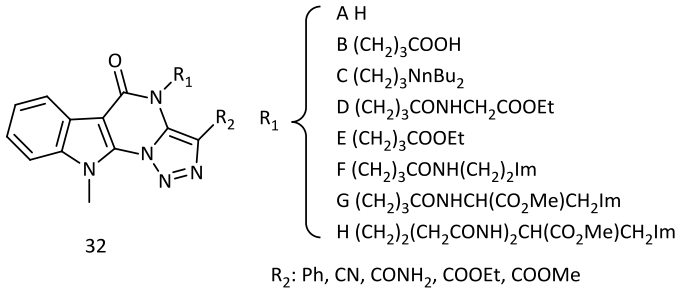

Indolo[3,2-e][1,2,3]triazolo[1,5-a]pyrimidine derivatives with anti-tumor activity.

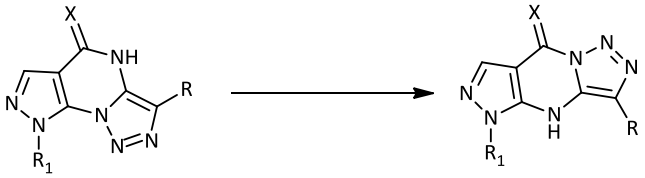

R=Ph,CN,$CONH_2$
R1=Ph,Me
X=NH,O

Scheme 8. Synthetic rout to pyrazolo[3,4-*d*][1,2,3]triazol[1,5-*a*]pyrimidine core structure.

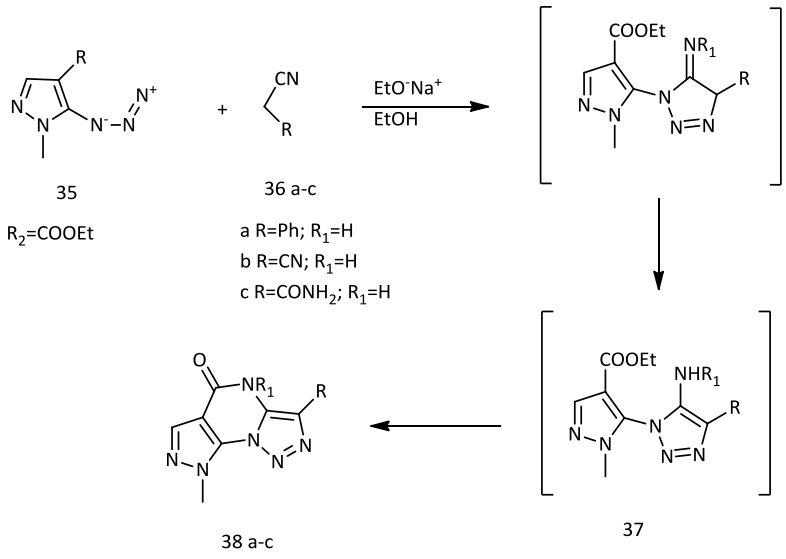

Scheme 9. Routs to pyrazolo[3,4-*d*][1,2,3]triazol[1,5-*a*]pyrimidine ring systems.

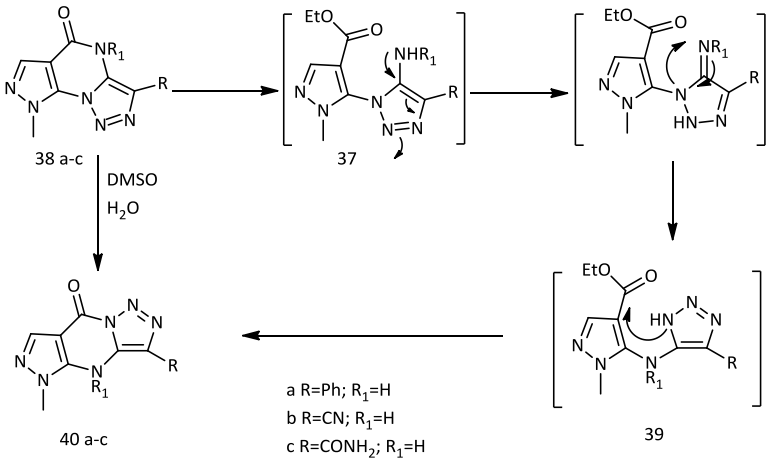

Scheme 10. Dimroth rearrangement mechanism.

Table 25. DNA fragment docking results (GSCORE)

Entry	R_1							
	A	**B**	**C**	**D**	**E**	**F**	**G**	**H**
38a	-5.84	-5.76	-7.50	-6.22	-5.69	-7.80	-6.94	-7.54
38b	-6.01	-6.10	-7.14	-6.12	-5.91	-7.71	-7.29	-7.02
38c	-7.21	7.03	-9.34	-8.33	-7.81	-8.48	-7.61	-6.96
40a	-5.62	-5.34	-6.69	-5.72	-5.22	-7.77	-7.47	-6.53
40b	-5.56	-5.74	-6.78	-5.75	-5.39	-7.05	-6.95	-6.50
40c	-5.82	-5.55	-6.41	-5.17	-5.44	-7.53	-6.81	-6.48
32 (R_2=ph)	-5.5	-6.19	-7.47	-6.18	-6.06	-8.19	-7.37	-7.16
Mean	-5.95	-5.96	-7.33	-6.21	-5.93	-7.79	-7.21	-6.88

A: H; B: $(CH_2)_3COOH$; **C:** $(CH_2)_3NnBu^2$; **D:** $(CH_2)_3CONHCH_2COOEt$; **E:** $(CH_2)_3COOEt$; **F:** $(CH_2)_3CONH(CH_2)_2Im$; **G:** $(CH_2)_3CONHCH(CO_2Me)CH_2Im$; **H:** $(CH_2)_2(CH_2CONH)_2$-$CH(CO_2Me)CH_2Im$.

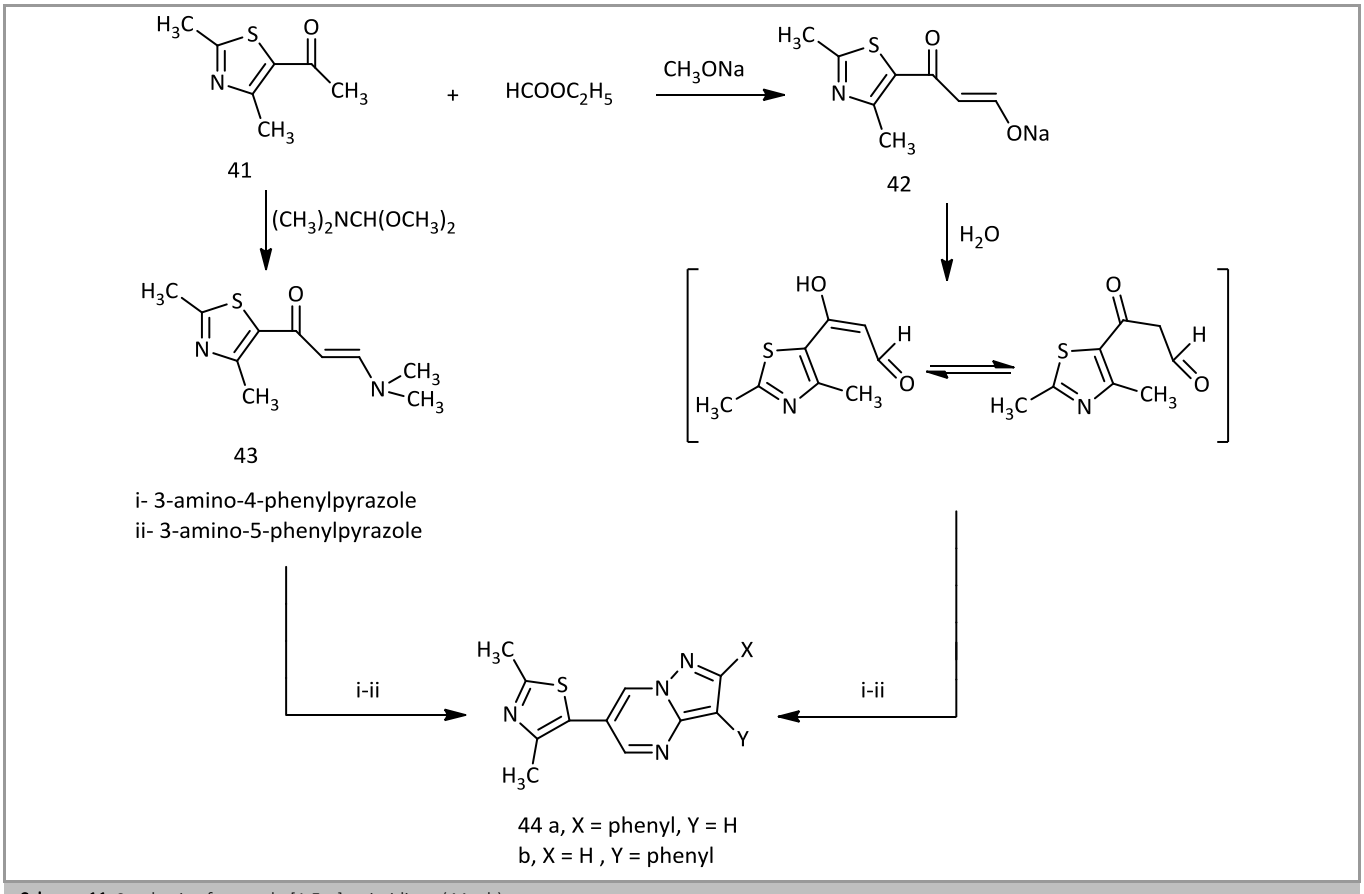

Scheme 11. Synthesis of pyrazolo [1,5-*a*]pyrimidines (44 a,b)

The compound 1-(2,4-dimethyl-1,3-thiazol-5-yl)ethanone (**41**) was reacted with ethyl formate in dried ether containing sodium methoxide forming the sodium salt of 3-hydroxy-1-(2,4-dimethylthiazol-5-yl) prop-2-en-1-one (**42**) that react with 3-amino-4-phenyl-1*H*-pyrazole or 3-amino-5-phenyl-1*H*-pyrazole in glacial acetic acid containing piperidenum acetate forming 5-(2,4-dimethyl-1,3-thiazol-5-yl)-3(or 4)-phenylpyrazolo[1,5-*a*]pyrimidines (**44a**,**b**).

Frequency computations were performed at a similar level of the theory in order to characterize the stationary points and to assess the zero-point energy

(ZPE), free energies (G) and enthalpies (H) at 298.15 K. TS_S had just a single imaginary frequency.

The 13DC reaction is demonstrated by utilizing the density functional theory (DFT). We notice a computational investigation of regioselectivity of 2, 4-dimethylthiazol **45** dipolarophiles. Our principle objective in acquiring these cycloadditions to acrylonitrile results is to compute the energy barrier for the 13DC reaction. B3LYP technique affirms that the **47** geometry is favoured by 3.789 kJ.mole^{-1}.

Activation barrier, enthalpy, free energy, and reaction energies are given in Table 27. As mentioned before, the studied 13DC reaction prefers structure **47** products with the lower activation energy (72.328 kJ. mol^{-1}) and high negative estimations of enthalpy and free energy [77].

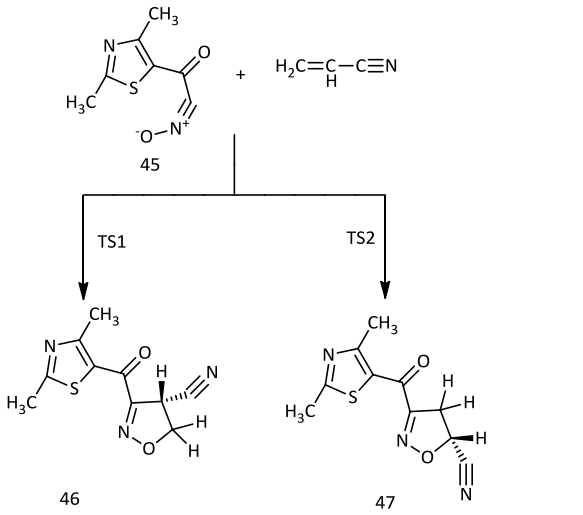

Scheme 12. Regioisomeric pathways for the studied cycloaddition reaction

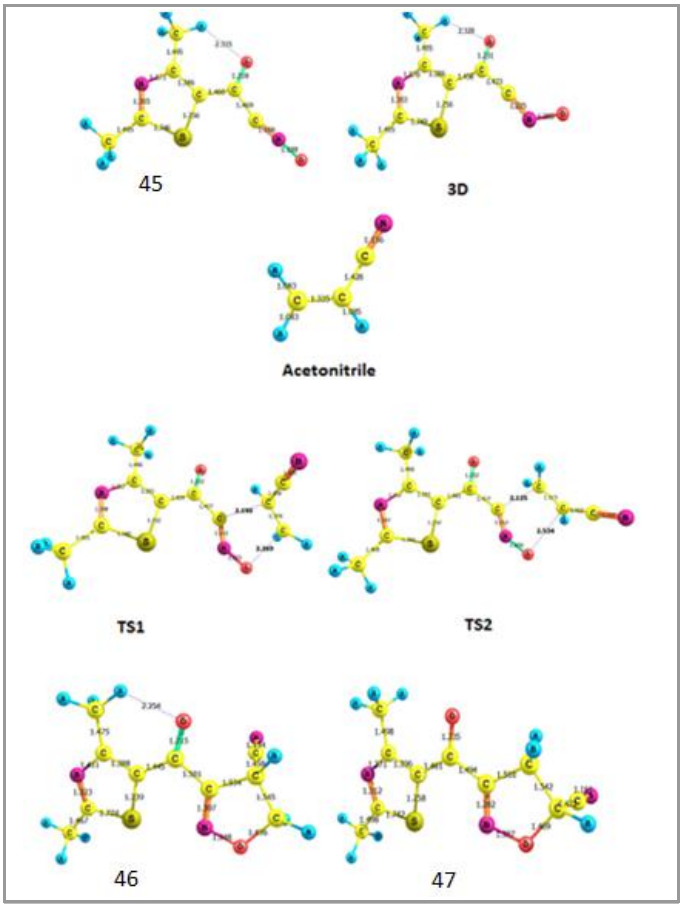

Figure 13. Optimized geometries obtained by B3LYP/6-311 ++G** of all spices in the studied 13DC reaction. The bond lengths are given in angstroms

Table 26. Zero point energy (ZPE), electronic energy (E), enthalpy (H) and free energies (G), total energy (E + ZPE) computed at 298 K of the stationary points involved in the studied 13DC reaction using B3LYP/6-311 ++G** level of theory.

Structure	ZPE	E	H	G	Et
Au					
acrylonitrile	0.05058	−170.88289	−170.82720	−170.85818	−170.83231
45	0.12172	−928.57717	−928.44370	−928.49390	−928.45545
3D	0.11855	−928.49839	−928.36910	−928.41635	−928.37984
TS1	0.17372	−1099.43404	−1099.24270	−1099.30732	−1099.26032
TS2	0.17355	−1099.43868	−1099.24740	−1099.31274	−1099.26513
46	0.17903	−1099.50842	−1099.30020	−1099.37243	−1099.32939
47	0.17858	−1099.50940	−1099.31520	−1099.37487	−1099.33082

Table 27. Enthalpies (ΔH) and free energies (ΔG), barrier energies E^{f}_{a}, E^{b}_{a} , relative energies (ΔE) computed at 298 K of the stationary points involved in the studied 13DC reaction utilizing B3LYP/6-311 ++G** level of theory

Product	ΔH (kJ/mole)	ΔG	E^{f}_{a}	E^{b}_{a}	ΔE
46	−273.437	−59.468	−72.328	−182.020	3.789
47	−274.012	−60.043	−65.549	−173.141	0

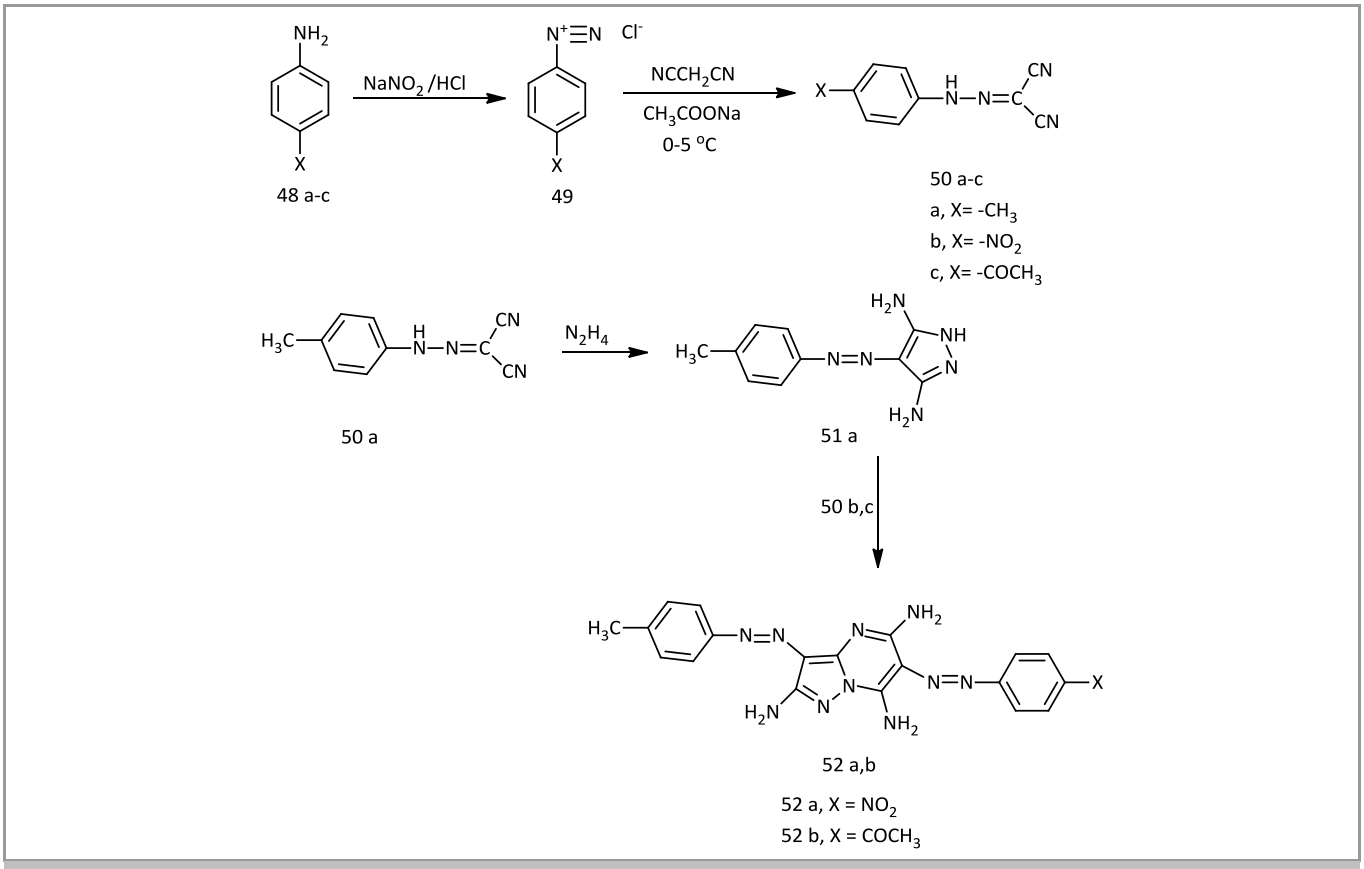

Scheme 13. Schematic diagram and synthesis route of the investigated dyes.

3.2. Synthesis of triaminopyrazolo[1,5-a]pyrimidine dyes

We have blended multifunctional dyes 3-(4-methyl-phenylazo)-6-(4-nitro-phenylazo)-2,5,7-triaminopyrazolo[1,5-*a*]pyrimidine 52a and 3-(4-methyl-phenylazo)-6-(4-acetyl-phenylazo)-2,5,7-tri aminopyrazolo[1,5-*a*]pyrimidine 52b, then characterized by IR, 1H NMR and 13C NMR techniques. Through density functional theory, the ground state geometries have been calculated.

This scheme obtain Synthesis of 3-(4-methyl-phenylazo)-6-(4-nitro-phenylazo)-2,5,7-Triaminopyrazolo[1,5-*a*] pyrimidine **52a** and 3-(4-methyl-phenylazo)6-(4-acetyl-phenylazo)-2,5,7-triaminopyrazolo[1,5-*a*]pyrimidine **52b**.

3.2.1. Synthesis of 3-(4-methyl-phenylazo)-6-(4-nitro-phenylazo)-2,5,7-Triaminopyrazolo[1,5-a]pyrimidine 52a and 3-(4-methyl-phenylazo)6-(4-acetyl-phenylazo)-2,5,7-triaminopyrazolo[1,5-a]pyrimidine 52b

Schematic diagram and synthesis route of the investigated dyes depicted in Scheme 8.

3.2.2. Computational details

Energy gap of HOMO–LUMO increases for **52b** while decreases for **52a** at ground state. The introduction of carboxylic group in place of nitro 53, raise the HOMO and LUMO energies. It was seen that energy gap of the **52b** is greater than the **52b**. We observed decrease in energy gap by using solvent for **52a** while solvent has no significant effect for **52b**.

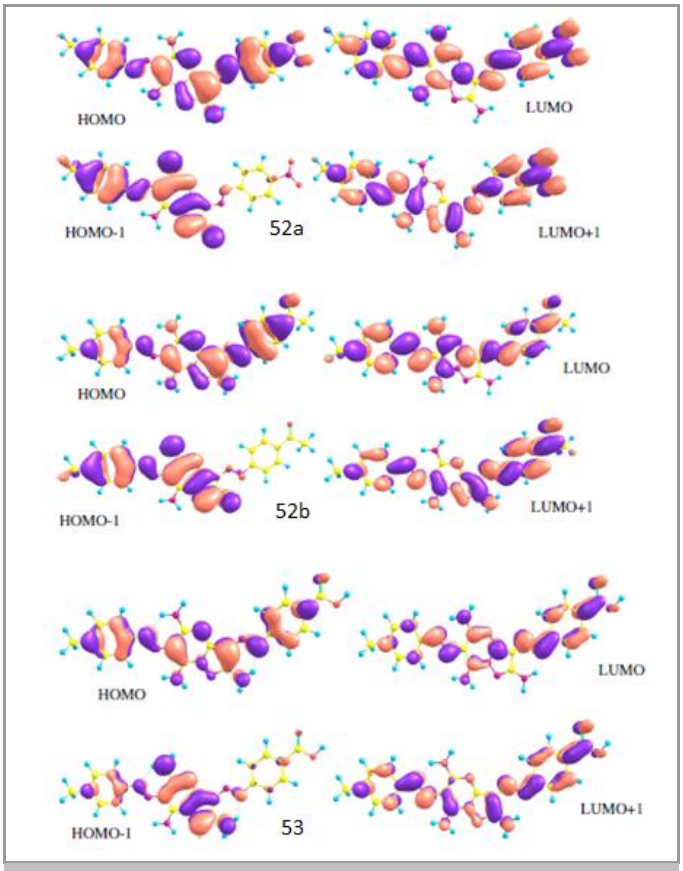

Figure 14. The distribution patterns of the frontier molecular orbitals (HOMOs and LUMOs) of 52a and 52b

Table 28. The HOMO energy (E_{HOMO}), LUMO energy (E_{LUMO}) HOMO–LUMO energy gap (E_{gap}) and dipole moment (μ) in eV for ground at B3LYP/6-31G*level of theory.

Dyes	E_{Homo}	E_{Lumo}	E_{gap}	μ
52a	-5.51	-2.62	2.89	14.78
52b	-5.29	-2.34	2.94	7.89
52a[a]	-5.60	-2.83	2.77	19.60
52b[a]	-5.47	-2.47	3.00	10.65
53	-5.30	-2.34	2.96	7.70

[a] The geometries have been optimized in solvent (methanol).

Table 29. Experimental[a] and calculated absorption wavelengths (λ) in nm of TD-B3LYP/6-31G* level of theory.

	F	Λ	Transition
52a[b]	1.1183	471	H → L
	0.1549	401	H→ L + 1
52b[b]	0.8718	464	H→ L
	0.4224	383	H→ L + 1
52a[c]	0.8970	504	H→ L
	0.2090	396	H-1→ L + 1
52b[c]	1.6978	466	H→ L
53[c]	0.4428	370	H-1→ L + 1
	1.6651	463	H → L
	0.4526	368	H-1→ L + 1

[a] Experimental absorption wavelengths of **52a** 479 nm while **52b** 465 nm.
[b] In gas phase.
[c] In solvent (methanol).

Table 30. The ΔG^{inject}. Oxidation potential, |VRP|, LHE of investigated dyes at TD-B3LYP/6-31G* and PCM-B3LYP/6-31G* level of theory**.**

System	ΔG^{inject}	E_{ox}^{dye}	E_{ox}^{dye*}	λ_{max}^{ICT}	LHE	$\lvert V_{RP}\rvert$
52a	-0.86	5.60	3.13	2.46	0.8732	0.43
52b	-1.19	5.47	2.80	2.66	0.9799	0.53
53	-1.18	5.50	2.82	2.68	0.9783	0.59

In Table 30, the ΔG^{inject}, Oxidation potential, and |VRP| of the studied dyes were presented. The values of electron injection and electronic coupling constant for **52a** are ‑0.86 and 0.43, respectively, while **52b** are ‑1.16 and 0.58, respectively. Al-Sehemi *et al.* demonstrated that, (HOMOs) the highest occupied molecular orbitals and lowest unoccupied molecular orbitals (LUMO) are delocalized and localized on throughout the backbone in **52b**, respectively. The HOMO and LUMO energies reduced from gas phase to solvent.

Solvent plays important role towards elevating the dipole moment. In solvent, the wavelengths of maximum absorption are red shifted. Further improvement towards efficient sensitizers occur when we attach anchoring groups having strong anchoring ability along with elongating the bridge as revealed in this study [78].

3.3. The regiodivergent palladium-catalysed C-H arylation of Pyrazolo[1,5-a]pyrimidine

As seen in Scheme 9, to achieve site selectivity at C7, using of the monodentate phosphine ligand SPhos proved crucial, giving the coveted item **55** a in great yield.

The HOMO orbital has critical electron density at the C3 position, and that this position has by far the highest "electrophile affinity" (Eα) value (Figure 15a) [79], on the other hand, they focused the significantly greater acidity of the C7-H group as detected by comparing the computed relative energies for the removal of each of the protons by acetate (Figure 15b) [80].

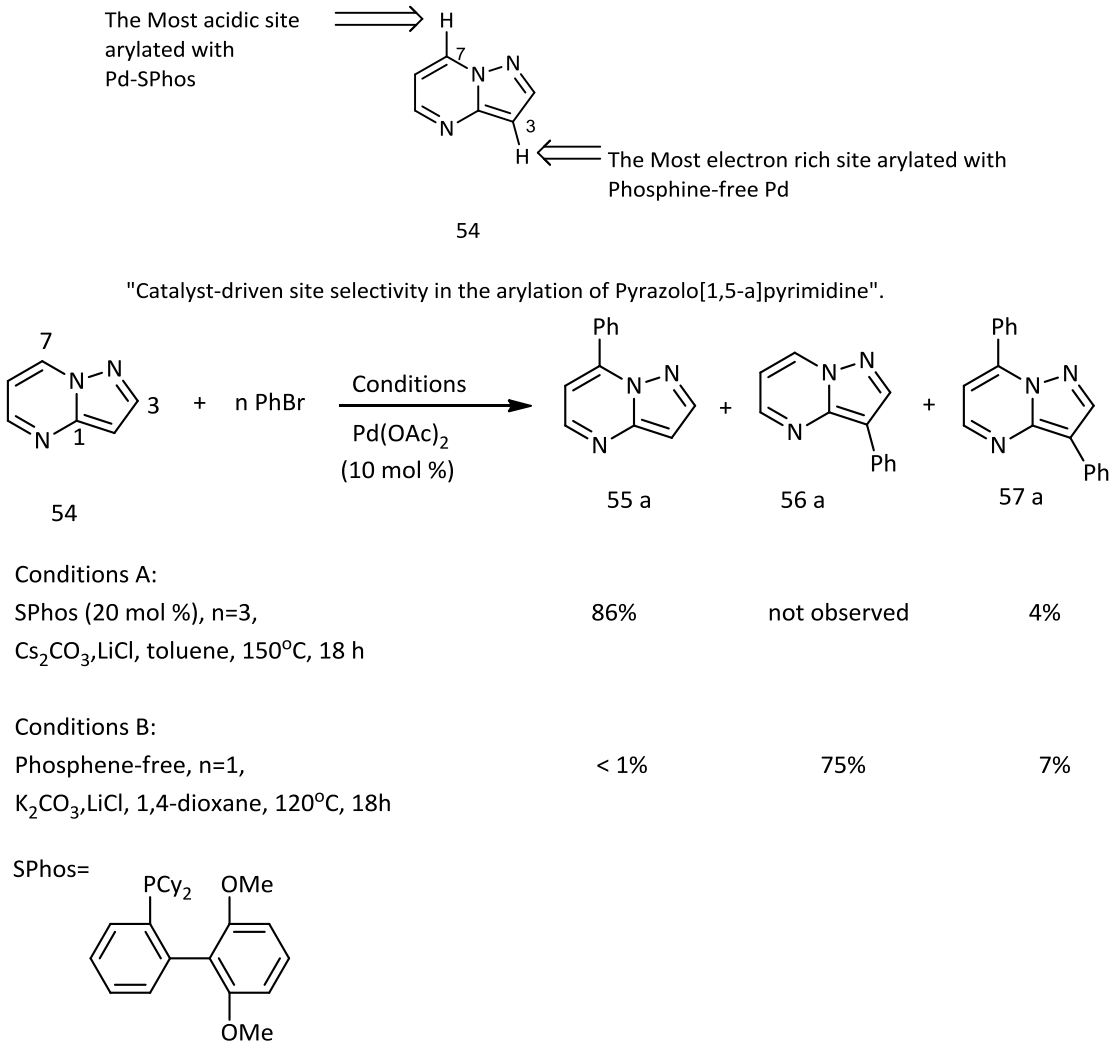

scheme 9: Results of optimization of reaction conditions. Yields determined by ^{1}HNMR spectroscopy (1,3,5 $(MeO)_3C_6H_3$ used as internal standard).

Scheme 14. Results of optimization of reaction conditions.

3.4. Synthesis of Pyrazolo[1,5-a]pyrimidin-7(4H)-one

Electronic absorption bands were observed and compared with the predicted transitions using a time-dependent DFT method (TDDFT). In all solvents utilized, except for DMF and acetonitrile, compounds **58** and **59** presented azo-hydrazone tautomerism. However, the ionized species were predominant in highly polar solvents for compounds **60** and **61**. In DMF, based on the molecular structure, all the investigated dyes presented either in acid-base equilibrium or in the ionized form. Hence, the values of the ionization constant (Kion) and Gibbs free energy (ΔG) of the equilibrium existing in solution were computed. In addition, the pKa values of the dyes is calculated by using the spectrophotometric method [81].

3.4.1. Quantum chemical calculations

The full geometrical optimization of the isolated molecules **58-61** is in this scheme. The transfer of the hydrogen atom related to N_4 either to the keto-oxygen (O_8) or to N_{11} creates annular and azo-hydrazone tautomerism, respectively. In addition, it is well-known that a variety of azo dyes can co-exist in acid-

base equilibrium particularly in basic solvents [82-84].

Using the B3LYP functional, The DFT calculations were calculated, in which Becke's nonlocal exchange [85,86] and the Lee-Yang-Parr correlation functional were used [46]. Compiles selected structural parameters detected only by geometrical optimization since no experimental geometrical data are shown in the literature for NH, OH and hydrazone tautomers calculated at PM6 levels and DFT.

Dissection of the spatial structure of the dyes **58-61** has uncovered that the fused heterocyclic fragment is completely planar in both NH and OH shapes but deviates slightly from planarity in the hydrazone tautomers as the torsion $C_6C_7N_{1a}N_1$ angle.

We can observe in Table 32, the NH tautomers have the lowest energy value among all the potential tautomers calculated at the B3LYP/6-31G** computational level.

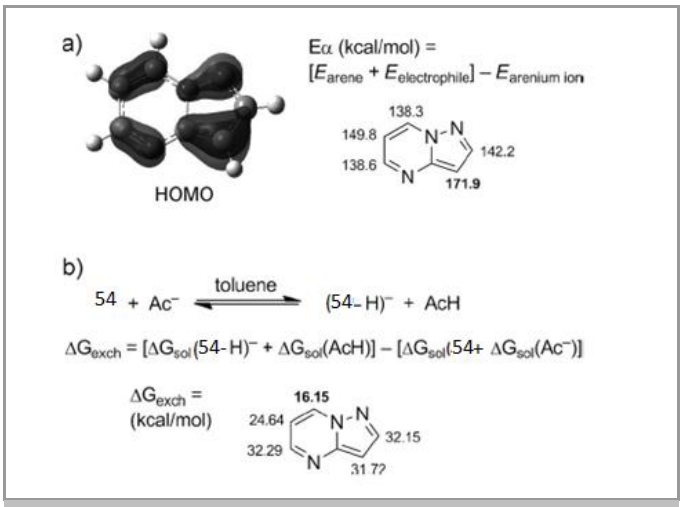

Figure 15. Results of DFT computational are summarized. **a)** Left: calculated (B3LYP-d2/6-311+ +G (d)) HOMO for **54** (isovalue ±0.05 (electron/ bohr³)$^{1/2}$), right: gas-phase electrophile affinity (Eα) values, determined using Br^+ as test electrophile (B3LYP/6-311+G (2d, 2p)). **b)** Calculated (B3LYP/6-311+ +G (2df, 2p)//B3LYP/6-31G (d)) free energies for the deprotonation of each of the CH groups of **54** by acetate

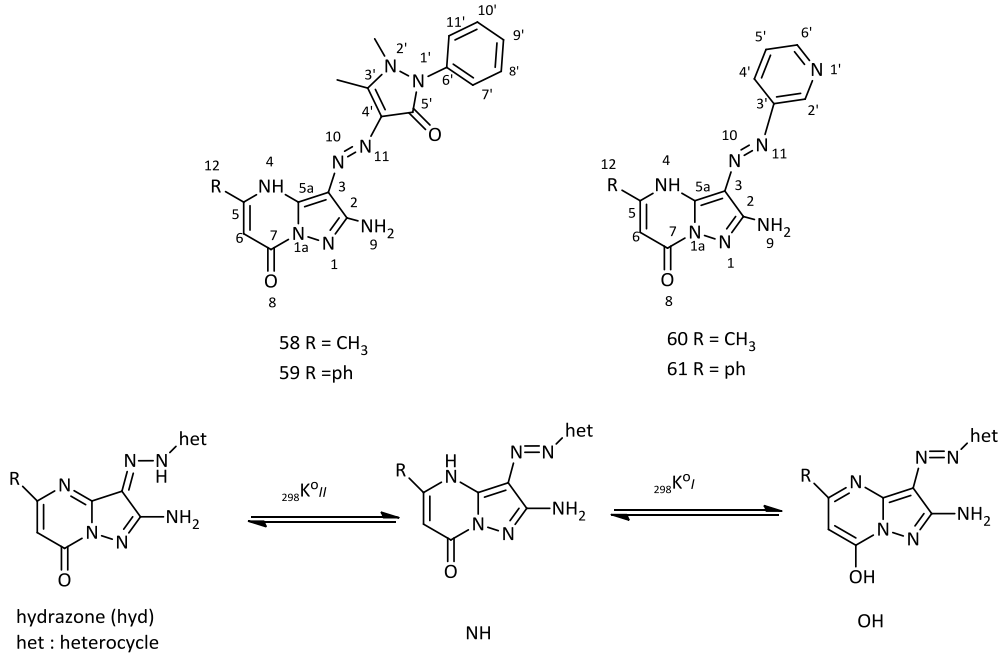

Scheme 15. Compounds and equilibria (298K0, equibrium constant) investigated with the number of atoms indicated

Table 31. The calculated (DFT, PM6) structural parameters (bond length in Å, angles in degree) of compounds **58-61**.

Compound	Parameter	DFT			PM6		
		NH	OH	Hyd	NH	OH	Hyd
58	N_4C_5	1.380	1.330	1.379	1.403	1.352	1.406
	C_6C_7	1.462	1.385	1.452	1.457	1.393	1.451
	C_7O_8	1.215	1.340	1.219	1.201	1.356	1.204
	$N_{10}N_{11}$	1.281	1.281	1.314	1.265	1.265	1.309
	$N_{10}N_{11}C_4\text{-}C_5$	-174.887	- 177.839	-179.185	-173.697	-178.991	-179.366
	$C_6C_7N_{1a}N_1$	-179.661	-179.861	178.404	-179.879	-179.942	-178.588
	$C_2C_3N_{10}N_{11}$	1.074	-0.297	-0.732	4.359	1.692	-2.112

	N_2-N_1-C_6-C_7	-162.192	161.417	21.021	-166.871	-167.524	-165.775
59	N_3C_4	1.381	1.336	1.380	1.401	1.349	1.406
	C_5C_6	1.460	1.385	1.450	1.458	1.392	1.454
	C_7O_8	1.216	1.340	1.219	1.201	1.356	1.204
	N_9N_{10}	1.281	1.281	1.313	1.265	1.265	1.308
	$N_{10}N_{11}C_4$-C_5	-176.320	-178.947	-179.148	-174.948	-177.697	-179.261
	$C_6C_7N_{1a}N_1$	179.694	-179.998	-178.00	-179.960	-179.931	-178.756
	$C_2C_3N_{10}N_{11}$	1.764	-0.229	0.996	4.343	1.883	-1.814
	$C_6C_5C_{12}C_{13}$	- 142.923	-161.981	-159.292	-112.810	-135.209	-136.199
	N_2-N_1-C_6-C_7	-160.657	161.023	-159.227	-166.834	-167.353	-165.640
60	N_3C_4	1.381	1.331	1.381	1.405	1.353	1.413
	C_5C_6	1.462	1.385	1.453	1.455	1.393	1.454
	C_7O_8	1.214	1.338	1.218	1.200	1.354	1.203
	N_9N_{10}	1.279	1.279	1.318	1.263	1.265	1.325
	$N_{10}N_{11}C_3$-C_2	178.850	-179.779	-175.332	-29.635	-179.378	-7.945
	$C_6C_7N_{1a}N_1$	179.848	-179.995	-178.321	179.814	179.930	-178.645
	$C_2C_3N_{10}N_{11}$	-0.521	0.038	0.555	0.148	-1.313	1.761
61	N_3C_4	1.382	1.337	1.383	1.403	1.354	1.412
	C_5C_6	1.459	1.385	1.451	1.457	1.393	1.456
	C_7O_8	1.215	1.339	1.219	1.200	1.354	1.203
	N_9N_{10}	1.279	1.280	1.318	1.263	1.265	1.324
	$N_{10}N_{11}C_3$-C_2	178.773	179.633	-175.890	28.007	175.766	8.254
	$C_6C_7N_{1a}N_1$	-179.869	179.963	177.744	-179.627	-179.869	178.746
	$C_2C_3N_{10}N_{11}$	-0.870	-0.106	-0.739	-0.288	1.196	-1.763
	$C_6C_5C_{12}C_{13}$	143.186	163.404	161.144	-116.397	140.751	-143.109

Table 32. Physicochemical features of the different tautomeric forms of compounds **58-61**. A piece of evidence supporting the above finding is the negative values of the computed HOMO and LUMO energies-following a full geometry optimization- by DFT for all the expected tautomers.

Computational	**Δ E**			**Natural charge at N_{11}**			**HOMO**			**LUMO**			**E_g^a**	**E_g^b**	**$\ln_{298}K_t^{oc}$**
level	**NH**	**OH**	**Hyd**	**NH**	**OH**	**Hyd**	**NH**	**OH**	**Hyd**	**NH**	**OH**	**Hyd**			
58															
DFT	0.00	31.39	16.27	-0.260	-0.274	-0.341	-0.196	-0.183	-0.202	-0.072	-0.060	-0.095	2.86	2.47	2.41 (2.07)
DFT (PCMeDMSO)	0.00	27.40	17.56	-0.283	-0.274	-0.316	-0.202	-0.183	-0.206	-0.075	-0.060	-0.096	2.93	2.54	2.37 (1.96)
DFT (PCM e C_2H_5OH)	0.00	28.09	17.81	-0.274	-0.280	-0.316	-0.202	-0.186	-0.206	-0.075	-0.063	-0.096	2.93	2.54	2.40 (1.97)
DFT (PCM e Acetone)	0.00	28.03	17.24	-0.271	-0.286	-0.321	-0.202	-0.189	-0.207	-0.075	-0.065	-0.096	2.93	2.56	2.40 (1.94)
DFT (PCM e $CHCl_3$)	0.00	30.99	16.85	-0.268	-0.281	-0.328	-0.200	-0.186	-0.206	-0.074	-0.063	-0.096	2.91	2.54	2.50 (1.92)
DFT (PCM e CCl_4)	0.00	31.63	17.78	-0.268	-0.281	-0.328	-0.200	-0.186	-0.206	-0.074	-0.063	-0.096	2.91	2.54	2.52 (1.97)
59															

DFT	0.00	26.26	15.75	- 0.261	- 0.274	- 0.339	- 0.196	- 0.190	- 0.202	- 0.072	- 0.064	- 0.097	2.86	2.42	2.37 (2.02)
DFT (PCMeDMSO)	0.00	21.31	13.99	- 0.268	- 0.293	- 0.335	- 0.202	- 0.193	- 0.208	- 0.076	- 0.072	- 0.099	2.91	2.51	2.08 (1.71)
DFT (PCM e C_2H_5OH)	0.00	22.12	14.04	- 0.268	- 0.293	- 0.335	- 0.202	- 0.193	- 0.208	- 0.076	- 0.072	- 0.099	2.91	2.51	2.14 (1.72)
DFT (PCM e Acetone)	0.00	22.42	13.78	- 0.271	- 0.294	- 0.318	- 0.202	- 0.193	- 0.208	- 0.076	- 0.073	- 0.098	2.91	2.54	2.15 (1.70)
DFT (PCM e $CHCl_3$)	0.00	24.73	13.64	- 0.265	- 0.289	- 0.331	- 0.198	- 0.192	- 0.205	- 0.074	- 0.072	- 0.098	2.86	2.47	2.25 (1.69)
DFT (PCM e CCl_4)	0.00	26.41	14.10	- 0.265	- 0.289	- 0.331	- 0.198	- 0.192	- 0.205	- 0.074	- 0.072	- 0.098	2.86	2.47	2.32 (1.72)
60															
DFT	0.00	35.40	31.51	- 0.276	- 0.293	- 0.350	- 0.216	- 0.204	- 0.215	- 0.082	- 0.069	- 0.106	2.86		2.44 (2.61)
DFT (PCMeDMSO)	0.00	28.88	23.63	- 0.284	- 0.309	- 0.344	- 0.215	- 0.205	- 0.218	- 0.081	- 0.076	- 0.102	2.91		2.45 (2.28)
DFT (PCM e C_2H_5OH)	0.00	28.88	26.26	- 0.286	- 0.303	- 0.343	- 0.215	- 0.205	- 0.216	- 0.081	- 0.076	- 0.104	2.91		2.47 (2.30)
DFT (PCM e Acetone)	0.00	31.51	26.26	- 0.286	- 0.305	- 0.333	- 0.215	- 0.205	- 0.217	- 0.081	- 0.076	- 0.102	2.91		2.64 (2.48)
DFT (PCM e $CHCl_3$)	0.00	31.51	26.26	- 0.281	- 0.302	- 0.345	- 0.216	- 0.204	- 0.215	- 0.082	- 0.074	- 0.106	2.86		2.55 (2.34)
DFT (PCM e CCl_4)	0.00	34.13	28.88	- 0.278	- 0.309	- 0.343	- 0.216	- 0.205	- 0.216	- 0.082	- 0.076	- 0.104	2.86		2.61 (2.41)
61															
DFT	0.00	30.96	29.32	- 0.276	- 0.294	- 0.349	- 0.215	- 0.205	- 0.215	- 0.082	- 0.072	- 0.108	3.07		2.40 (2.50)
DFT (PCMeDMSO)	0.00	23.63	21.00	- 0.282	- 0.310	- 0.349	- 0.215	- 0.206	- 0.215	- 0.082	- 0.079	- 0.108	3.07		2.23 (2.12)
DFT (PCM e C_2H_5OH)	0.00	26.26	23.63	- 0.283	- 0.307	- 0.328	- 0.215	- 0.206	- 0.218	- 0.082	- 0.079	- 0.104	3.07		2.28 (2.18)
DFT (PCM e Acetone)	0.00	23.63	21.00	- 0.281	- 0.299	- 0.328	- 0.215	- 0.202	- 0.218	- 0.082	- 0.075	- 0.104	3.07		2.27 (2.15)
DFT (PCM e $CHCl_3$)	0.00	28.88	23.63	- 0.280	- 0.294	- 0.342	- 0.215	- 0.201	- 0.216	- 0.083	- 0.075	- 0.106	3.04		2.37 (2.22)
DFT (PCM e CCl_4)	0.00	28.88	26.26	- 0.278	- 0.299	- 0.342	- 0.215	- 0.202	- 0.216	- 0.083	- 0.075	- 0.106	3.04		2.45 (2.31)

ΔE in kJ/mol, is the energy difference between OH, hydrazone and the NH forms. E_g^a, E_g^b in kcal/mol, are the energy gap between LUMO and HOMO for NH and hydrazone forms, respectively. The equilibrium constant values were obtained from ln_{298} K^o = - ΔG^o/RT equation.

[c] Values in parentheses represent the $ln_{298}K_{II}^o$ of the NHNH↔hydrazone equilibrium. HOMO and LUMO, in eV, indicate the energies of the highest occupied and lowest unoccupied molecular orbitals.

The sensitivity of its λ_{max} to the type of the substituent attached and the nature of the solvent. This CT originates mainly from the pyrazolo[1,5-*a*]pyrimidine-7-(4*H*)-one ring as a donor to the terminal heterocyclic moiety.

Electronic absorption spectra from time-dependent DFT calculations of the tautomers were expected here in Table 34.

The values of ΔG and K_{ion} of the ionization equilibrium existing in solution are cited in Table 35. The negative values of the free energy change of the ionization process indicate that this process is spontaneous. In general, the experimental results presented in this table show that the values of K_{ion} and ΔG of the compounds investigated in mixed solvent depend upon R and increase in the following sequence **58** (R=CH_3)> **59** (R=Ph) and **60** (R=CH_3) >**61** (R=Ph) Values of pKa were determined by using three different spectrophotometric methods, namely the half curve-height, the limiting absorbance and the isosbestic point methods [87, 88]. The obtained values are in Table 36.

The similarity between the experimental and theoretical results shows that the DFT/B3LYP/6-31G** method has powerful role in explaining the features and tautomeric phenomena of the compounds under investigation. In the light of the obtained calculations of the energy gap (ε_{LUMO}_ε_{HOMO}) and time-dependent DFT, the visible absorption bands of compounds **58** and **59** are successfully assigned. The phenyl substituent at C_5 in compound **59** diminishes the energy gap between HOMO and LUMO and consequently absorbs light at relatively long wavelengths relative to compound [81].

Table 33. Experimental electronic absorption compounds havig spectral data of **58-61** moiety.

Compound	C_2H_5OH		DMF		DMSO		CH_3CN		Acetone		$CHCl_3$		CCl_4	
	λ_{max}	Log ε	λ_{max}	log ε	λ_{max}	log ε	λ_{max}	log ε	λ_{max}	log ε	λ_{max}	log ε	λ_{max}	log ε
58	404	4.48	440	4.38	426	4.29	442	4.34	407	4.33	405	4.38	405_{sh}	4.30
	367	4.56	375_{sh}	4.13	375_{sh}	4.19	367_{sh}	3.88	370	4.38	370	4.46	373	4.38
	246	4.52												
	208	4.61												
59	438_{sh}	4.41	454	4.60	452_{sh}	4.33	438	4.52	448_{sh}	4.02	409	4.49	410	4.47
	415	4.48	372	4.10	423	4.37	372_{sh}	4.08	412	4.46	372	4.55	372	4.55
	374_{sh}	4.36			376_{sh}	4.24			372	4.44				
	257	4.66												
	217	5.10												
60	430	4.26	451	4.25	439	3.99	436	4.19	428_{sh}	3.90	374	4.06	376	4.21
	280	3.80			385	4.02			377	4.02				
	236_{sh}	4.24												
	209	4.58												
61	436	4.48	457	4.54	458	4.41	431	4.45	447	4.46	410	4.27	405	4.24
	297	4.05												
	253	4.57												
	215	4.94												

λ_{max} – position of band maxima in absorption spectra (in nm), ε– absorption coefficients (in M^{-1} cm^{-1}), sh - shoulder.

Table 34. Wavelengths (λ_{nm}) and oscillator strengths (f) of electronic absorption transitions calculated at TDDFT method and the transition energies of the experimental (CT) absorption bands.

Compound	Time-dependent DFT calculations						E_T (kJ/mol)	
	NH		OH		hyd			
	λ (nm)	f	λ (nm)	f	λ (nm)	f	NH	Hyd
58	386	0.62	399	0.78	464	0.52	0.33	0.30
	340	0.18	331	0.12	347	0.08		
	248	0.19	251	0.22	259	0.06		
			214	0.05	217	0.01		
59	394	0.52	429	0.32	415	0.10	0.32	0.29
	343	0.09	378	0.25	361	0.13		
	249	0.19	293	0.16	260	0.26		
	226	0.21	244	0.10	213	0.03		
60	356	0.82	369	0.64	455	0.39	0.28	
	286	0.12	315	0.12	364	0.11		
	212	0.08	262	0.13	342	0.24		
	209	0.11	232	0.40	246	0.09		
61	362	0.74	396	0.45	468	0.28	0.27	
	256	0.04	344	0.55	422	0.18		
	218	0.02	273	0.23	360	0.22		
			218	0.18	256	0.24		
					245	0.10		

Table 35. Values of K_{ion} and -ΔG for the ionization process of the investigated compounds

System	Compound							
	58		59		60		61	
	K_{ion}	-Δ G	K_{ion}	-Δ G	K_{ion}	-Δ G	K_{ion}	-Δ G
DMF–C_2H_5OH	11.01	1.42	4.20	0.85	7.52	1.19	5.07	0.96
DMF–acetone	6.84	1.14	5.31	0.96	5.84	1.04	3.41	0.73
DMF–$CHCl_3$	10.78	1.40	6.07	1.10	7.03	1.15	4.65	0.91
DMF–CCl_4	9.79	1.35	3.45	0.73	6.63	1.12	4.21	0.85

Table 36. Values of acidity constants (pKa) and lamda max of the neutral and ionic forms of the compounds **58-61**

Compound	pK_a				SD	λ_{max}, nm	
	Method 1	Method 2	Method 3	Mean		Neutral	Ionic
58	8.67	8.60	8.66	8.64	±0.04	366	425
59	7.38	7.39	7.25	7.34	±0.08	366	430
60	7.23	7.23	7.20	7.22	±0.02	372	425
61	6.32	6.19	6.33	6.28	±0.08	370	429

3.5. Synthesis of 7-hydroxy-6-phenyl-3-(phenyldiazenyl)Pyrazolo[1,5-a]pyrimidine-2,5(1H,4H)-Dione

Synthesise of 7-hydroxy-6-phenyl-3-(phenyldiazenyl)pyrazolo[1,5-*a*]pyrimidine-2,5(1H,4H)-dione derivatives were obtained from the reaction of (chlorocarbonyl)phenyl ketene and 5-aminopyrazolones produce great yields and take short reaction times. To optimize the structures, calculate the energies and vibrational frequencies IR and 1H NMR shielding tensors of the desired products by

using Density Functional Theory (DFT). There are new methods to synthesize heterocyclic compounds by using condensation of (chlorocarbonyl) ketenes **63** with 1,3-dinucleophiles [89-91]. The reaction of (chlorocarbonyl) ketenes **63** with 5-aminopyrazoles **62** for the synthesis of 7-hydroxy-6-phenyl-3-(phenyldiazenyl)Pyrazolo[1,5-*a*]pyrimidine-2, 5(1H, 4H)-Dione derivatives **64a-e**, is reported in Scheme 16.

The endocyclic nitrogen atom will attack the central carbon atom of the ketene group, which have a low-lying LUMO. Subsequent cyclization gives compound **66**. Compound **64a-e** is given by H^+ elimination.

3.5.1. Theoretical studies

To anticipate the spectroscopic properties of the most stable structure, DFT approach was utilized in the Gaussian software. The computed wave numbers were scaled with the scaling factor in order to figure out how the predicted vibrational spectra are in agreement with experimental ones.

Vibrational examination of molecule was computed by using B3LYP level with basis set 6-311 G. The identified and predicted vibrational spectrum with results of fundamental vibrational modes were given in Table 37.

Table 37, in the range of 3300-2800 cm−1 the experimental N-H and O-H stretching frequencies showed for compound **64a-e**, the theoretically presaged IR for N-H and O-H stretching frequencies too were seen in the same range ~ 3199-2902 cm-1 by B3LYP/6-311G. The strongly intense peaks from B3LYP/6-311+G (d,p) agree well to the intensities obtained experimentally.

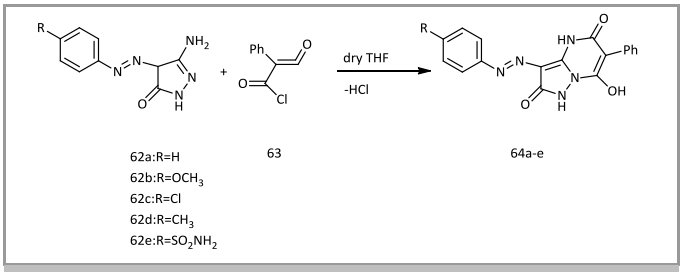

Scheme 16. Synthesis of 7-hydroxy-6-phenyl-3-(phenyldiazenyl)Pyrazolo[1,5-*a*]pyrimidine-2, 5(1H,4H)-dione derivatives 64a-e.

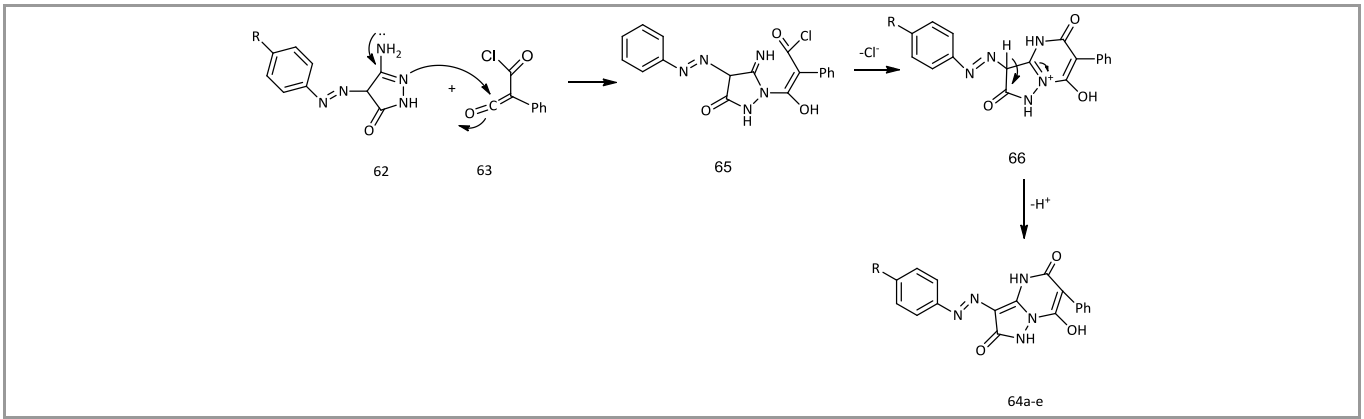

Scheme 17. Proposed mechanism for the formation of 7-hydroxy-6-phenyl-3-(aryldiazenyl)Pyrazolo[1,5-*a*]pyrimidine-2, 5(1H,4H)-dione derivatives.

Table 37. Calculated IR frequency of synthesized compound by B3LYP/6-311G

Compound	Experimental IR(cm^{-1})	Theoretical IR(cm^{-1}) B3LYP/6-311G
64a	(NH,OH) 3200-2900,(C=O) 1657 ,1625,1481,1550	(NH,OH) 3209-2902,(C=O) 1651,1660,1624,1633, 1543,1552,1480,1489
64b	(NH,OH) 3200-2900,(C=O) 1668,1628,1554,1491	(NH,OH) 3199-2893,(C=O) 1669,1624,1633, 1552,1489,1498
64c	(NH,OH)3200-2900,(C=O) 1672,1593,1549,1484	(NH,OH) 3209-2902,(C=O) 1670,1679,1588,1597, 1543,1480,1489
64d	(NH,OH)3200-2900,(C=O) 1672,1628,1552,1492	(NH,OH) 3207-2902,(C=O) 1669,1678,1624,1633,1552, 1561,1489,1498
64e	(NH_2) 3639,3547,(NH,OH)3300-2800,(C=O) 1688,1630,1596,1486	(NH,OH) 3325-2803,(C=O) 1687,1624,1633,1642,1588, 1597,1480,1489

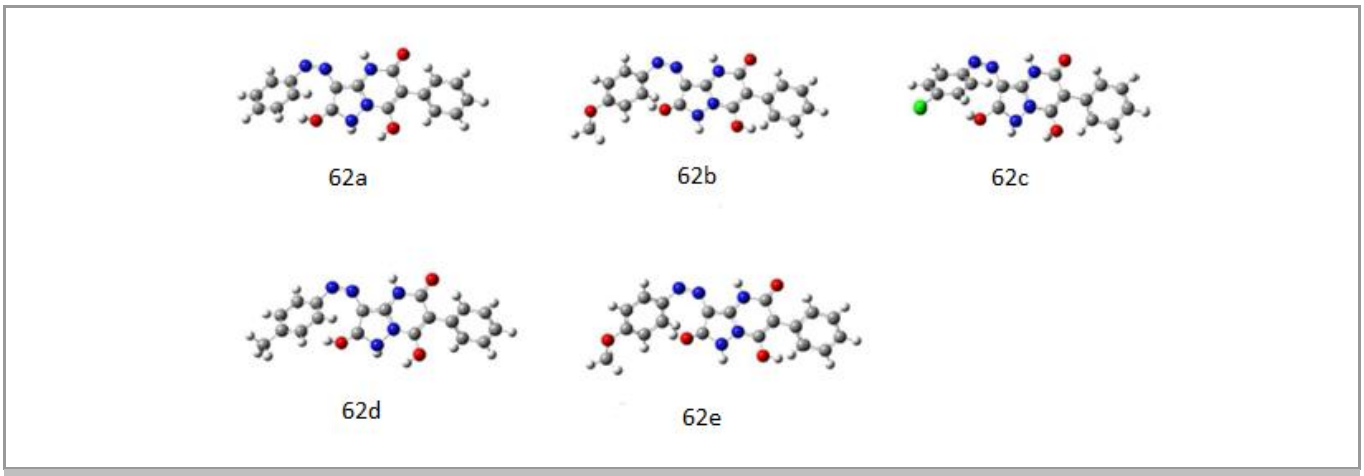

Figure 16. The optimized geometries of the compounds 64a-e

Table 38. The Nuclear Magnetic Resonance spectra of the ground state geometry of molecule has been indicated by DFT/GIAO method". To calculate isotropic nuclear magnetic used The GIAO method that is one of the most common methods. In table the predicted and measured NMR values were listed by B3LYP/6-311G

Experimental NMR(ppm)					**Theoretical NMR(ppm) B3LYP/6-311G**				
^{13}C NMR					**^{13}C NMR**				
64a	**64b**	**64c**	**64d**	**64e**	**64a**	**64b**	**64c**	**64d**	**64e**
160.04	160.58	161.13	160.08	160.52	159.71	159.06	159.51	159.83	159.00
159.80	160.48	160.35	159.85	160.43	154.94	157.75	152.63	153.00	156.16
151.36	158.78	151.36	151.31	153.78	149.63	149.75	149.28	149.69	155.05
145.94	150.49	145.54	146.12	145.48	145.92	149.24	146.56	145.66	148.70
143.69	146.20	134.50	141.10	141.66	130.44	140.89	146.12	136.29	147.12
134.35	134.59	131.10	136.81	134.48	129.65	132.99	130.44	130.45	130.50
129.22	129.26	130.39	134.47	130.52	128.24	129.31	130.05	129.96	127.93
127.51	126.48	129.54	129.80	129.82	127.96	128.17	129.69	128.73	126.36
126.88	123.32	127.48	127.61	128.29	126.29	127.62	127.68	128.15	125.68
123.31	119.88	123.26	123.40	127.60	125.97	123.34	126.08	126.90	122.12
123.01	118.51	120.23	123.10	123.42	124.19	118.31	125.51	125.90	120.93
117.76	114.70	116.85	117.77	118.41	115.81	116.19	115.83	115.76	115.94
84.32	84.26	84.27	84.40	84.48	110.77	104.55	110.85	110.29	108.90
67.93	66.30	67.64	64.85	67.02	100.40	96.46	101.71	100.34	103.17
	55.46		20.62			50.13		15.37	

Table 39. Showing Gibbs free energy for each compound at 298 K. According to these data, the reactant has Energy surface lower than the product energy surface at room temperature. This happen obtained the reaction will be done by external energy.

Comp	**63**	**62a**	**62b**	**62c**	**62d**	**62e**	**64a**	**64b**	**64c**	**64d**	**64e**	**THF**	**HCl**
$\Delta G°_f$ (j)×10^4	-2.51	-1.83	-6.70	-4.86	-6.53	-1.04	-3.13	-3.43	-4.34	-6.67	-4.72	-6.10	-1.21

Where 7-hydroxy-6-phenyl-3-(phenyldi azenyl) Pyrazolo[1,5-*a*]pyrimidine-2,5(1*H*,4*H*)-dione **62a** 7-hydroxy-3-((4-methoxyphenyl)diazenyl)-6-pheny lpyrazolo[1,5-*a*]pyrimidine-2,5(1*H*,4*H*)-dio ne **62b** , 3-(4-chlorophenyl) diazenyl)-7-hydroxy-6-phenyl pyrazolo[1,5-*a*]pyrimidine-2,5(1*H*,4*H*)-dione **62c** ,7-hydroxy-6-phenyl-3-(p-tolyldiaze nyl)Pyrazolo [1,5-*a*]pyrimidine-2,5(1*H*,4*H*)-dione **62d**, 4-((7-hydroxy-2,5-dioxo-6-phenyl-1,2,4,5-tetrahydropy razolo[1,5-*a*]pyrimidin-3-yl)diazenyl) benzenesulfonamide **62e.**
Activity energy surface of reactant and product in THF depicted in Figure 17.
Calculation by Gibbs free energy accordance with experimental process illustrated this reaction can be done at THF boiling point, correct products of this reaction also showed by using NMR data also showed in the experiment . Calculated parameters predicted that this reaction theoretically suitable for experimental synthesis [92].

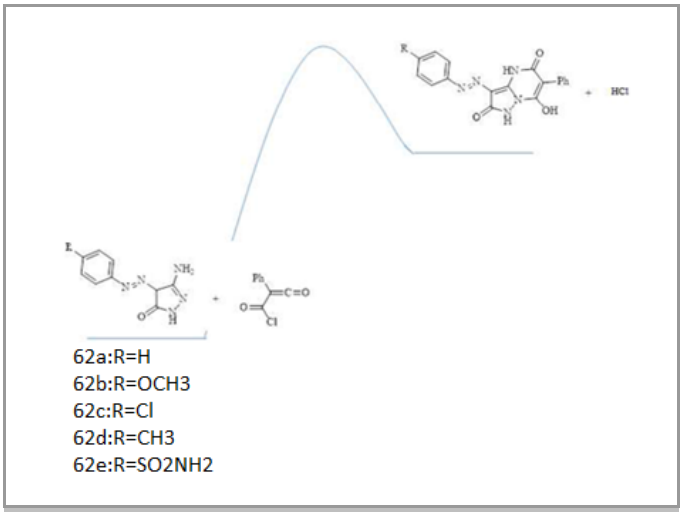

Figure 17. Activity energy surface of reactant and product in THF.

3.6. Synthesis of 5-tolyl-2-phenylpyrazolo[1,5-c]pyrimidine-7(6H)thione(Tolyl), 5-tolyl-2-phe-enylpyrazolo[1,5-c] pyrimidine-7(6H)one(Inon)

It was investigated as corrosion inhibitors utilizing density functional theory (DFT) at the B3LYP/6-31 + G (d, p) level of theory. The computed quantum chemical parameters associated to the inhibition proficiency are: the highest occupied molecular orbital energy (EHOMO), the lowest unoccupied molecular orbital energy (ELUMO), the energy gap (ΔEL-H), ionization energy (I), dipole moment (μ), electron affinity (A), absolute electronegativity (χ), absolute softness (σ), absolute hardness (η), the fraction of electron transferred (ΔN), and the total energy (Etot) which were studied.
Figure 18 shows the optimized structures of Tolyl and Inon inhibitors along with atomic numbering. For Tolyl and Inon molecules, the computed quantum chemical properties as E_{HOMO}, E_{LUMO}, ΔE_{L-H} and dipole moment (μ) are obtained in Table 40.

Table 40. Calculated quantum chemical parameters of Tolyl and Inon molecules calculated at B3LYP/6-31 + G (d, p) level of theory

Quantum parameters	Unit	Tolyl	Inon
E_{HOMO}	(eV)	−0.21463	−0.21943
E_{LUMO}	(eV)	−0.06821	−0.06535
ΔE_{L-H}	(eV)	0.14642	0.15408
μ	(debye)	7.2231	6.8992

Table 41. Calculated quantum chemical parameters of Tolyl and Inon molecules calculated at B3LYP/6-31 + G(d,p) level of theory.

Quantum parameters	Unit	Tolyl	Inon
$I=-E_{HOMO}$	(au)	0.21463	0.21943
$A=-E_{LUMO}$	(au)	0.06821	0.06535
$\chi = (I+A)/2$	(au)	0.14142	0.14239
$\eta = (i-A)/2$	(au)	0.07321	0.07704
$\sigma = 1/\eta$	(au^{-1})	13.65934	12.98027
$\omega=\mu^2/2\,\eta$	(au)	356.32546	308.92370
$\Delta N=(\chi_{FE}-\chi_{inh})/2(\eta_{fe}+\eta_{inh})$		46.84182	44.50681
E_{tot}	(au)	−1295.56608	−972.61603

Tolyl with the softness value of 13.65934 eV has the most elevated inhibition efficiency contrasted with 12.98027 eV of Inon; this result is also in agreement with the experimental finding.
Utilizing the DFT/B3LYP/6-31 + G (d,p) level of hypothesis, the inhibition efficiency of two Pyrazolo[1,5-*c*] pyrimidine derivatives is indicated prompting the accompanying conclusions.
Through DFT calculations, a relationship between parameters identified with the electronic and molecular structures of these derivatives and their ability to stop the corrosion process could be set up.
The inhibition efficiency of these derivatives acquired quantum chemically increases with the increase in E_{HOMO}, and decrease in E_{LUMO} and energy gap ΔE_{L-H}. Tolyl has the highest inhibition efficiency because it had the highest HOMO energy [93].

67 68

The molecular structures of the investigated in-hibitors: **(67)** 5-tolyl-2-phenylpyrazolo[1,5-c]pyrimidine-7(6H) thione (Tolyl), **(68)** 5-tolyl-2-phenylpyrazolo[1,5-c]pyrimidine-7(6H)one (Inon).

67

68

Figure 18. Optimized geometries of **67** Tolyl and **68** Inon molecules along with atomic numbering calculated at B3LYP/6-31 + G(d, p) level of theory

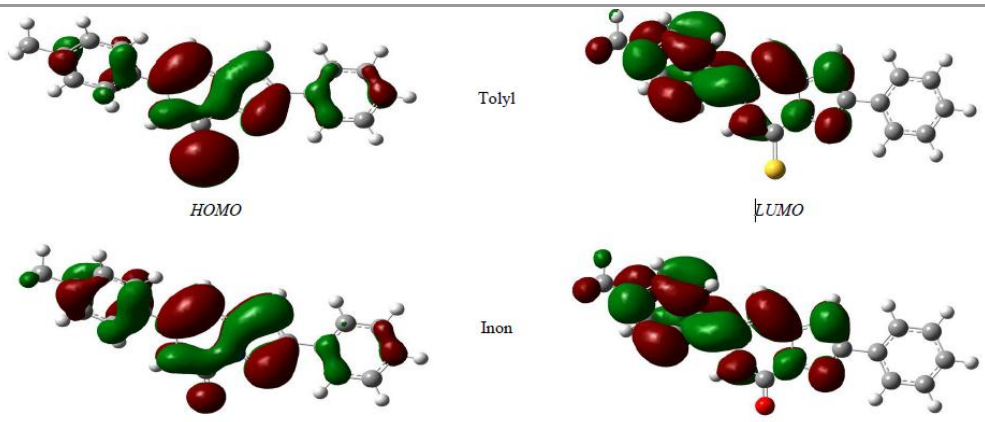

Figure 19. Frontier molecular orbitals (FMO) of Tolyl and Inon molecules calculated at B3LYP/6-31 + G(d,p) level of theory

4. Conclusion

In this study, the synthesis of different pyrazolopyrmidines derivatives and their computational analysis by density functional theory level (utilizing HF/6−311+G and B3LYP/6−311+G) were evaluated. Charge transfer occured through the molecule was shown by calculating the HOMO and LUMO energies. The electric dipole moment values (l) of the molecule were counted as calculations of the DFT. Some geometrical and structural parameters including, the total energies (E), relative energies (DE), (bond length in Å, angles in degree), energy gap, relative Gibbs free energy, dipole moment, and molecular electrostatic potentials (MEP) were studied.

Acknowledgement

The authors would like appreciate Dr. Yasser Zaky, from Organic Chemistry, Faculty of Science, Beni-Suef University, Mrs. Ghada Mayhoob and Arwa Ali from the Faculty of Science, Beni-Suef University for their support.

References

[1] Ahmed, S. A., Elghandour, A. H., & Elgendy, H. S. (**2014**). Synthesis of pteridines

derivatives from different heterocyclic compounds. *Der Pharma Chemica*, *6*(3), 194-219..

[2] Ahmed, S. A., Elgendy, H. S., & Younis, W. O. (**2015**). Pyrazolopyrimidines: Synthesis, Chemical Reactions and Biological Activity. *ChemInform*, *46*(14), no-no.

[3] Hussein S. H. Mohamed, M. N., Sayed A. Ahmed. (**2018**) Novel synthesis and characterization of Aryl Benzothiazoles with antimicrobial activity, *der pharma chemical 10*(5), 121-127.

[4] Contreras, J. G., Seguel, G. V., & Gnecco, J. A. (**1992**). The IR and Raman spectra of 2-amino pyrimidine complexes of some Zn (II), Cd (II) and Hg (II) halides. *Spectrochimica Acta Part A: Molecular Spectroscopy*, *48*(4), 525-532.

[5] Pullman, B., & Pullman, A. (**1971**). Electronic aspects of purine tautomerism. In *Advances in Heterocyclic Chemistry*(Vol. 13, pp. 77-159). Academic Press.

[6] Contreras, J. G., & Seguel, G. V. (**1982**). Solid State Vibrational Spectra of Tetrapropylammonium Tribromomercurate (II). *Spectroscopy Letters*, *15*(9), 671-677.

[7] Hayat, F., Salahuddin, A., Umar, S., & Azam, A. (**2010**). Synthesis, characterization, antiamoebic activity and cytotoxicity of novel series of pyrazoline derivatives bearing quinoline tail. *European journal of medicinal chemistry*, *45*(10), 4669-4675.

[8] Budakoti, A., Abid, M., & Azam, A. (**2007**). Syntheses, characterization and in vitro antiamoebic activity of new Pd (II) complexes with 1-N-substituted thiocarbamoyl-3, 5-diphenyl-2-pyrazoline derivatives. *European journal of medicinal chemistry*, *42*(4), 544-551.

[9] Parveen, H., Hayat, F., Mukhtar, S., Salahuddin, A., Khan, A., Islam, F., & Azam, A. (**2011**). Synthesis, characterization and biological evaluation of novel 2, 4, 6-trisubstituted bis-pyrimidine derivatives. *European journal of medicinal chemistry*, *46*(9), 4669-4675.

[10] Siddiqui, S. M., Salahuddin, A., & Azam, A. (**2013**). Pyrazolo [3, 4-d] pyrimidine analogues: synthesis, characterization and their in vitro antiamoebic activity. *Medicinal Chemistry Research*, *22*(2), 775-781.

[11] Hussein S. H. Mohamed, H. S. B., Sayed A. Ahmed. (**2017**) Evaluation of N-Sulfanoamide Pyridines from Chalchon with Anticancer Effect, *nternational Journal of Innovative Research in Science, Engineering and Technology 6*, 15972-15981.

[12] Hussein S. H. Mohamed, M. N., Sayed A. Ahmed. (**2017**) Synthesis, Chemical reactions and applications of Aryl azo Thiazole, *International Journal of advanced research*, *5*(7), 2426-2496.

[13] Azzama, E. M., Ahmedb, S. A., Mohamedb, H. H., Adlyb, M. A., & Gada, E. A. (**2019**). Removal of iron (II) from wastewater in oil field using 3-(p-methyl) phenyl-5-thionyl-1, 2, 4-triazoline assembled on silver nanoparticles. *DESALINATION AND WATER TREATMENT*, *142*, 244-251.

[14] Bekhit, A. A., & Abdel-Aziem, T. (**2004**). Design, synthesis and biological evaluation of some pyrazole derivatives as anti-inflammatory-antimicrobial agents. *Bioorganic & medicinal chemistry*, *12*(8), 1935-1945..

[15] Sayed A. Ahmed, H. S. E. (**2014**) Synthesis of some new purine and mercaptopurine analogues as antimetabolites, *International Journal of advanced research*, *2*(5), 865-876.

[16] Yadava, U., Singh, M., & Roychoudhury, M. (**2013**). Pyrazolo [3, 4-d] pyrimidines as inhibitor of anti-coagulation and inflammation activities of phospholipase A 2: insight from molecular docking studies. *Journal of biological physics*, *39*(3), 419-438..

[17] Elion, G. B., Callahan, S., Nathan, H., Bieber, S., Rundles, R. W., & Hitchings, G. H. (**1963**). Potentiation by inhibition of drug degradation: 6-substituted purines and xanthine oxidase. *Biochemical Pharmacology*, *12*(1), 85-93.

[18] Schenone, S., Brullo, C., Musumeci, F., & Botta, M. (**2010**). Novel dual Src/Abl inhibitors for hematologic and solid malignancies. *Expert opinion on investigational drugs*, *19*(8), 931-945.

[19] Sayed A. Ahmed, O. M. A., Hussein S. Elgendy. (**2014**) Novel Synthesis of Purine analogues derivatives and Thieno [2,3-b]pyridine derivatives with anticancer and antioxidant activity, *Journal of pharmacy research*, *8*(9), 1303-1313.

[20] Casini, N., Forte, I. M., Mastrogiovanni, G., Pentimalli, F., Angelucci, A., Festuccia, C., ... & Botta, M. (**2015**). SRC family kinase (SFK) inhibition reduces rhabdomyosarcoma cell growth in vitro and in vivo and triggers p38 MAP kinase-mediated differentiation. *Oncotarget*, *6*(14), 12421.

[21] Carlomagno, F., Vitagliano, D., Guida, T., Basolo, F., Castellone, M. D., Melillo, R. M., ... & Santoro, M. (**2003**). Efficient inhibition of RET/papillary thyroid carcinoma oncogenic kinases by 4-amino-5-(4-chloro-phenyl)-7-(t-

butyl) pyrazolo [3, 4-d] pyrimidine (PP2). *The Journal of Clinical Endocrinology & Metabolism*, *88*(4), 1897-1902.

[22] Fogarasi, G., Pulay, P., & Durig, J. R. (**1985**). Vibrational spectra and structure. *Vibrational Spectra and Structure*, *14*, 125.

[23] Schaefer, H. (Ed.). (**2012**). *Applications of electronic structure theory* (Vol. 4). Springer Science & Business Media.

[24] Islam, M. J., Kumer, A., Sarker, N., Paul, S., & Zannat, A. (**2019**). The prediction and theoretical study for chemical reactivity, thermophysical and biological activity of morpholinium nitrate and nitrite ionic liquid crystals: A DFT study. *Advanced Journal of Chemistry-Section A (Theoretical, Engineering and Applied Chemistry)*, *2*(4, pp. 266-385), 316-326.

[25] Javanshir, Z., Jameh-Bozorghi, S., & Peyki, P. (**2018**). DFT calculations of the neighboring groups effects on cheletropic reaction of 2, 5-Dihydrothiophene sulfone. *Advanced Journal of Chemistry-Section A*, *1*(2. pp. 66-126), 117-126.

[26] Arivazhagan, M. (**2011**). Vibrational analysis of 4-amino pyrazolo (3, 4-d) pyrimidine A joint FTIR, Laser Raman and scaled quantum mechanical studies. *Spectrochimica Acta Part A: Molecular and Biomolecular Spectroscopy*, *82*(1), 228-234.

[27] Fekri, M. H. (**2019**). Study of Electrochemical and Electronical Properties on the Some Schiff Base Ni Complexes in DMSO Solvent by Computational Methods. *Advanced Journal of Chemistry-Section A*, *2*(1, pp. 1-93.), 14-20..

[28] Kumer, A., Sarker, N., Paul, S., & Zannat, A. (**2019**). The Theoretical Prediction of Thermophysical properties, HOMO, LUMO, QSAR and Biological Indics of Cannabinoids (CBD) and Tetrahhdrocannabinol (THC) by Computational Chemistry. *Advanced Journal of Chemistry-Section A (Theoretical, Engineering and Applied Chemistry)*, *2*(3. pp. 184-265), 190-202.

[29] Sanz, F., Manaut, F., José, J., Segura, J., Carbó, M., & De la Torre, R. (**1988**). Automatic determination of MEP patterns of molecules and its application to caffeine metabolism inhibitors. *Journal of Molecular Structure: THEOCHEM*, *170*, 171-180.

[30] Abood, N. A. (**2013**). SH Hlban J. Chem. *Pharm. Res*, *5*, 324-331.

[31] Yang, J., Yan, H., Wang, G., Zhang, X., Wang, T., & Gong, X. (**2014**). Computational investigations into the substituent effects of–N 3,–NF 2,–NO 2, and–NH 2 on the structure, sensitivity and detonation properties of N, N′-azobis (1, 2, 4-triazole). *Journal of molecular modeling*, *20*(4), 2148.

[32] Scrocco, E., & Tomasi, J. (**1973**). The electrostatic molecular potential as a tool for the interpretation of molecular properties. In *New concepts II* (pp. 95-170). Springer, Berlin, Heidelberg.

[33] March, N. H. (**1996**). Electrostatic Potential, Bond Density and Bond Order in Molecules and Clusters. In *Theoretical and Computational Chemistry* (Vol. 3, pp. 619-647). Elsevier.

[34] Gomaa, E. G. A., Abdel Hady, M. H., Mahmoud, M. H., & El Kot, D. A. (**2019**). Cyclic Voltammetry of Aqueous CoCl2 in the Presence of Ceftriaxone Disodium Salt (Cefs) at 298.65 K. *Advanced Journal of Chemistry-Section A*, *2*(1, pp. 1-93.), 1-13.

[35] Hariharan, P. C., & Pople, J. A. (**1973**). The influence of polarization functions on molecular orbital hydrogenation energies. *Theoretica chimica acta*, *28*(3), 213-222.

[36] Hosseini, P., & Rezaei Sameti, M. (**2019**). The AIM, RDG, NBO, Quantum and Structural Study of Adsorption of Phosgene Gas on the Surface of Pristine and Al, P Doped Ga12N12 Nano Cluster: A DFT Method. *Chemical Methodologies*, *3*(5, pp. 519-683), 607-625.

[37] Mosallanejad, B. (**2019**). Phthalimide Derivatives: New Promising Additives for Functional Electrolyte in Lithium-ion Batteries. *Chemical Methodologies*, *3*(2. pp. 145-275), 261-275.

[38] Ahmadinejad, N., & Talebi Trai, M. (**2019**). Computational NQR− NBO Parameters and DFT Calculations of Ampicillin and Zwitterion (Monomer and Dimer Structures). *Chemical Methodologies*, *3*(1. pp. 1-144), 55-66.

[39] Frisch, M. J., Trucks, G. W., Schlegel, H. B., Scuseria, G. E., Robb, M., Cheeseman, J. R., ... & Nakatsuji, H. (**2009**). Gaussian 09, Revision D. 01, Gaussian. *Inc.: Wallingford, CT*.

[40] Rezaei Sameti, M., & Amirian, B. (**2018**). A Quantum, NBO, RDG study the interaction of cadmium ion with the pristine, C, P and C&P doped (4, 4) armchair boron nitride nanotube (BNNTs). *Asian Journal of Nanosciences and Materials*, *1*(4. pp. 172-293), 262-270.

[41] Houshmand, F., Neckoudaria, H., & Baghdadi, M. (**2019**). Host-guest interaction in chitosan–MX (3-chloro-4-(dichloromethyl)-5-hydroxy-2 (5H)-furanone) complexes in water solution:

Density Functional Study. *Asian Journal of Nanosciences and Materials*, *2*(1, pp. 1-119.), 49-65.

[42] Korivand, N., & Rezaei-Sameti, M. Asian Journal of Nanoscience and Materials.

[43] Prabavathi, N., Nilufer, A., Krishnakumar, V., & Akilandeswari, L. (**2012**). Spectroscopic, electronic structure and natural bond analysis of 2-aminopyrimidine and 4-aminopyrazolo [3, 4-d] pyrimidine: A comparative study. *Spectrochimica Acta Part A: Molecular and Biomolecular Spectroscopy*, *96*, 226-241.

[44] Frisch, M. J. E. A., Trucks, G. W., Schlegel, H. B., Scuseria, G. E., Robb, M. A., Cheeseman, J. R., ... & Nakatsuji, H. (**2009**). Gaussian 09, revision a. 02, gaussian. *Inc., Wallingford, CT*, *200*, 28.

[45] Becke, A. D. (**1993**) Density-functional thermochemistry. III. The role of exact exchange, *The Journal of chemical physics*, *98*(7), 5648-5652.

[46] Lee, C., Yang, W., & Parr, R. G. (**1988**). Development of the Colle-Salvetti correlation-energy formula into a functional of the electron density. *Physical review B*, *37*(2), 785.

[47] Krishnakumar, V., & Dheivamalar, S. (**2007**). Density functional theory studies on tautomeric stability and infrared and Raman spectra of some purine derivatives. *Spectrochimica Acta Part A: Molecular and Biomolecular Spectroscopy*, *68*(3), 823-832.

[48] Xue, Y., Xu, D., Xie, D., & Yan, G. (**2000**). Density functional theory studies on tautomeric stability and infrared spectra of 2-chloroadenine. *Spectrochimica Acta Part A: Molecular and Biomolecular Spectroscopy*, *56*(10), 1929-1938.

[49] Datta, A., & Pati, S. K. (**2004**). Effects of dipole orientations on nonlinear optical properties of oxo-bridged dinitroaniline systems. *The Journal of Physical Chemistry A*, *108*(2), 320-325.

[50] Shunmugam, R., & Sathyanarayana, D. N. (**1984**). Raman and polarized infrared spectra of pyridine-2-thione. *Spectrochimica Acta Part A: Molecular Spectroscopy*, *40*(8), 757-761.

[51] Mukherjee, V., Singh, N. P., & Yadav, R. A. (**2011**). Optimized geometry and vibrational spectra and NBO analysis of solid state 2, 4, 6-tri-fluorobenzoic acid hydrogen bonded dimer. *Journal of Molecular Structure*, *988*(1-3), 24-34.

[52] Hamilton, H. W., Ortwine, D. F., Worth, D. F., & Bristol, J. A. (**1987**). Synthesis and structure-activity relationships of pyrazolo [4, 3-d] pyrimidin-7-ones as adenosine receptor antagonists. *Journal of medicinal chemistry*, *30*(1), 91-96.

[53] Squarcialupi, L., Colotta, V., Catarzi, D., Varano, F., Filacchioni, G., Varani, K., ... & Di Cesare Mannelli, L. (**2013**). 2-Arylpyrazolo [4, 3-d] pyrimidin-7-amino derivatives as new potent and selective human A3 adenosine receptor antagonists. Molecular modeling studies and pharmacological evaluation. *Journal of medicinal chemistry*, *56*(6), 2256-2269.

[54] Massey, V., Komai, H., Palmer, G., & Elion, G. B. (**1970**). On the mechanism of inactivation of xanthine oxidase by allopurinol and other pyrazolo [3, 4-d] pyrimidines. *Journal of Biological Chemistry*, *245*(11), 2837-2844.

[55] Falchi, F., Manetti, F., Carraro, F., Naldini, A., Maga, G., Crespan, E., ... & Botta, M. (**2009**). 3D QSAR Models Built on Structure-Based Alignments of Abl Tyrosine Kinase Inhibitors. *ChemMedChem: Chemistry Enabling Drug Discovery*, *4*(6), 976-987.

[56] Alkorta, I., & Elguero, J. (**2017**). The structure of N-arylindazoles and their aza-derivatives in the solid state: A systematic analysis of the Cambridge Structural Database coupled with DFT calculations. *Journal of Molecular Structure*, *1137*, 186-192.

[57] Ali, H. I., Fujita, T., Akaho, E., & Nagamatsu, T. (**2010**). A comparative study of AutoDock and PMF scoring performances, and SAR of 2-substituted pyrazolotriazolopyrimidines and 4-substituted pyrazolopyrimidines as potent xanthine oxidase inhibitors. *Journal of computer-aided molecular design*, *24*(1), 57-75.

[58] Avasthi, K., Rawat, D. S., Maulik, P. R., Sarkhel, S., Broder, C. K., & Howard, J. A. (**2001**). 1H NMR and X-ray crystallographic analysis of 1, 2-bis (4, 6-diethylthio-1H-pyrazolo [3, 4-d] pyrimidin-1-yl) ethane and its 'propylene linker'-analog: molecular recognition versus crystal engineering. *Tetrahedron Letters*, *42*(40), 7115-7117.

[59] Avasthi, K., Aswal, S., Kumar, R., Yadav, U., Rawat, D. S., & Maulik, P. R. (**2005**). Fine tuning of folded conformation by change of substituents: 1H NMR and crystallographic evidence for folded conformation due to arene interactions in pyrazolo [3, 4-d] pyrimidine core based 'propylene

linker'compounds. *Journal of molecular structure*, *750*(1-3), 179-185.

[60] Maulik, P. R., Avasthi, K., Biswas, G., Biswas, S., Rawat, D. S., Sarkhel, S., ... & Bhakuni, D. S. (**1998**). A stacked pyrazolo [3, 4-d] pyrimidine-based flexible molecule. *Acta Crystallographica Section C: Crystal Structure Communications*, *54*(2), 275-277.

[61] Avasthi, K., Aswal, S., & Maulik, P. R. (**2001**). A stacked pyrazolo [3, 4-d] pyrimidine-based flexible molecule: the effect on stacking of an ethyl group in comparison with a methyl group. *Acta Crystallographica Section C: Crystal Structure Communications*, *57*(11), 1324-1325.

[62] Avasthi, K., Tewari, A., Rawat, D. S., Sharon, A., & Maulik, P. R. (**2002**). A stacked pyrazolo [3, 4-d] pyrimidine-based flexible molecule: the effect of a bulky benzyl group on intermolecular stacking in comparison with methyl and ethyl groups. *Acta Crystallographica Section C: Crystal Structure Communications*, *58*(8), o494-o495.

[63] Avasthi, K., Farooq, S. M., Aswal, S., Raghunandan, R., & Maulik, P. R. (**2007**). 1H NMR and crystallographic evidence for tolerance of bulky electron withdrawing methanesulfonyl group on robustness of the U-motif in pyrazolo [3, 4-d] pyrimidine core based 'Leonard linker'compounds and formation of plus (+) motif. *Journal of molecular structure*, *827*(1-3), 88-94.

[64] Avasthi, K., Bhagat, D., Bal, C., Sharon, A., Yadav, U., & Maulik, P. R. (**2003**). Unusual molecular conformation in dissymmetric propylene-linker compounds containing pyrazolo [3, 4-d] pyrimidine and phthalimide moieties. *Acta Crystallographica Section C: Crystal Structure Communications*, *59*(8), o409-o412.

[65] Avasthi, K., Rawat, D. S., Sarkhel, S., & Maulik, P. R. (**2002**). A dimeric layered structure of a 4-oxo-4, 5-dihydro-1H-pyrazolo [3, 4-d] pyrimidine compound. *Acta Crystallographica Section C: Crystal Structure Communications*, *58*(6), o325-o327.

[66] Yadava, U., Singh, M., & Roychoudhury, M. (**2011**). Gas-phase conformational and intramolecular π–π interaction studies on some pyrazolo [3, 4-d] pyrimidine derivatives. *Computational and Theoretical Chemistry*, *977*(1-3), 134-139.

[67] Laarej, K., Bouachrine, M., Radi, S., Kertit, S., & Hammouti, B. (**2010**). Quantum chemical studies on the inhibiting effect of bipyrazoles on steel corrosion in HCl. *Journal of Chemistry*, *7*(2), 419-424.

[68] Chtita, S., Larif, M., Ghamali, M., Adad, A., Rachid, H., Bouachrine, M., & Lakhlifi, T. (**2013**). Studies of two different cancer cell lines activities (MDAMB-231 and SK-N-SH) of imidazo [1, 2-a] pyrazine derivatives by combining DFT and QSAR results. *Studies*, *2*(11).

[69] Elidrissi, B., Ousaa, A., Ghamali, M., Chtita, S., Ajana, M. A., Bouachrine, M., & Lakhlifi, T. (**2014**). Journal of Computational Methods in Molecular Design, 2014, 4 (4): 140-149. *Journal of Computational Methods in Molecular Design*, *4*(4), 140-149.

[70] Krishnakumar, V., Prabavathi, N., & Muthunatesan, S. (**2008**). Structure and vibrational frequencies of 1-naphthaldehyde based on density functional theory calculations. *Spectrochimica Acta Part A: Molecular and Biomolecular Spectroscopy*, *69*(2), 528-533.

[71] El-Mansy, M. A. M., & El-Nahass, M. M. (**2014**). On the spectroscopic analyses of Perylene-66. *Spectrochimica Acta Part A: Molecular and Biomolecular Spectroscopy*, *130*, 568-573.

[72] Shukla, B. K., Yadava, U., & Roychoudhury, M. (**2015**). Theoretical explorations on the molecular structure and IR frequencies of 3-phenyl-1-tosyl-1H-pyrazolo [3, 4-d] pyrimidin-4-amine in view of experimental results. *Journal of Molecular Liquids*, *212*, 325-330.

[73] Kasula, M., Samunuri, R., Chakravarty, H., Bal, C., Baba, M., Jha, A. K., & Sharon, A. (**2016**). Regioselective Synthesis of Pyrazolo [3, 4-D] Pyrimidine Based Carbocyclic Nucleosides as Possible Antiviral Agent. *Nucleosides, Nucleotides and Nucleic Acids*, *35*(1), 43-52.

[74] Khan, S. A. (**2017**). Green synthesis, spectrofluorometric characterization and antibacterial activity of heterocyclic compound from chalcone on the basis of in vitro and quantum chemistry calculation. *Journal of fluorescence*, *27*(3), 929-937.

[75] Asiri, A. M., & Khan, S. A. (**2012**). Synthesis, characterization, and in vitro antibacterial activities of macromolecules derived from bis-chalcone. *Journal of Heterocyclic Chemistry*, *49*(6), 1434-1438.

[76] Lauria, A., Abbate, I., Patella, C., Gambino, N., Silvestri, A., Barone, G., & Almerico, A. M. (**2008**). Pyrazolo [3, 4-d][1, 2, 3] triazolo [1, 5-a] pyrimidine: a new ring system through

Dimroth rearrangement. *Tetrahedron Letters*, *49*(35), 5125-5128.
[77] Zaki, Y. H., Sayed, A. R., & Elroby, S. A. (**2016**). Regioselectivity of 1, 3-dipolar cycloadditions and antimicrobial activity of isoxazoline, pyrrolo [3, 4-d] isoxazole-4, 6-diones, pyrazolo [3, 4-d] pyridazines and pyrazolo [1, 5-a] pyrimidines. *Chemistry Central Journal*, *10*(1), 17.
[78] Al-Sehemi, A. G., Irfan, A., & Fouda, A. M. (**2013**). Synthesis, characterization and density functional theory investigations of the electronic, photophysical and charge transfer properties of donor–bridge–acceptor triaminopyrazolo [1, 5-a] pyrimidine dyes. *Spectrochimica Acta Part A: Molecular and Biomolecular Spectroscopy*, *111*, 223-229.
[79] Koleva, G., Galabov, B., Wu, J. I., Schaefer III, H. F., & Schleyer, P. V. R. (**2009**). Electrophile affinity: a reactivity measure for aromatic substitution. *Journal of the American Chemical Society*, *131*(41), 14722-14727.
[80] Bedford, R. B., Durrant, S. J., & Montgomery, M. (**2015**). Catalyst-Switchable Regiocontrol in the Direct Arylation of Remote C□ H Groups in Pyrazolo [1, 5-a] pyrimidines. *Angewandte Chemie International Edition*, *54*(30), 8787-8790.
[81] Ebead, Y. H. (**2012**). Spectrophotometric investigations and computational calculations of prototropic tautomerism and acid–base properties of some new azo dyes. *Dyes and Pigments*, *92*(1), 705-713.
[82] Hihara, T., Okada, Y., & Morita, Z. (**2003**). Reactivity of phenylazonaphthol sulfonates, their estimation by semiempirical molecular orbital PM5 method, and the relation between their reactivity and azo-hydrazone tautomerism. *Dyes and Pigments*, *59*(3), 201-222.
[83] Hammam, A. M., Rageh, N. M., & Ibrahim, S. A. (**1997**). Solvatochromic studies on 2-[(2-hydroxypheny) azo]-4-5-diphenylimidazole. *dyes and Pigments*, *35*(3), 289-296.
[84] Karcı, F., Şener, N., Yamaç, M., Şener, İ., & Demirçalı, A. (**2009**). The synthesis, antimicrobial activity and absorption characteristics of some novel heterocyclic disazo dyes. *Dyes and Pigments*, *80*(1), 47-52.
[85] Becke, A. D. (**1988**). Density-functional exchange-energy approximation with correct asymptotic behavior. *Physical review A*, *38*(6), 3098.
[86] Becke, A. D. (**1993**). A new mixing of Hartree–Fock and local density-functional theories. *The Journal of chemical physics*, *98*(2), 1372-1377.
[87] Issa, R. M., Sadek, H., & Ezzat, I. I. (**1971**). Spectrophotometric studies on dihydric phenols. *Zeitschrift für Physikalische Chemie*, *74*(1_2), 17-25.
[88] Issa, R. M., Hammam, A. S., & Etaiw, S. H. (**1972**). The Electronic Absorption Spectra of Some 2, 3-Benzcarbazoloquinones. *Zeitschrift für Physikalische Chemie*, *251*(1), 177-182.
[89] Zahedifar, M., & Sheibani, H. (**2014**). Unexpected Products from Mesoionic 1, 3-Thiazinium and Oxazinium Olates: A Novel Access to 3, 5-Diaryl-1, 3-thiazine-2, 4, 6-trione and Alkoxy-3, 5-diphenyl-3H-1, 3-oxazine-2, 6-dione Derivatives. *Australian Journal of Chemistry*, *67*(9), 1201-1204.
[90] Zahedifar, M., & Sheibani, H. (**2016**). Reaction of α-oxoketenes with 2-substituted benzothiazoles and benzimidazoles: synthesis of benzo [4, 5] thiazolo [3, 2-a] pyridinone and N-(1, 3-benzothiazol-2-yl)-3-oxopropanamide derivatives. *Chemistry of Heterocyclic Compounds*, *52*(1), 41-44.
[91] Sheibani, H., & Zahedifar, M. (**2009**). The condensation of (chlorocarbonyl) phenylketene with 1, 3-dinucleophiles (2) Preparation of 2-hydroxy-3-phenyl-4H-pyrimido [2, 1-b][1, 3] benzothiazol-4-ones and thioxo dihydro-4, 6 (1H, 5H)-pyrimidinones. *Heterocycles*, *78*(4), 1015-1022.
[92] Zahedifar, M., Razavi, R., & Sheibani, H. (**2016**). Reaction of (chloro carbonyl) phenyl ketene with 5-amino pyrazolones: Synthesis, characterization and theoretical studies of 7-hydroxy-6-phenyl-3-(phenyldiazenyl) pyrazolo [1, 5-a] pyrimidine-2, 5 (1H, 4H)-dione derivatives. *Journal of Molecular Structure*, *1125*, 730-735.
[93] Wazzan, N. A., & Mahgoub, F. M. (**2014**). DFT calculations for corrosion inhibition of ferrous alloys by pyrazolopyrimidine derivatives. *Open Journal of Physical Chemistry*, *4*(01), 6.

How to cite this manuscript: Hussein S. H. Mohamed, Sayed A. Ahmed, Reviewing of Synthesis and Computational Studies of Pyrazolo Pyrimidine Derivatives, Journal of Chemical Reviews, **2019**, 1(3), 183-232.